REVIEW

Transforming Surgical Planning and Procedures through Synergistic Use of Additive Manufacturing, Advanced Materials and Artificial Intelligence: Challenges and Opportunities

Received 00th January 20xx,
Accepted 00th January 20xx

DOI: 10.1039/x0xx00000x

Shivi Tripathi[1,2], Aftab Alam Ansari[1,2,3], Manisha Singh[4], Madhusmita Dash[2,5,6], Prasoon Kumar[6,7**], Harpreet Singh[8], Biranchi Panda[9], Syam Nukavarapu[10], Gulden Camci-Unal[11], Bingbing Li[12,13,14], Prashant Kumar Jain[3], Rengaswamy Jayaganthan[15], Hassan Mehboob[16], Harri Junaedi[16], Himansu Sekhar Nanda[1,2,13 *], Guoping Chen[17], Subhas C Kundu[18]

Additive manufacturing (AM) is a powerful approach in healthcare to augment the functionalities of patient-specific medical products and surgical tools. One such area of the healthcare industry is surgical planning and procedures, where the benefits of AM can revolutionize the industry. AM technologies, commonly known as three-dimensional (3D) printing, can change the conventional surgical methodology from "open-detect-operate-close" mode to "detect-open-operate-close" mode. However, the use of 3D printing in surgical planning has been hampered due to the limited availability of literature reports thoroughly examining the advantages and drawbacks of this technology in clinical settings. Hence, this review explores the widespread use of additive manufacturing, multi-materials, metamaterials, 4D printing, and artificial intelligence in surgical planning for complex surgical procedures in spine, orthopedics, dentistry, cardiology, gynecology, and neurology. This review focuses on meticulously adjusting the lattice structure of metamaterial during 3D printing to achieve specific mechanical properties. It further delves into 4D printing to achieve dynamic capabilities in 3D printed models for better integration with host tissue. Furthermore, it highlights the key aspects of combining AM with Artificial Intelligence/Machine Learning (AI/ML) models in healthcare to automate 3D model production, reducing human intervention. This comprehensive review offers bioengineers, clinical scientists, and clinicians a platform to explore AM and its potential for addressing pre- and post-surgical operations challenges, providing valuable insights for biomedical engineering and healthcare advancements.

Wider Impact

The review article "Transforming Surgical Planning and Procedures through Synergistic Use of Additive Manufacturing, Advance Materials, and Artificial Intelligence: Challenges and Opportunities" represents a pioneering effort to consolidate the latest advancements in additive manufacturing technologies for personalized surgical planning and procedures. This aims to promote the use of personalized 3D anatomical models and surgical guides for real-time simulation of complex surgeries in orthopedics, dentistry, cardiology, gynecology, and neurology. Unlike the published reports focusing on limited aspects, our comprehensive review article offers a unified perspective, providing a comprehensive understanding of the role of advanced materials, processes, and additive manufacturing technologies in surgical planning and their execution. This review explores the synergistic use of additive manufacturing, multi-materials, metamaterials, 4D printing, and artificial intelligence to address the challenges in conventional surgical models. The discussion also includes dynamic and patient-specific 3D models to replicate anatomical and intricate biological properties of tissues and organs, offering potential solutions to global health problems. These transformative approaches in additive manufacturing for surgical planning ensure safer and more efficient diagnoses and treatments for both pre-and post-surgical challenges, paving the way for a promising future in healthcare.

1. Introduction

The current additive manufacturing (AM) market is about $13 billion and is expected to reach $70 billion by 2030. [1] AM, often known as three-dimensional (3D) printing, is a revolutionary technology that has found its broad use in the healthcare industry.[2] The advantage AM offers over conventional manufacturing techniques is its extensive customization for medical applications based on patient-specific data.[3] Due to this, AM is being explored for several activities in the healthcare industry, such as medical device prototyping, surgical planning, monitoring, and outcome analysis.

One of the procedures in hospitals is surgical planning, which is traditionally carried out through 3D computer visualization. The visualization quality depends on the volume rendering of stacks of two-dimensional (2D) image scans.[4] Compared to CT scans, radiologists often prefer MRI for soft tissue imaging due to its high-resolution tissue characterization and absence of ionizing radiation exposure.[5] Nevertheless, CT is still being used for challenging tissue imaging. Advanced imaging techniques gather multi-parametric and multidimensional data, allowing for high-resolution imaging that realistically reconstructs anatomy and characterizes the tissues.[6] However, such image models are still in virtual platforms with no physical feel of the actual tissue or organ. The lack of haptic feedback in 3D virtual models hinders learning and eventually affects surgical outcomes. By enabling physical interaction such as touching, rotating, and examining anatomical structures, 3D printed models effectively overcome the lack of tactile feedback found in virtual simulations.[7] To support realistic surgical training, the materials used for these models must provide accurate force feedback, allowing trainees to sense and respond to different pressure levels. [8] Additionally, these materials must endure sterilization processes to maintain hygiene and structural integrity during repeated use, helping to minimize infection risk. Several polymers, including polylactic acid[9], polymethyl methacrylate, polyethylene terephthalate, polyamides, and thermoplastic polyurethane, fulfill these requirements. Anatomical models created through 3D printing have proven especially valuable for simulating complex structures and procedures. [10][11] For example, Kiraly et al.[12] created 3D-printed prototypes of malformed hearts to explore complex spatial relationships at the aortic arch and simulate the operative procedure for congenital heart disease (CHD). Intraoperative assessment confirmed the anatomical precision of the 3D models. In another study by Kiraly et al.[13], rigid "blood volume" and flexible "hollow" heart models were used for the preoperative planning of CHD. The results showed that 3D models refined diagnostics in 13 out of 15 cases and provided new anatomical information in 9 out of 15 cases. The prototypes significantly improved or altered the surgical approach and intracardiac repair in 13 cases, with no operative morbidity or mortality. Extending this precision to renal surgery, researchers leveraged 3D-printed kidney models to simulate surgical scenarios accurately.[14] Wake et al.[15] used 3D-printed models for patient education in renal and prostate cancer. Patients completed a 5-point Likert scale survey twice on disease and surgical procedure understanding. The Likert scale uses a numerical scale, where one means strongly disagree, two means disagree, three means neutral, four means agree, and five means strongly agree. Initially, the investigators used imaging alone, then repeated the survey after reviewing imaging and a 3D model. The result of the questionnaire given to the patient suggested that the 3D model was beneficial for the patients to understand the cancer size (4.60 ± 0.54, $p < 0.001$), cancer location (4.75 ± 0.50, $p < 0.001$), and treatment plan (4.69 ± 0.57, $p = 0.013$).

Apart from 3D-printed surgical models, AM enables the creation of patient-specific surgical guides, enhancing precision and efficiency in complex bone surgeries and improving patient outcomes. Schweizer et al.[16] investigated the benefits of using patient-specific guides for treating scaphoid non-unions compared to freehand techniques. Postoperative results showed that 3D-printed guides improved reconstruction accuracy, reducing misalignment to 7° compared to 26° with freehand surgery. This enhanced accuracy effectively addressed scaphoid non-union, a common complication in scaphoid fracture treatment. Practicing on patient-specific prototypes can save time in surgery. 3D-printed models and surgical guides reduced surgery time by 12-62 minutes and lowered treatment costs to $3720/case compared to multiple CT scans/MRI images.[17] 3D-printed models are helpful for pre-operative planning and diagnosing complex structural defects, such as atrial septal defect (ASD) and

[1]*Biomaterials and Biomanufacturing Laboratory, Department of Mechanical Engineering, PDPM Indian Institute of Information Technology Design and Manufacturing, Jabalpur, Madhya Pradesh 482005, India.*
[2]*International Centre for Sustainable and Net Zero Technologies, PDPM-Indian Institute of Information Technology Design and Manufacturing Jabalpur, Madhya Pradesh 482005, India.*
[3]*Fused Filament Fabrication Lab, PDPM-Indian Institute of Information Technology, Design and Manufacturing Jabalpur, Madhya Pradesh 482005, India.*
[4]*Institute for Medical Engineering and Science, Massachusetts Institute of Technology, Cambridge, Massachusetts 02142, United States of America.*
[5]*School of Minerals, Metallurgical and Materials Engineering, Indian Institute of Technology Bhubaneswar, Argul, Khordha, Odisha 752050, India.*
[6]*Iota Design & Innovations Lab Private Limited, 111, FTBI, NIT Rourkela, Rourkela, Odisha 769008, India*
[7]*Biodesign and Medical Device Laboratory, Department of Biotechnology and Medical Engineering, National Institute of Technology, Rourkela, Odisha 769008, India.*
[8]*Dr B R Ambedkar National Institute of Technology Jalandhar, GT Road Bypass, Jalandhar, Punjab 144011, India.*
[9]*Department of Mechanical Engineering, Indian Institute of Technology Guwahati, Assam, 781039, India.*
[10]*Biomedical Engineering, Materials Science & Engineering, University of Connecticut, 260 Glenbrook Road, Unit 3247 Storrs, CT, 06269, United States of America.*
[11]*Department of Chemical Engineering, University of Massachusetts Lowell, Lowell, MA 01854-2827, United States of America.*
[12]*Laboratory for Sustainable and Additive Manufacturing, Manufacturing Systems Engineering, California State University, Northridge, CA 91324, United States of America.*
[13]*Terasaki Institute for Biomedical Innovation, 21100 Erwin St Los Angeles, CA 91367, United States of America.*
[14]*Department of Mechanical and Aerospace Engineering, UCLA Samueli School of Engineering, University of California Los Angeles, Los Angeles, CA 90095-1597, United States of America.*
[15]*Department of Engineering Design, Indian Institute of Technology Madras, Chennai, Tamil Nadu 600036, India.*
[16]*Department of Engineering and Management, College of Engineering, Prince Sultan University, Riyadh 12435, Saudi Arabia*
[17]*Research Center for Macromolecules and Biomaterials, National Institute for Materials Science, 1-1 Namiki, Tsukuba Ibaraki 305-0044, Japan.*
[18]*3Bs Research Group, I3Bs - Research Institute on Biomaterials, Biodegradability and Biomimetics, University of Minho, Headquarters of the European Institute of Excellence on Tissue Engineering and Regenerative Medicine, AvePark, Barco 4805-694, Guimaraes, Portugal.*
**Corresponding author's e-mail:*
***kumarprasoon@nitrkl.ac.in (P. Kumar) and *himansu@iiitdmj.ac.in (H. S. Nanda)*

ventricular septal defect (VSD), in conditions such as CHD.[18] These models provide a comprehensive view of anatomy, aiding in the accurate diagnosis of these challenging conditions compared to 2D images.[19] Liang et al.[20] evaluated the effectiveness of 3D-printed models for diagnosing CHD. The models improved diagnostic accuracy to 97% from 81.25% with CT scans and echocardiography. This progress helps physicians to identify complex diseases and overcome barriers associated with complex anatomical structures. Overall, 3D-printed models simulate complex surgeries in real-time, improving visualization and tissue mimicry, allowing precise bone osteotomies and fixation without affecting neighbouring tissues.[21]

However, there are notable research gaps in using 3D-printed surgical models for preoperative planning. The first challenge occurs during the data preparation stage when medical images are processed for 3D printing. [22] This involves segmenting medical imaging data, such as CT or MRI scans, to isolate the region of interest. The process of manual contouring, which is commonly used, is highly laborious, cumbersome, and time-consuming. This challenge is especially pronounced when working with soft tissues, as they often appear with low contrast in imaging. [23] As a result, accurately distinguishing soft tissues from surrounding structures becomes difficult, leading to segmentation errors and significant variability in the resulting anatomical models. The second challenge concerns the material limitations of current 3D-printed models. Most of the existing models effectively replicate hard tissues such as bone but are inadequate for mimicking soft tissues. [24] There is an apparent mismatch between the mechanical properties of the printed models and those of actual soft tissues. This discrepancy reduces the realism and effectiveness of the models during surgical simulation and planning, especially for procedures involving delicate or deformable tissues. The third challenge concerns the static nature of current 3D-printed surgical implants. [25] Once fabricated, these implants maintain fixed physical and mechanical characteristics. [26] They cannot dynamically respond or adapt to changes in the biological environment, such as variations in pressure, temperature, or biochemical signals. This lack of adaptability limits their functionality in complex or evolving surgical contexts where interaction with surrounding tissues is critical. [27][28] Additionally, the absence of real-time predictive insights limits the effectiveness of existing patient specific 3D-printed models for supporting immediate surgical decision-making. Therefore, this review is unique in its combined focus on several key advancements to overcome limitations in 3D-printed surgical models.

The current review discusses how artificial intelligence (AI), particularly generative AI, can improve medical image processing and segmentation. It also examines the use of metamaterials and multi-materials to replicate soft tissue better and mimic the mechanical behavior of surgical models. The relationship between a structure and the properties of a polymer is crucial for surgical models, affecting their mechanical properties and printability [29]. Meticulous control of these properties allows for customization, closely mimicking specific tissues for a lifelike training experience.[30,31] Due to the composite nature of the tissue, multi-materials with anisotropic properties are desirable for mimicking 3D tissue constructs. The 3D printing of multi-material and metamaterials enhances tissue characteristics for more realistic haptic feedback in surgical simulations. [8] [32][33] The review also highlights the role of 4D printing in transforming static implants into dynamic systems capable of responding to physiological changes within the body. [34][35] Additionally, to address the lack of real-time predictive insights during surgery, the review also explores the potential of digital twin technology of AI to support more accurate and immediate decision-making. The review presents various additive manufacturing (AM) techniques used for fabricating surgical models and emphasizes the dimensional accuracy and value of patient-specific 3D printed models in medical education. It then provides a detailed evaluation of these models in clinical areas such as orthopedics, dentistry, gynecology, cardiology, and neurology, highlighting existing limitations in replicating soft tissues. The discussion continues with key challenges in using AM for surgical planning that require further attention. This is followed by multidisciplinary strategies to enhance surgical outcomes, culminating in forward-looking insights to inspire future innovations. **Figure 1** offers a detailed overview of the current focus of available literature and how the topic covered in this review aims to address and alleviate these challenges.[36]

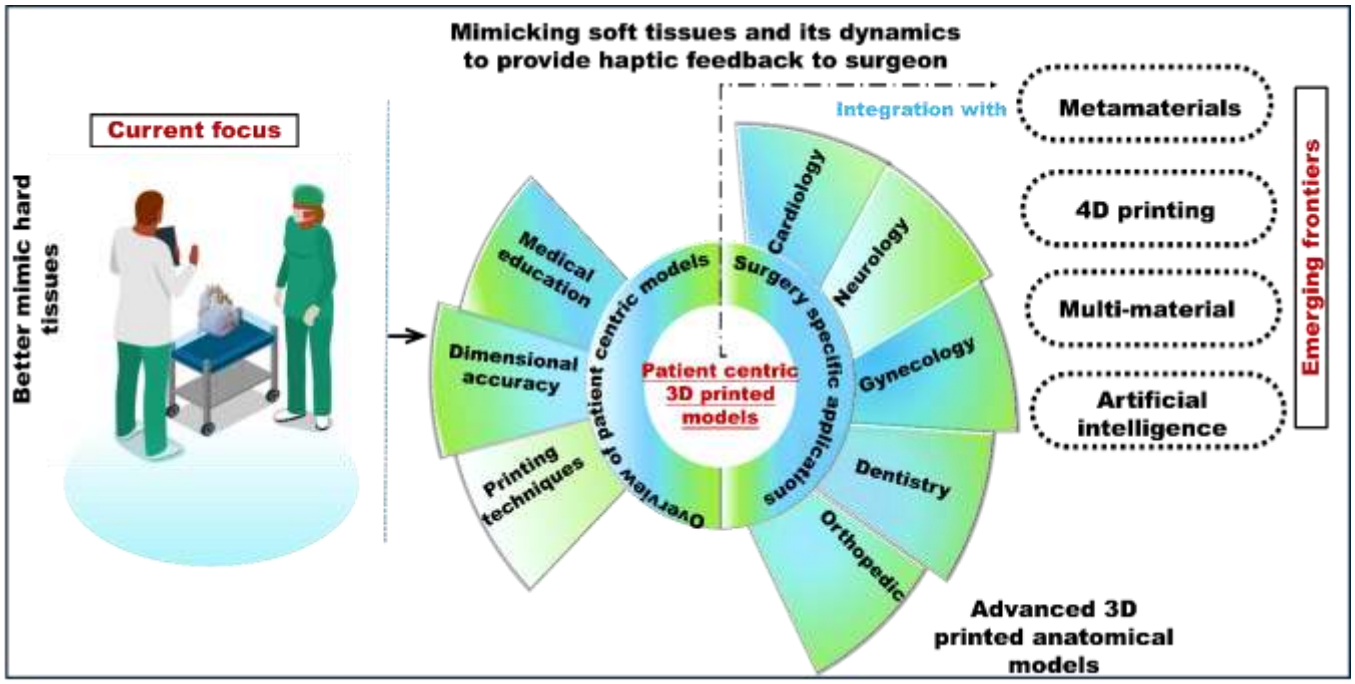

Figure 1. Schematic of the topics covered in the review for advancing patient-centric 3D printed models

2. 3D printing for preparation of patient-centric surgical models

2.1 3D printing technologies for surgical prototypes

The application of 3D printing for surgical planning generally follows four fundamental procedures: obtaining raw medical data, preprocessing, fabricating the components, and conducting post-processing. During preprocessing, the region of interest (ROI) is isolated from surrounding tissues to target a specific area. The key highlights of the standard volume rendering software are provided in **Table 1** for selecting ROI. After outlining the tissue's ROI, the 3D model is smoothed and wrapped to remove defects for a high-quality print. The smoothed model is then prepared for 3D printing. The 3D model is converted to a surface triangulation language (STL) file format, representing its surface as a mesh of triangles.[37] This mesh is then sliced into 2D layers, creating G-code for 3D printer tool paths.[38] Finally, the sliced file is used by 3D printers to produce a physical model using a specific material.[39] AM employs layer-by-layer assembly of materials by dispensing either the melt material through an extruder (fused filament) [40], binding powder material through a chemical agent (binder)[41], or changing the state of the material through a power laser (sintering/melting)[42] to print the desired 3D models. The American Society for Testing and Materials (ASTM) classifies AM technologies based on the underlying fabrication method. The major AM technologies are discussed below based on their practical relevance to surgical planning.

Table 1. Standard volume rendering software employed in image processing and 3D model reconstruction.

Volume Rendering software	**3D Slicer** [43]	**Invesalius** [44]	**Osirix** [45]	**Mimics** [46]
Image data Supported	DICOM, NRRD, VTK, Analyze, Nifti	DICOM, Analyze, Nifty, jpg, png	DICOM, JPEG MPEG	DICOM, BMP, jpg
Language	C++, Python	Python, C++	Objective C	C++, Java, Python
Algorithm	Interpolation	-	-	Matching cubes

Resolution (pixels)	1280×1024	1024×768	1800×1800	1920×1080
Advantages	Simple user interface, open software	Operating system compatibility	Automatic surface and volume rendering produce high-quality models	User-friendly, able to map surfaces of the model
Disadvantages	High-quality products cannot be obtained	User interface issues	Lacks Material inclusion option, does not allow measurements in 3D	Challenging to measure precisely, time-consuming process to create 3D models
Approval status for clinical applications	Not approved	Not approved	Approved	Approved

2.1.1 Material jetting

Material jetting (MJ) technology is gaining popularity in various sectors, such as biomedicine, dentistry, manufacturing, and aviation, due to its capability to produce highly accurate and smooth products.[47] MJ utilizes a variety of polymers, including photopolymer resins, thermosets, and elastomers, each with distinct mechanical properties.[48] PolyJet is a prominent droplet-based MJ 3D printing method that uses a 200 DPI nozzle to deposit layers.[49] The process involves jetting and precisely placing photopolymer droplets, which are then rapidly cured and solidified to form the intended 3D structure.[50] PolyJet technology employs multiple heads to spray acrylic-based photopolymer droplets with high precision, achieving a resolution of approximately 16 microns, comparable to some laser-based systems.[51] This technology is ideal for prototyping and model-making applications, offering exceptional precision and versatility.[52] Polyjet technology was employed by Zein et al.[53] to fabricate 3D-printed livers for developing and studying liver transplants. This approach aimed to depict the spatial relationships between vascular and biliary anatomical structures, thereby facilitating surgery and minimizing intraoperative complications. PolyJet technology can also create anatomical replicas of sinus passages, helping doctors improve patients understanding of their condition and treatments. Sander et al.[54] used polyjet technology to fabricate human nasal sinus models to explain the diseased state to the patients. The findings validated that using 3D-printed nasal models effectively alleviates surgical procedure-related anxiety in 97.5% of the patients. Despite having several benefits, it is essential to note that printing materials are currently confined to photopolymers, limiting the range of options available for polyjet printing. Moreover, the high costs associated with jet printers make this technology more suitable for only large-scale production scenarios.[55,56]

2.1.2 Powder bed fusion

The powder bed fusion (PBF) process is gaining popularity in research communities due to its high-quality results and affordability.[57] The PBF technique can produce 3D components using various materials, including plastics, glass, metals, and alloys.[34] The PBF method maximizes resource efficiency by reusing powder, enabling the creation of more components.[58] Particle sintering, de-powdering, and post-processing are critical in powder-based 3D printing.[59] The polymer powder undergoes partial melting, retaining its solid core. Densification occurs through reorganizing solid-phase particles and bonding the liquid phase, resulting in a solidified 3D structure with higher density. Solid-phase particles directly contribute to the higher density of the printed model.[60] PBF utilizes various heat sources for powder melting, including thermal, electric, and laser.[61,62] Laser fusion is divided into selective laser melting (SLM) for metals[63] and selective laser sintering (SLS) for plastics.[64]

Among powder-based 3D printing techniques, SLS stands out for its ability to produce complex, intricate components without requiring support structures, allowing for the creation of internal structures, undercuts, and thin walls(**Figure 2a**).[65] A significant benefit of SLS for biomedical applications is its compatibility, as it does not involve using organic solvents.[66] Furthermore, it can process nearly any powdered material, including photo polymers, glass-reinforced polymers, metals, and metal/polymer composites.[67] Polyamide 12 (PA12) is frequently used in SLS due to its biocompatibility, making up the majority of SLS powders.[68] For example, Pacurar et al.[69] used PA12 to fabricate personalized medical implants via the SLS technique. The study evaluated the surface roughness of the PA 12 hip implant. The surface of the PA 12 particles was cleaner, potentially resulting in improved surface quality of the hip implants. Furthermore, PBF techniques can employ various hydrogels for soft tissue applications, leveraging their biomimetic properties, customization potential, and biocompatibility. Apart from native tissue mimicry, the SLS-printed models are lightweight; for example, prosthetic sockets printed through SLS were 17% lighter than the traditionally manufactured ones.[70] Beyond direct fabrication, SLS also contributes indirectly to soft tissue engineering by enabling the creation of precise molds. This becomes particularly valuable when working with soft materials like PVA or PHY hydrogels and agarose, which present challenges in direct large-scale printing due to poor printability and structural consistency. Otero et al. [71] combined SLS with FDM to create a two-part mold to address this issue. The inner

mold parts, representing features such as veins, tumors, and the biliary tract, were printed using PA12 with an SLS printer selected for its ability to produce rigid components with a layer thickness of 0.08 to 0.1 mm. The outer mold was printed using PLA filament with an FFF printer, which provides a dimensional accuracy of ±0.2 mm and a layer thickness of 25 micrometers. This combination allowed for the accurate casting of soft tissue models of the brain and liver using various hydrogels, and their mechanical properties were assessed using dynamic mechanical analysis, the Shore durometer scale, and the Warner-Bratzler shear test. Postoperative results showed a less than 1 %-dimensional error between the actual liver and the 3D model, with a fabrication cost of $387.55.

The study identified 1% agarose as the best material to mimic liver tissue, while 4% GelMA combined with 1% agarose best-mimicked brain tissue (**Figure 2b and 2c)**. Despite these advantages, SLS also possesses limitations, including inadequate texture and inferior material characteristics.[72] As a result, the manufactured components using SLS do not meet the native microstructural and mechanical behavior of native tissues.[73] Post-processing treatments like heat treatment, de-powdering, cleaning, spraying, and coating strategies mitigate these shortcomings, but they are insufficient for many biomedical applications.[74]

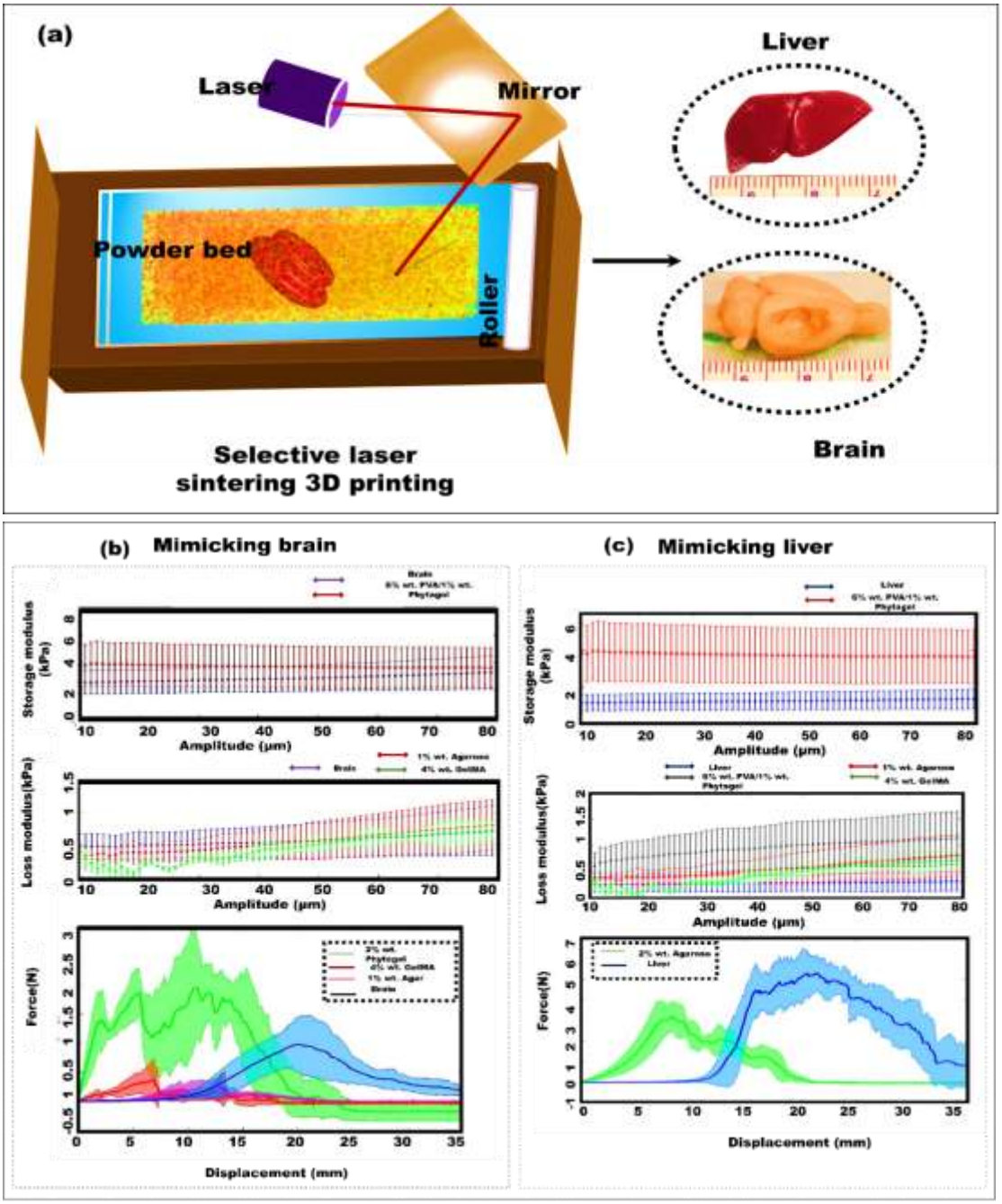

Figure 2. (a) Schematic representation of SLS technology of 3D printing; Figure reproduced from Wong et al.[65] (b) Different hydrogel materials like agarose and GelMA composites mimicking the brain and (c) Different hydrogel materials like agarose and GelMA composites mimicking the liver; Figure reproduced from Otero et al.[75]

2.1.3 Material extrusion

Material extrusion is the most popular AM method due to its compact size and user-friendliness.[76] It allows rapid production through instant part fabrication.[77,78] Fused Filament Fabrication (FFF), also known as Fused deposition modeling (FDM), relies on the material extrusion-based method has gained much interest for its simplicity and cost-effectiveness.[55,79] The biocompatibility, biodegradability, and low melting temperatures of PLA and PCL make them ideal for FDM 3D printing, creating prosthetic parts that can interact with living tissues without causing adverse reactions.[80] However, users can also select from various materials for FDM, including acrylonitrile butadiene styrene (ABS), nylon, and Polyvinyl alcohol (PVA).[81] Muta et al.[82] used a chairside FDM 3D printer to create temporary dental crown covers from PVA, comparing the accuracy of digital and conventional prosthetic methods. The 3D digital superimposition analysis revealed significantly higher root means square values for the PVA/original typodont model (310 ± 50 µm) compared to the conventional/original typodont model (120 ± 40 µm) ($p < 0.05$). Chairside FDM printers (**Figure 3**) offer a cost advantage, with in-house 3D printed prostheses costing an average of $8.34, compared to $350 to $925 for prostheses made by off-site dental laboratories. Apart from dental models, FDM-printed models effectively mimic the craniofacial skeleton for maxillofacial surgeries.[83] Consumer-grade FDM processes show similar accuracy to industrial SLS printers, with minor deviations from the virtual design.[84] Naghiegh et al.[85] used the FDM to fabricate a 3D model of a patient-specific skull for the preoperative planning of maxillofacial reconstruction. The study demonstrated that the difference between the virtual models in the software and the 3D-printed skull models was 1.4%.

Despite having various advantages of FDM, the high temperatures used for heating the material during extrusion may alter the chemical composition of biomaterials, making it unfit for low-temperature biomaterials such as hydrogels and, in some cases, high temperature leads to warpage in the 3D printed parts.[86] Direct Ink Writing (DIW) technology, on the other hand, operates in a heat-free environment, addressing these high-temperature concerns.[87] DIW handles various materials, including tungsten carbide-cobalt**,** metal-infused PLA, porous metals, carbon-based nanomaterials, polymers, and ceramics.[88] The DIW technique has become a viable method for modifying crucial structural elements of biomedical implants. Kalaba et al.[89] reviewed that small spaces between mesh fibers (< 1 mm) in polymeric mesh architectures may create inadequate tissue integration, promote inflammation, and accelerate bridging fibrosis. With DIW, all the necessary geometrical details, including mesh shape, dimensions, infill density, and opening size, can be customized to meet specific requirements. Ajdari et al. [90] used the DIW technique to fabricate mesh implants from chitosan and nanocellulose. The mesh openings of 53 ± 1.2% on the fabricated meshes helped to integrate the mesh with the neighbouring tissue. Xu et al.[91] utilized the DIW technique to fabricate biodegradable metal iron (Fe) scaffolds with fine pore sizes ranging from 50 µm to 300 µm and complex bone implant models. DIW precisely controls filament deposition to create high-quality pores, avoiding blockages, which is advantageous for fabricating metallic bone implants with interconnected pores. Despite having various advantages, material extrusion technologies face limitations in printing complex parts with overhangs, such as the left ventricular cavity, lacking intrinsic support.[92] While support structures can solve this, they lead to material waste and affect the surface finish, especially for functional surgical tools.[93]

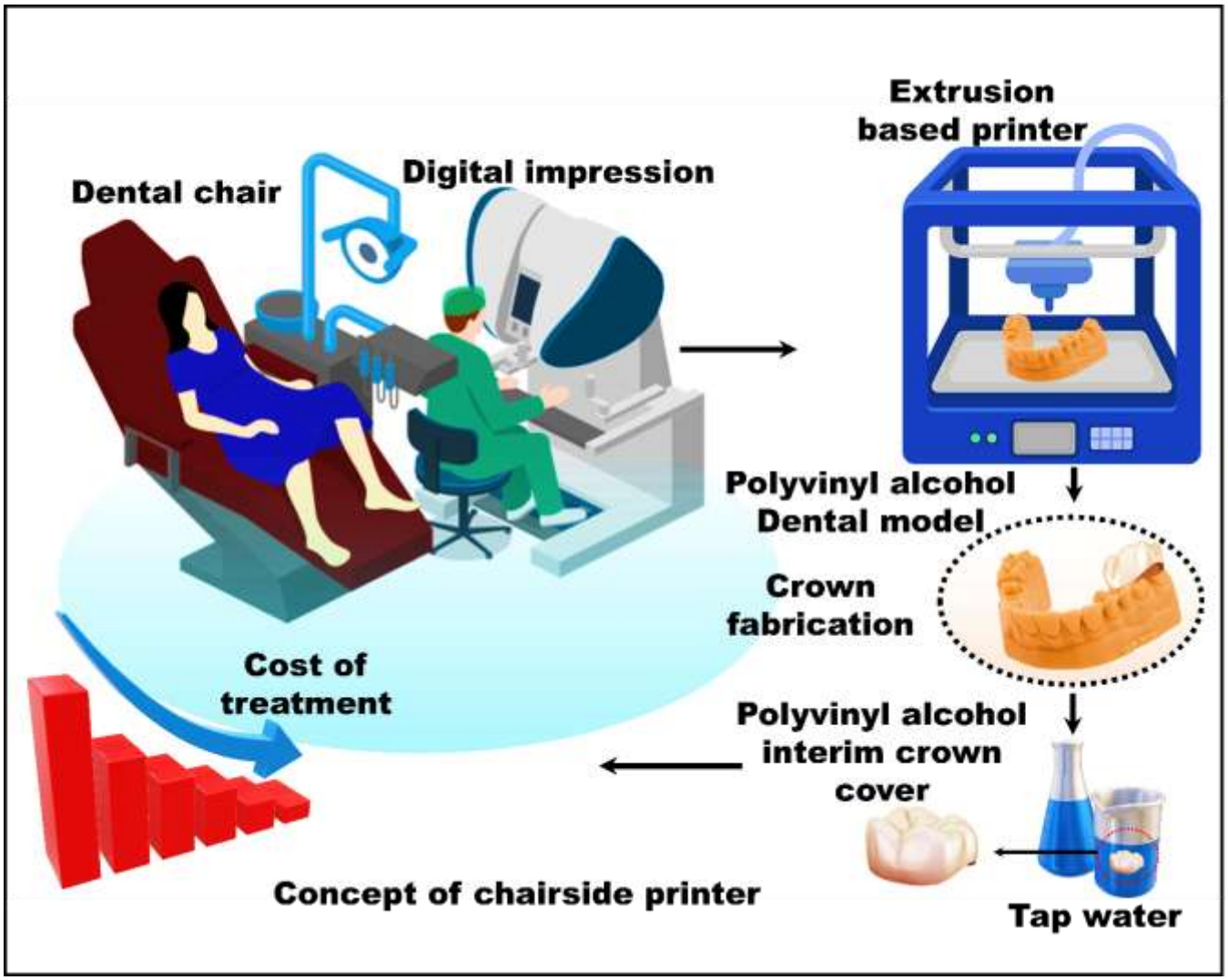

Figure 3. Concept of chair-side FDM printer technology for fabricating dental interim cover crown; Figure reproduced from Muta et al. [82]

2.1.4 Vat polymerization

Vat polymerization is a widely adopted AM technique known for its exceptional resolution and smooth surface finish.[94] It utilizes 3D photopolymerization, where a liquid resin solidifies layer-by-layer under specific light wavelengths to construct the object.[95] Selecting biomaterials for light-based 3D printing in surgical planning involves ensuring biodegradability, biocompatibility, and the inclusion of photoreactive moieties (like methacrylate acrylate or thiol-ene groups) for rapid solidification.[96,97] Common choices for these materials include natural options like gelatin methacrylate and collagen and synthetic choices like polyethylene glycol and PLA. Some of the vat polymerization technologies are digital light processing (DLP),[98] Digital light synthesis (DLS)[99], and stereolithography (SLA).[100] SLA is a resin-based technology that uses ultraviolet light to cure liquid resin into a solid through photopolymerization.[101] It is well known for producing intricate structures with exceptional feature resolution (as low as 25 µm) and surface smoothness (1.41 µm to 2.28 µm), making it ideal for surgical applications.[102] For example, Haider et al.[103] used an SLA printer to fabricate cutting guides for the surgical planning of maxillofacial reconstruction. The study revealed that the virtual preoperative planning and custom-fabricated cutting guides for maxillofacial reconstruction enhanced the bony reconstruction accuracy and overall operational efficiency. Within the domain of maxillofacial reconstruction, orbital floor fractures are the biggest challenge for clinicians due to misalignment of the orbit, which is caused by a discrepancy between the implant's geometries and the patient's anatomical structure at the affected site.[104] The orbital floor is a lower part of the eye socket, which protects the human eye from injuries.[105] Guillaume et al.[106] used the SLA technique to create a flexible, patient-specific implant from poly(trimethylene carbonate) with 40 wt.% hydroxyapatite (Osteo-PTMC) for orbital floor treatment and compared it with standard titanium meshes. The results showed that implanted titanium meshes led to fibrous tissue encapsulation. In contrast, Osteo-PMTC promoted rapid neovascularization and bone morphogenesis ectopically and in the orbital floor region without the need for additional biotherapeutics like bone morphogenic proteins. The complete workflow of the fabrication of Osteo-PTMC and titanium implants used in the surgery, along with the post-follow-up results, are shown in **Figure 4**.

DLP is another vat polymerization AM technique, which operates a digital projector for curing photo resin; however, printing the soft polymer on DLP printers is cumbersome due to the layer-by-layer printing method. In contrast, DLS technology is a more advanced vat polymerization process that constructs the entire 3D object in a single exposure, substantially decreasing the printing time. The printed components are outlined by light from a projector or digital micromirror device, which then solidifies them through selective exposure into the desired shape. The efficient curing process in DLS printers produces high-resolution pixels of about 75 μm, resulting in 3D-printed parts with enhanced structural integrity. This improvement allows DLS-printed parts to withstand higher strain rates. For example, Hossain et al.[107] used UV-curable DLS technology to create elastomer polyurethane (EPU). The results showed that the 3D-printed EPU40 can stretch over 600% before rupturing, indicating its exceptional stretchability. Aravena et al.[108] used the highly stretchable EPU polymers to create patient-specific stents using DLS. These stents support the patient's tracheobronchial wall. The 3D-printed EPU polymer stent effectively prevents the biofilm formation and mucus retention, an issue commonly associated with conventional stents.

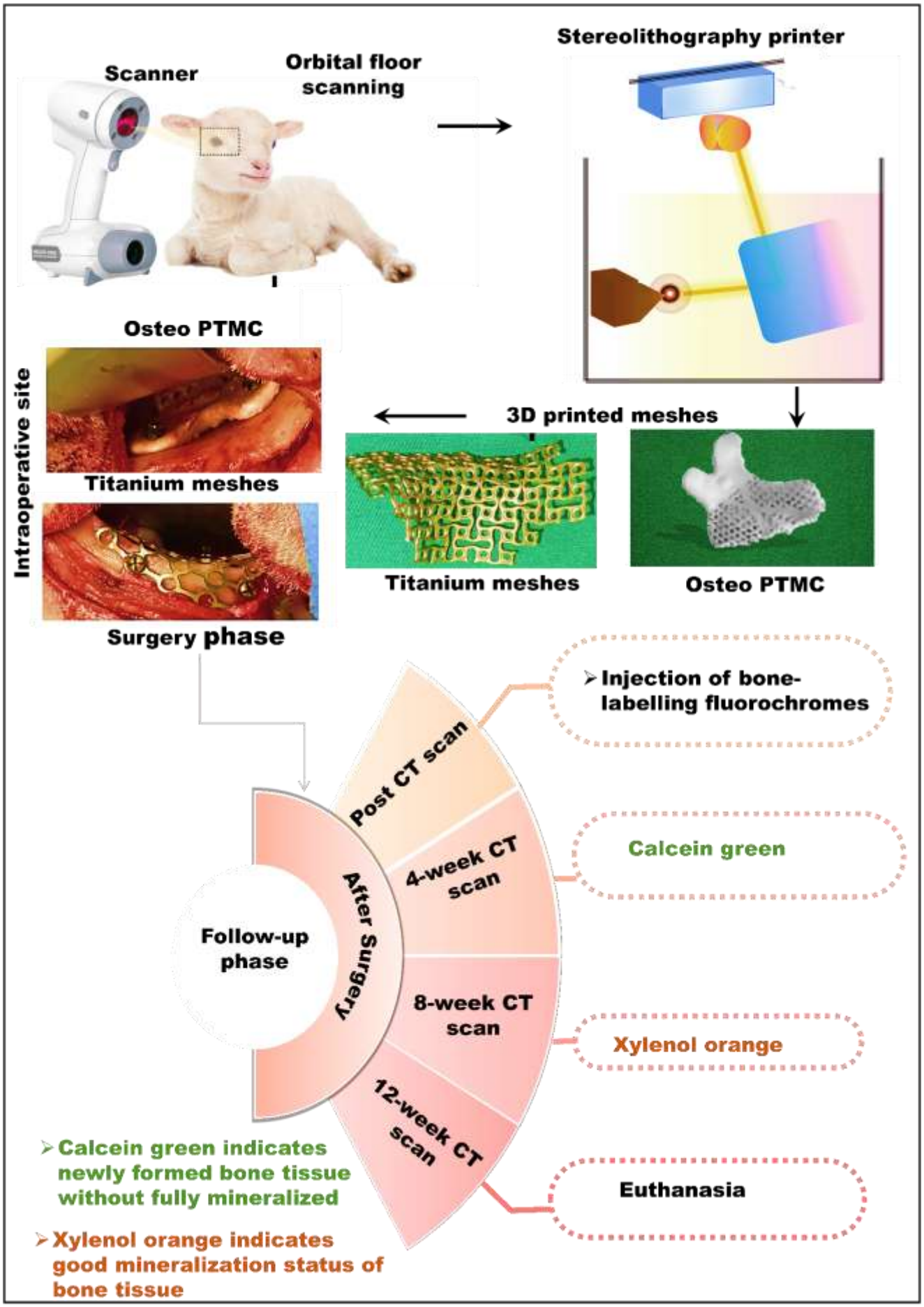

Figure 4. Workflow diagram representing the scanning of sheep orbital floor area and using SLA fabricated osteo-PTMC meshes for surgery along with the post-surgical results at four, eight, and twelve weeks; Figure reproduced from Guillaume et al.[106] with permission from Elsevier, copyright (2020)

2.1.5 Binder jetting 3D printing

Binder jetting is an AM method that selectively bonds a thin layer of powder (≤100 µm) using a binder to form the desired shape.[109] The resulting parts need further processing, such as sintering or infiltration, to improve their mechanical properties for final use.[110] Binder and powder properties significantly influence the geometry and strength of the parts.[41,111] The powders investigated for binder jetting include iron, ferrous alloys, nickel, nickel alloys, titanium, its alloys, and ceramics.[111] Binder jetting technology offers many advantages, such as its compatibility with various powders and operation in ambient conditions. It reduces the need for sealed chambers and minimizes residual stresses, thereby increasing mechanical properties.[112,113] Khademitab et al. [114] studied the mechanical properties of cobalt-chromium-molybdenum (Co-Cr-Mo) alloy parts printed using binder jetting. These parts, intended for hip joints, dentures, and small-scale knee joints, exhibited higher hardness, yield strength, and ultimate tensile strength than Co-Cr-Mo alloy parts made by casting process. However, the risk of defects arising from specific steps in the binder jetting process is a notable disadvantage.[115] These defects can manifest as pores in the prototypes, compromising their thermal conductivity, transmittance, and mechanical properties.[116] Accurate and precise printed parts are essential for effective surgical planning models.[117] However, these defects in the binder jetting process can cause minor deviations in geometry, surface finish, and material properties, compromising overall performance and reliability for surgical planning.

2.1.6 Directed energy deposition

In Direct Energy Deposition (DED), materials like powder or wire are melted by an energy source (laser, electron, or electric arc) and deposited from various angles onto existing surfaces using four- or five-axis machines.[118] DED 3D printing can deposit high-performance materials like shape memory alloys, ceramics, composites, metal alloys, high-entropy alloys, and functionally graded materials.[119] These materials find applications in various surgeries, including cranial and maxillofacial implants, spinal treatments, and limb and dental implants [120]. For example, Yan et al.[121] the DED-based electron beam melting (EBM) technique was used to create a biocompatible Ti-6Al-4V titanium alloy mesh for mandibular prostheses, showing good biocompatibility. Nguyen et al.[122] also utilized EBM to produce Ti6Al4V hip stems, revealing lower fatigue limits than traditionally machined surfaces. Additionally, Hollander et al. [123] employed DED to manufacture Ti-6Al-4V alloy vertebral bodies, demonstrating osteoblast proliferation on meshes with 500, 700, and 1000 µm pore sizes. Despite its advantages, challenges in DED technology must be addressed for medical applications. Issues like powder scalability due to varying blown powder content and metallurgical compatibility need attention.[124,125] The fast cooling rates of DED can lead to incomplete fusion and microstructural inconsistencies, affecting the mechanical properties of 3D-printed parts and potentially compromising surgical instrument and implant performance.[126] In addition to the abovementioned techniques, sheet metal lamination is another type of AM that creates 3D objects by cutting and joining sheets. However, the literature lacks sufficient reports on using sheet metal lamination for surgical applications due to the inconsistent strength of the fabricated models.

Overall, the detailed overview of all the 3D printing methods covers every aspect, from materials to capabilities to applications in surgery. Extrusion-based techniques, especially "DIW," show great potential for future personalized surgical planning due to their cost-effective and eco-friendly use of various biomaterials. While binder jetting, direct energy deposition, and sheet metal lamination are rarely used in surgical planning. Thus, detailed discussions and applications of these methods are excluded from the review to maintain focus and relevance for future readers. However, the primary 3D printing technologies adapted for medicine to develop the various 3D models and fabrication parameters, printing resolution, estimated cost, biomaterials used, advantages, limitations, and possible applications have been summarized in **Table 2**. [103,127–129]

2.1.7 Hydrogel based bioprinting

While various 3D printing techniques mentioned above have been widely explored for medical applications, bioprinting represents a specialized branch that focuses on the fabrication of functional tissues and organs by precisely arranging living cells and bioactive materials in a spatiotemporal manner.[130] To achieve structural and functional fidelity, strategies such as biomimicry, self-assembly, and modular tissue units are employed to mimic native tissue architecture. Implementing these strategies requires suitable materials. Hydrogels are ideal material (bioinks) for bioprinting because they can be printed in a 3D, hydrophilic network supporting high cell viability and exchanging nutrients and growth factors.[131] Some hydrogels also interact with cellular integrins, enhancing cell adhesion, proliferation, migration, and differentiation. Four major bioprinting techniques widely used are (i) extrusion-based, (ii) inkjet-based, (iii) laser-assisted, and (iv) stereolithography.[132] Among these, extrusion-based methods, particularly Direct Ink Writing (DIW), are widely used for printing hydrogel-based bioinks due to their versatility and material compatibility.[133] In DIW, bioinks must exhibit specific rheological properties, particularly shear-thinning behavior, for smooth extrusion and shape retention. Their flow behavior is described by the Herschel–Bulkley model: $\sigma = \sigma dyn + K\gamma^n$.[134] Here, σdyn (dynamic yield stress) ensures flow stability, while σstat (static yield stress) initiates the flow. The maximum shear rate at the nozzle wall is given by $\gamma_{max} = 4Q/\pi r^3$, indicating that smaller nozzles require optimized ink properties to manage higher shear rates. The filament error measures printability (ε): $\varepsilon = (D_{filament} - D_{nozzle})/D_{nozzle} \times 100$. Lower ε values indicate better fidelity. Inks with higher dynamic yield stress (σdyn) tend to produce filaments with diameters that more closely match the nozzle size, limiting filament expansion and improving precision. This behavior is essential for high-resolution printing, which relies on minimizing post-extrusion spreading and carefully controlling the ink's flow characteristics. Expanding the

scope of DIW, Wu et al.[135] Introduced a sacrificial-free Direct Ink Writing (SF-DIW) method for creating vascularized organ models without sacrificing sacrificial materials. This high-resolution technique allows one-step printing of complex hollow structures. Using SF-DIW, hepatic metastasis models representing different cancer types were created and integrated into the perfusion system with micropumps and agar casting to enhance physiological relevance. These models activated a prodrug that inhibited breast cancer growth, highlighting SF-DIW's utility in drug testing and disease modeling. The method is straightforward, cost-efficient, and adaptable for generating various vascularized tissues. Apart from DIW bioprinting, light-based bioprinting is also gaining attention. Moon et al.[136] demonstrated the potential of hydrogel-based bioprinting for fabricating thick, metabolically active liver tissue (>1 cm^3) using a polyethylene glycol/gelatin methacrylate (PEG/GelMA) bioink with human hepatocytes (HepG2). A gyroid-inspired structure ensured uniform perfusion and shear stress. The constructs, printed using digital light projection (DLP), maintained over 85% cell viability for 30 days under perfusion. Endothelial cells lined the vascular channels, while hepatocytes formed the viable clusters. Functional assays confirmed stable albumin and bilirubin production, mimicking key liver functions. Overall, in 3D bioprinting, functional, implantable biological structures are created based on a series of interconnected processes. First, cell sorting ensures that different cell types are precisely placed within specific scaffold regions, preserving the tissue-specific composition.[137] Following this, tissue fusion occurs as cells adhere to one another, forming continuous, cohesive tissue structures that enable communication and integration within the printed scaffold. Finally, tissue maturation involves the growth and differentiation of these cells, leading to fully functional tissues with the necessary mechanical and biological properties.

This maturation process is crucial for ensuring the printed tissues can integrate with the body and perform their intended functions after implantation.[138] However, the ongoing challenge is achieving long-term stability and seamless integration of bioprinted tissues with the body's natural extracellular matrix. Another important concern in bioprinting technology is the tendency of certain stem cells to develop into teratomas, which are tumors containing a mix of different tissue types and can pose serious health risks. Although these challenges persist, ongoing progress in biomaterials, stem cell control, and printing techniques is steadily advancing the development of safe and more effective bioprinted tissue therapies.

Table 2. 3D printing technologies are used in the development of medical 3D models.

3D printing method	Polyjet	SLS	FDM	SLA	DLS
Speed [mm hr^{-1}]	-	48[139]	50-100[140]	14[141]	125-250[142]
Resolution [mm]	0.0017[143]	0.08[139]	0.25[140]	0.05[144]	0.1[98]
Estimated Cost	$43,000[145]	$6,000	$5,000[146]	$11,000[144]	$20,000[147]
Material	Photopolymer[148]	Powdered materials like ceramic powder, metal powder, polymer powder, others. [72]	Thermoplastic polymers such as PLA, ABS, PC) polyether ether ketone (PEEK), etc. [149]	Photosensitive resin, including methacrylate polycaprolactone, etc[150]	Polyurethanes, silicone, cyanate ester, epoxy, and EPU 40[151]
Advantage	Extremely high resolution; Can print with multiple colors on one single print[152]	Can print polymers or metals; Batch production; No supports needed[153]	Cheaper technology; Great layer bonding[154]	Precise and highly accurate. Can accommodate complex designs[150]	Better surface finish, high quality and consistency in products, high speed and flexibility, and

					minimum wastage of material[155]
Limitation	Low mechanical properties; Limited heat resistance; Costly maintenance of printer heads[156]	Requires high printing infrastructure; Use of fine powders can be hazardous[157]	Only thermoplastic materials[158]	Limited range of materials. Post-curing is required, but support structures can hamper surface finish. [159]	Expensive, limited selection of materials[155]
Application	Cardiac surgery, liver surgery[160]	Functional prototypes, orthopedic components, medical devices[150]	Educational templates, tools[161]	Dental models, surgical guides and splints, orthodontic devices (aligners and retainers), castable crowns, and bridges, etc[162]	COVID swabs, mouthguards, and other dental implements[142]

2.2 Dimensional accuracy of printed models for surgical planning

AM enables the creation of 3D models from clinical imaging. Yet, accuracy varies based on data acquisition, image processing, and model fabrication.[163] Each stage introduces geometric errors in the printed model. Thresholding, a commonly used segmentation technique, involves dividing a volume by including voxels with intensities exceeding a specified threshold value.[164] A voxel's threshold value corresponds to its predominant tissue type. For example, suppose a voxel comprises both high-density tissue (40%) and low-density substances (60%). In that case, it's assigned a low-density threshold value.[165] This non-uniform distribution of voxel intensities undermines the accuracy of threshold-based segmentation and ultimately leads to dimensional inaccuracies in the final 3D printed models. Similarly, slicing is also a potential source of dimensional errors for 3D-printed models. For example, if a slicing algorithm fails to design support structures properly, it can result in incorrect slice orientation. This error can lead to 3D model distortion, resulting in the sagging of the overhanging structures. 3D printing capacities such as printer calibration, ambient temperature, printing parameters, and resolution of different 3D printing technologies also play a crucial role in determining the accuracy of a 3D printed model. Msallem et al.[166] assessed the accuracy of 3D printed mandibular models created using different established and commonly used 3D printing technologies like SLS, SLA, and FDM. The deviation patterns were examined for trueness and precision. The results showed that the SLS printer achieved the highest overall trueness of 3D-printed mandibular models (RMS 0.11- 0.016 mm). In contrast, the highest overall precision is achieved by the FDM printer (RMS 0.05 - 0.005 mm). Ogden et al. [167] compared the dimensional accuracy of 3D printed models of an L1 vertebra, produced from cadaver spine CT data, with the original vertebra. The comparison details are presented in **Table 3.** The investigation showed that the overall accuracy of the dimensional measurements was good, and the coefficient of variance was less than 1%, which is acceptable to the medical surgeons. Wu et al.[168] investigated the accuracy of 3D-printed models of the acetabulum (part of the cadaveric pelvis). Acetabulum models were printed and measured using the Vernier Calipers scale. Vernier Caliper's reading showed a good correlation (P value = 0.794) between the actual acetabulum and the 3D-printed acetabulum model (**Figure 5**). The available literature revealed an excellent correlation between the reference object and the simple 3D-printed model, with accuracy varying from 97.7% to 99.1%.[169] However, some complex anatomical shapes, such as the skull, involve several steps in 3D model construction, which leads to the possibility of inaccuracies. Huotilainen et al. [170] highlighted significant inaccuracies in 3D-printed skull models caused by errors in converting DICOM data to STL/CAD data. These conversion errors amplified discrepancies, preventing precise replication of the patient's skull. Overall, there are no single reasons for the dimensional inaccuracies in the 3D-printed models.[171]

Clinicians need to be aware of these sources of errors in medical models due to dimension loss from CAD transmission, STL generation, and slicing or 3D printing capacity and resolution. Quality control is essential for resolving such errors, which involves different processes that help monitor and prevent quality issues to meet the necessary standards for process performance and product quality.[172] This quality control flow diagram consists of 18 go/no-go gates, implemented before, during, or after critical processes depending on their importance and the availability of quality control technologies (**Figure 6**).[173] Go/no-go gates ensure that product quality attributes at each stage are met before proceeding to the following process. Each quality control gate requires documentation with checklists and control diagrams to monitor quality variations at each stage. Quality control at each stage is essential to ensure dimensional accuracy, prevent errors, and achieve precise patient-specific models and implants for accurate preoperative planning in complex surgeries.[174]

Table 3. Comparison of dimensions of an original vertebra with a 3D-printed model.

Dimensions	Original Vertebra [mm]	Unfiltered model [mm]
Upper-end plate width	48.3±0.12	48.2±0.00
Spinal canal width	24.3±0.03	23.9±0.03
Upper-end depth	31.5±0.81	31.5±0.15
Lower end width	49.5±0.24	49.6±0.15
Spinal canal depth	21.1±0.13	20.5±0.17

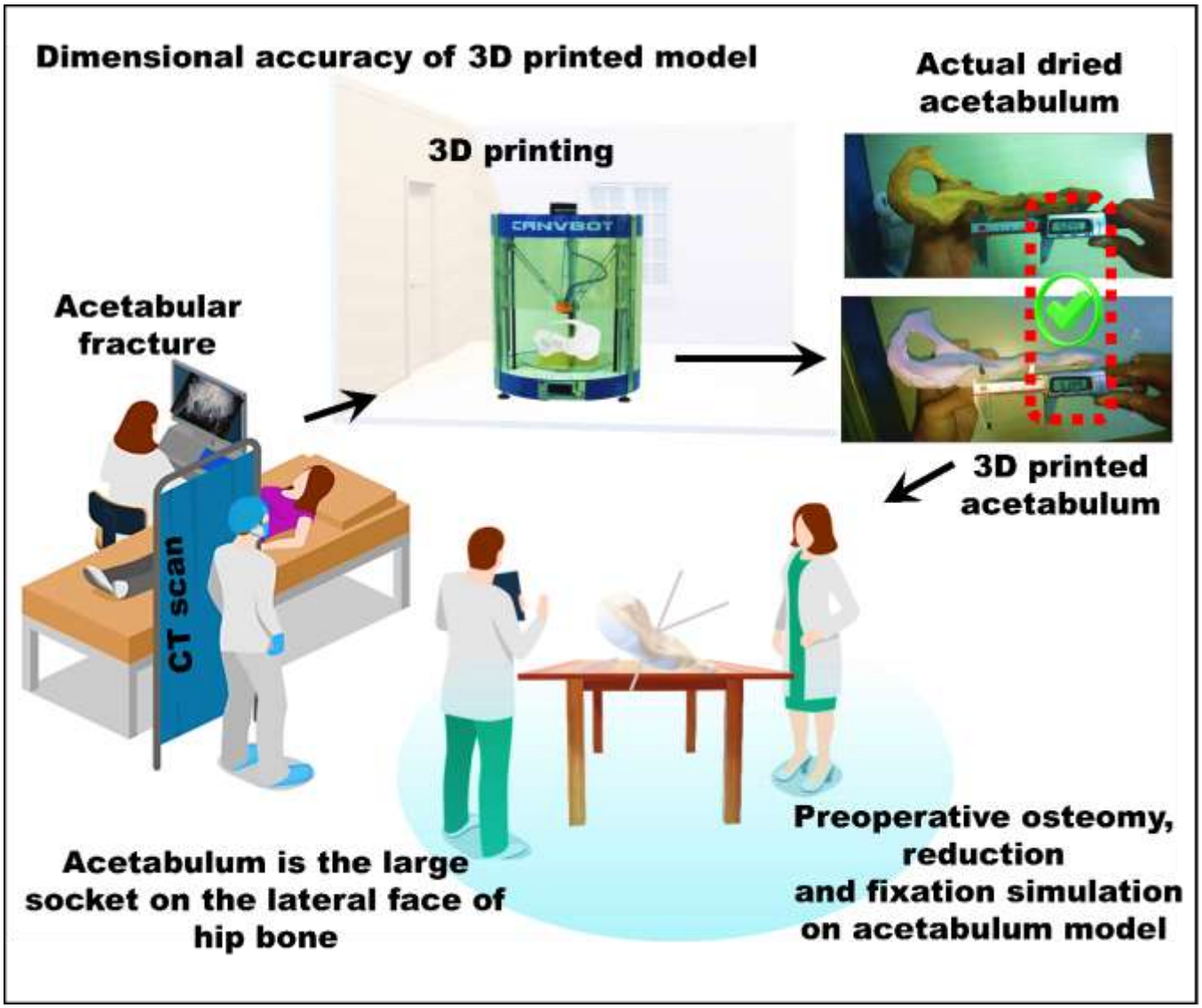

Figure 5. The comparison of an original dried acetabulum provided by the Beijing Anatomic Association and 3D printed acetabulum; Figure reproduced from Wu et al. [168]

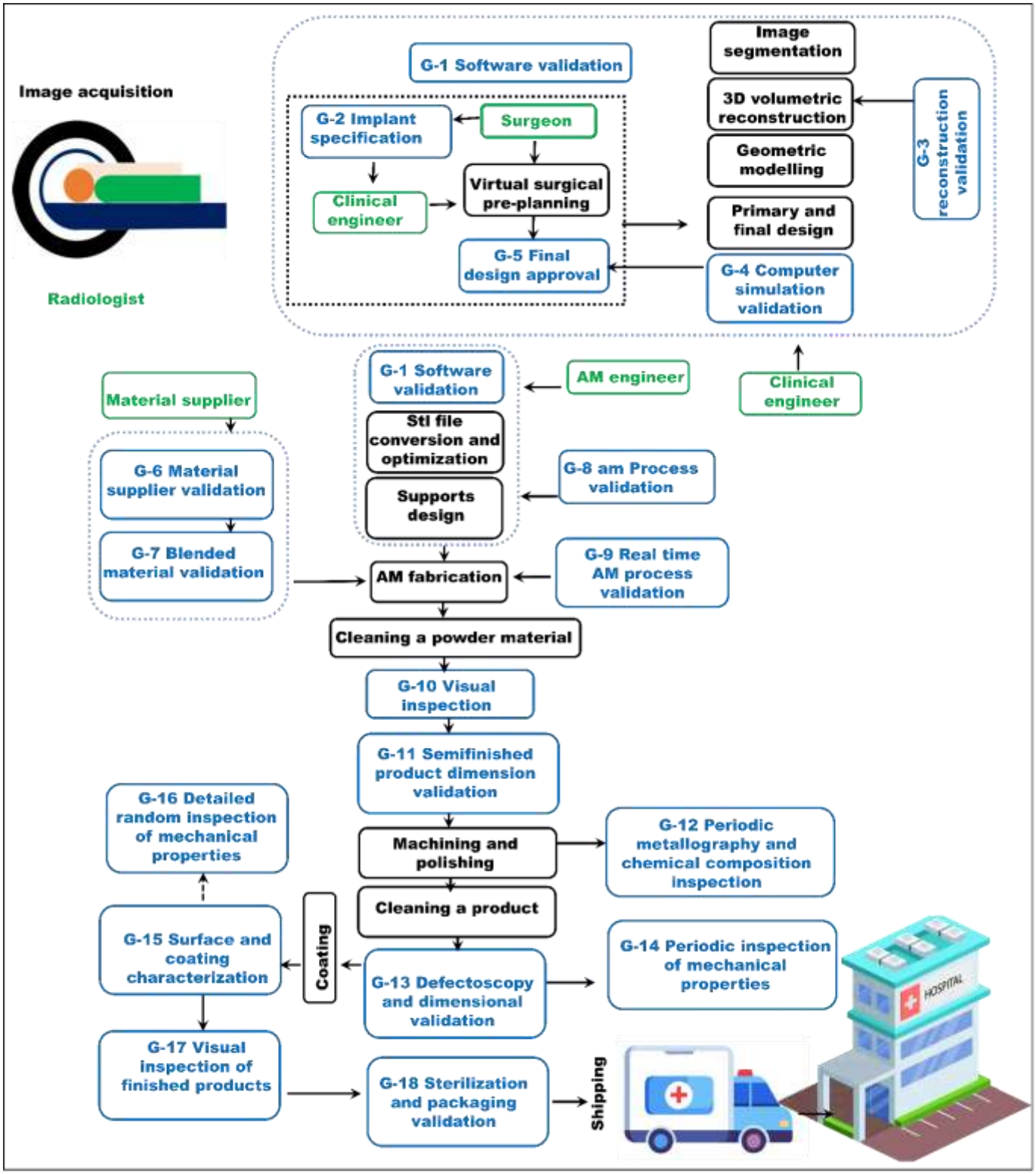

Figure 6. Integrated quality control workflow with 18 gates for designing and fabricating patient-specific implants using AM. The meanings of the operators in the chart are as follows: black solid outlined boxes = processes; black dash outlined boxes = overarching processes; blue solid

outlined boxes = quality control gates; blue dash outlined boxes = overarching quality control gates; yellow boxes = experts/staff; solid arrows = online processes; dashed arrow = off-line processes; Figure reproduced from Marquez et al.[173]

3 Revolutionizing healthcare progress through personalized 3D printed models

3.1 Medical education and patient counseling

Augmented Reality (AR) and Virtual Reality (VR) are getting significant attention for showing complete tissue or delineated portions of damaged tissue for teaching medical students human anatomy and various complex diseases.[6,175,176] Although AR/VR displays a variety of facts from image data, these technologies lack the realistic experience essential for the training and education of medical students and resident doctors.[177] To compensate for this issue of AR/VR, 3D anatomical prototypes enhance visualization and provide haptic feedback while teaching human anatomy to medical students. 3D anatomical models significantly increase the student's knowledge and understanding of human anatomy compared to conventional classroom teaching tactics and AR/VR approaches.[178] These models could effectively help identify and visualize complicated organ systems, boosting the confidence level of budding doctors and patients. Jones et al.[179] surveyed 51 participants, including 50 surgeons and 1 medical student, after creating 3D models of the breast, lung, aneurysm, and liver with tumors to evaluate their utility in surgical planning and education. The investigation showed that 74% of the participants believed 3D-printed models could help plan surgeries and teaching. Therefore, medical students and junior doctors improved their grasp of basic anatomy and pathology using anatomical models, including those depicting liver and kidney tumors (top of **Figure 7a**).[180] Likewise, Yan et al.[181] employed 3D-printed models of pelvic fractures to demonstrate the injury mechanism to medical students **(**bottom of **Figure 7a)**. The study revealed that students who had access to the 3D-printed models spent less time answering the questions related to pelvic fractures than those who did not have access to those models. Similarly, Hanisch et al.[182] employed the polyjet 3D printing technique to fabricate personalized surgical training models for dental surgeries involving root tip rejection. These models offered medical students and doctors a life-like educational platform, enabling practical training and skill development. Waran et al.[183] demonstrated the utilization of a 3D-printed head model containing a small thalamic lesion placed deep inside for surgical training in a biopsy procedure. It enabled the trainers to perform the surgical operations more precisely. Surgical simulation on the head model and root tip rejection in the dental model is shown in **Figure 7b**.

Besides educational purposes, the 3D-printed models also advocate counseling patients with complex diseases such as craniosynostosis and cardiac surgeries to avoid complexities and optimize patient outcomes.[184] Family members often notice patient abnormalities, prompting consultations for complex conditions. Therefore, the involvement of the patient and s is important in finalizing treatment plans and understanding risks, especially in high-risk surgical planning [185]. A direct approach is required to clarify the exact pathology and anticipated preoperative plan. The patients and family members can better understand the treatment plan with 3D printed anatomy models than with 2D scanned images.[186] Anwar et al.[187] used 3D heart models to counsel patients and caregivers for CHD. The 11 caregivers involved in the survey between 2014 and 2017 gave 5 out of 5 scores to 3D models for generating a clear understanding of CHD. Hence, accurate simulation of diseased tissue by 3D-printed surgical models is beneficial for training surgeons and counseling patients, thereby reducing surgery-related anxiety for patients and their families.

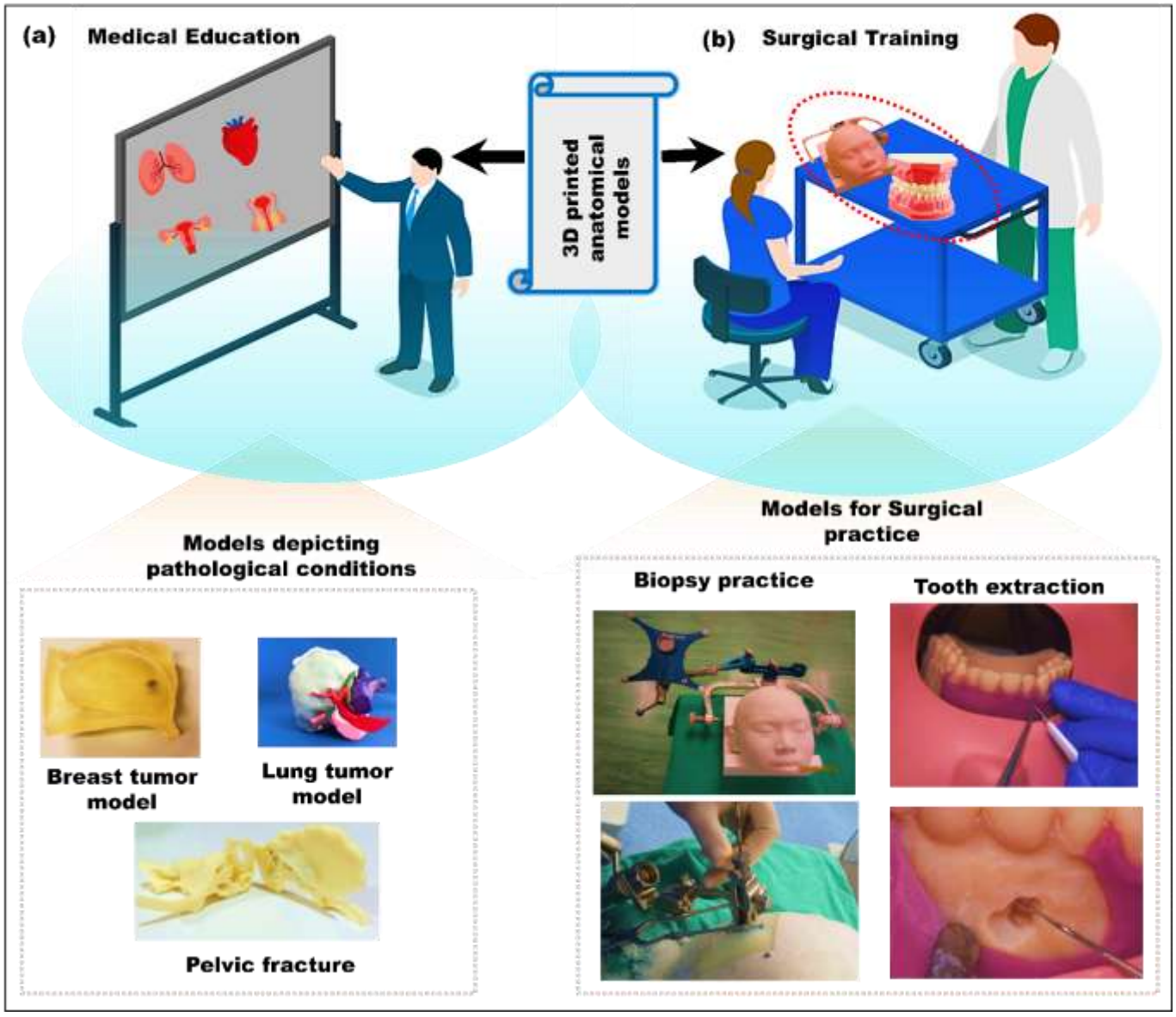

Figure 7. 3D printed models for education and surgery practice. (a) 3D printed models representing liver tumors, kidney tumors, and pelvic fractures; Figure reproduced from Amparore et al. and Yan et al. [180,181] with permission from Elsevier, copyright (2022) (2023) (b) The head model along with the process of biopsy on the left; Figure reproduced from Waran et al.[183] with permission from Elsevier, copyright (2014) and root tip rejection simulation on the right side; the Figure reproduced from Waran et al. [183] with permission from Elsevier, copyright (2014)

3.2 Surgery specific applications

The increase in the geriatric population globally shows a growing demand for tissue/organ transplantation-associated complicated surgeries.[188] Therefore, using AM is of utmost importance in upgrading surgeons' performance, leading to better surgical approaches and improving quality of life.[189] There is a need for precise preoperative planning to ensure zero percent error during surgery.[190] Otherwise, the post-operative surgical outcomes might lead to a high mortality rate in patients.[191] Broadly, 3D printing applications in surgery can be classified into three groups: i. anatomic models, ii. implants and prostheses, and iii. surgical instruments.[192] Subsequent sections have extensively discussed the importance of 3D-printed surgical models in spine, orthopedics, dental, cardiac, gynecological, and neurological surgeries. These surgeries utilized

3D-printed anatomical models, implants, or surgical instruments to improve treatment outcomes.

3.2.1 Spine surgery

X-rays, CT scans, and MRI images have traditionally been used for diagnosing spine diseases and planning spine surgeries. However, integrating 3D-printed models in surgical planning for spine pathology provides a more detailed representation of a patient's anatomy than 2D images.[193] Mobb et al.[194] examined two craniocervical junction chordoma (spinal deformity) cases. Custom-designed and custom-built implants simplify surgery, shorten the overall time of surgical procedures, and eliminate the need for complex reconstruction procedures, such as harvesting and shaping rib or fibular grafts to fit the defect. The radiological follow-up for both the cases showed successful fusion at 9 and 12 months, respectively. One of the most successful methods of treating cervical spinal malignancies is En-bloc resection with sagittal osteotomy.[195] En-bloc resection is a process of completely removing a tumor without damaging its capsules.[196] Xiao et al.[197] investigated the feasibility of 3D printed spinal models for En-bloc resection of primary malignant bone tumors of the cervical spine of 5 patients. The investigation showed that 3D printing provided more precise anatomical awareness of the tumor–cervical interaction than the 2D MRI and CT scan images. The average surgical time was 465 minutes (ranging from 390 minutes to 540 minutes), with an average blood loss of 1290 mL at the time of surgery with no intraoperative infections. **Figure 8a** depicts the tumor rejection in a female patient, while **Figure 8b** demonstrates the tumor rejection in a male patient. Wu et al.[198] evaluated 3D-printed spine models to enhance the precision of pedicle screw insertion in patients with congenital scoliosis. Precision and accuracy in the placement of pedicle screws with the help of 3D-printed models were compared with the traditional fluoroscopy. The investigation showed that the 3D printing technique for preoperative and perioperative planning enhances the effectiveness of pedicle screw placement. The accuracy of screw placement with 3D-printed spine models was 97.9%. The incidences of misplaced screws were 6%, which was far less than 28% to 43% in the case of traditional fluoroscopy. Li et al.[199] used a personalized 3D-printed titanium alloy (Ti6AL4V) porous implant to reconstruct the multilevel cervical spine (C2-C4) in a middle-aged female patient after resecting metastatic papillary thyroid carcinoma. The surgical investigation showed no implant displacement or subsidence after 12 months of post-surgery. Similarly, Leary et al.[200] used patient-specific 3D printed models for surgical planning in a series of complicated primary spine tumors and real-time intraoperative guidance (**Figure 8c**). The model demonstrated its usefulness in designing osteotomies by enabling the precise monitoring of tumor expansion within the membrane at a very detailed level. The 3D printing also aids in treating kyphoscoliosis, an abnormal spine bending in the sagittal and coronal planes. Severe cases of ankylosing spondylitis require spinal osteotomy to restore alignment.[201] Tu et al. [202] used patient-specific 3D-printed guiding templates to position the osteotomy plane and determine the trajectories for the pedicle screws for treating kyphoscoliosis. The average correction at the osteotomy site was 65.9°. No patients had severe complications, such as misplaced screws or neurological problems. At the final follow-up, radiography revealed no implant dysfunction in any patients. The correction of severe spinal deformity is shown in **Figure 8d**.

The abundance of literature that supports the effectiveness of 3D printing in spine surgery indicates a greater likelihood of its widespread adoption.[203] However, rigorous and multi-center trials are necessary to establish the safety and clinical benefits of 3D-printed technologies in spine surgeries.

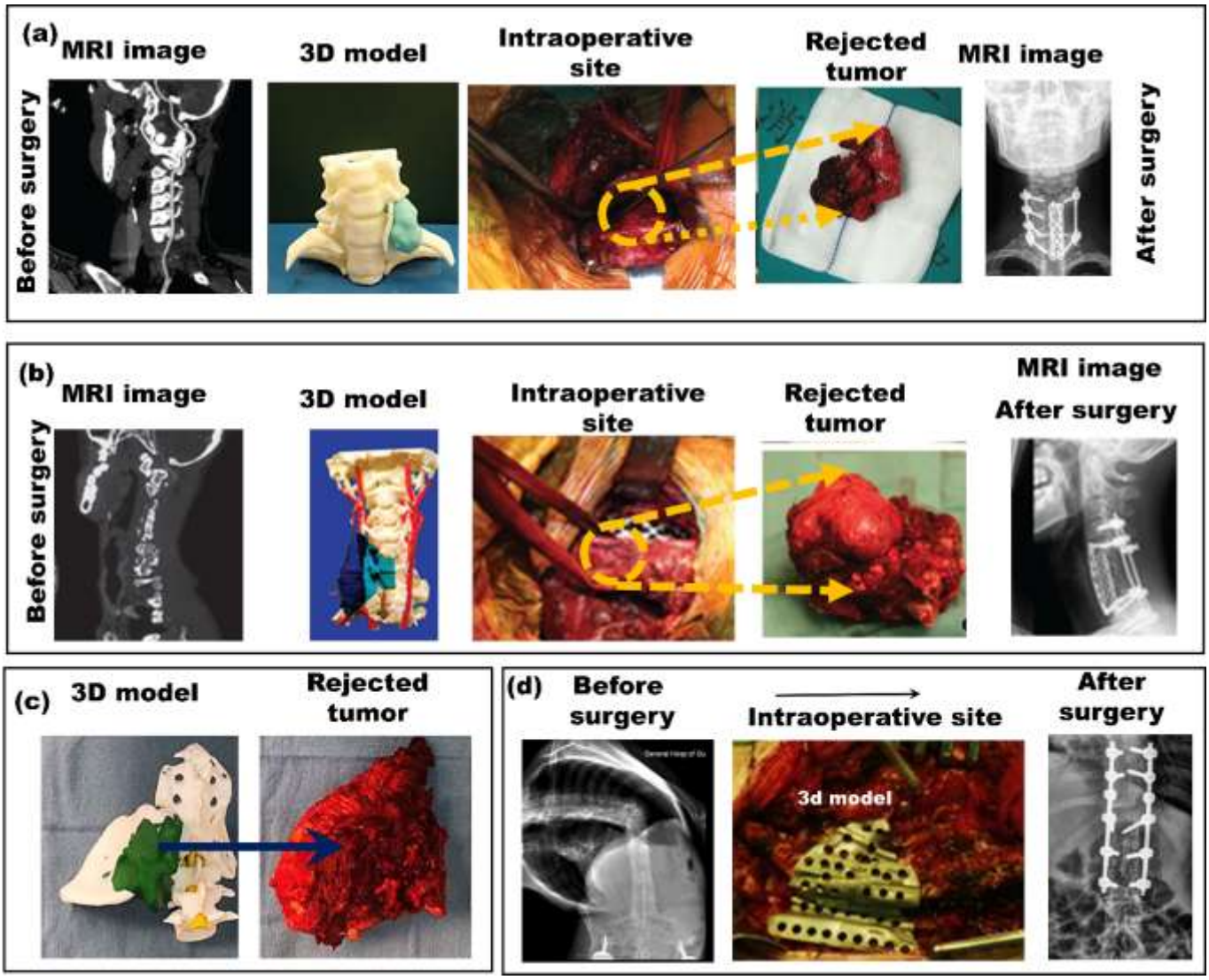

Figure 8. (a) En-bloc removal of the tumor, Figure reproduced from Xiao et al.[194] (b) removal of a tumor in the right vertebral artery; Figure reproduced from Yang et al. [197] with permission from John Wiley and Sons, copyright (2016) (c) A 3D-printed model of the extracted tumor; Figure reproduced from Li et al.[200](d) surgical correction of severe kyphoscoliosis by customized guiding templates. The process from the CT scan before surgery on the upper left to the post-operative CT scan on the right; Figure reproduced from Tu et al. [202] with permission from Elsevier, copyright (2019)

3.2.2 Orthopedic trauma

Orthopedic trauma, caused by incidents like accidents or brutal assault, often requires complex reconstructive surgery to address these injuries.[204] Consequently, the prosthetics market is growing steadily and is expected to reach $1,460.77 million by 2027 from $879.35 million in 2021.[205] Reconstructed orthopedic surgery relies on precisely identifying bone landmarks and anatomical axes. For example, attaching substitute grafts in medial patellofemoral ligament reconstruction for the knee and medial ulnar collateral ligament reconstruction for the upper limb is crucial for joint stabilization and function.[206] The upper limb involves various fractures, such as clavicular, proximal humeral, metacarpals, and acromial fractures [207]. The acromion forms through the fusion of multiple ossification centers, and incomplete fusion leads to the Os acromiale defect.[208] Belien et al. [209] used 3D acromion models to pre-bend osteosynthesis plates for surgical planning in cases of acromial fractures and Os Acromiale defects (**Figure 9a**). Using a patient-customized plate resulted in a complete healing of non-union in all cases, demonstrating its effectiveness in achieving proper fixation and lesion repair. Like acromion, the clavicle is a crucial part of shoulder anatomy, supporting stability and movement. Clavicular injuries are minor injuries, accounting for 2 to 5% of all upper extremities fractures, which often occur in active, young people.[210] Jeong et al.[211] used contoured clavicular locking plates for mid-shaft fractures. Bending plates with 3D-printed clavicle models took 3 hours, facilitating easier fracture reduction and reducing soft tissue damage and post-surgery scars. Uninjured clavicle models helped to select personalized pre-contoured plates (**Figure 9b**).

Besides clavicular injuries, Proximal humeral rupture (PHF) is a frequent upper extremity fracture, accounting for 45% of humerus fractures and 4% of general fractures [212]. You et al.[213] investigated the feasibility of 3D printing technology versus CT scans for treating

complex PHF in 66 geriatric patients (**Figure 9c**). The test group, consisting of 34 cases, utilized 3D-printed fracture models for surgical planning. In contrast, the control group, with 32 cases, relied on CT scans. The test group demonstrated shorter surgery times (77.65 ± 8.09 minutes) and lower blood loss (235.29 ± 63.40 mL) compared to the control group (92.03 ± 10.31 minutes, 281.25 ± 57.85 mL, respectively; $P < 0.05$). Moreover, the control group had higher fluoroscopy scores (10.59 ± 1.36 vs. 7.12 ± 1.57, $P < 0.05$), potentially reducing radiation exposure with 3D-printed models. The test group had a shorter time to fracture union (8.36 ± 1.00 weeks) than the control group (8.50 ± 1.22 weeks, $P > 0.05$), emphasizing the advantages of the 3D-printed proximal humeral fracture models. Cubitus varus deformity is also an upper extremity issue that appears due to supracondylar fracture malunion (bone healing in a misaligned position). The quantification of such malunions is difficult with 2D scan images due to internal rotational deformity.[214] Therefore, Zhang et al.[215] used a reversed engineering approach to design personalized osteotomy template models (**Figure 9d**) for cubitus varus patients. The postoperative surgical analysis was based on the elbow's range of motion and the elbow carrying angle. The carrying angle observed after the surgery was 7.3° with 21.9° as a mean correction. The elbow movement was from 12° of flexion contracture to 128° of further flexion. Gemalamz et al.[216] used personalized 3D-printed resection guides (**Figure 9e**) for a 40º cubitus varus deformity. Post-operative X-rays confirmed precise repair, improved bone contact, and perfect fixation without cosmetic issues. Similarly, Goma et al.[217] used 3D printed models for treating eight different upper extremity trauma cases. 3D printed models aid in planning for multidirectional elbow instability and improve accuracy in distal radius and metacarpal surgeries, addressing challenges in determining ligament reconstruction sites. Additionally, the thumb is vital in the upper extremity, responsible for around 40% of hand function and 80% of gripping activities. Toe transplantation has been the primary surgical approach for reconstructing the thumb (or finger) for over fifty years.[218] The essence of 3D printing can also be seen in thumb reconstruction surgeries when Zhang et al.[219] used a 3D-printed donor toe model for thumb reconstruction. The post-operative results confirmed that the mean flexion angle of the reconstructed thumb was 47°, and the extension angle of the reconstructed thumb was 16°. All patients were satisfied with the thumb function and the reconstructed thumb's appearance.[220]

Beyond upper extremity fractures, over 8 million people also suffer from lower extremity peripheral arterial disease (PAD), which is linked to significant morbidity and mortality.[221] 3D printing technology enhances surgeons' ability to address complex surgeries in the lower extremities [222]. Ankle joint fractures, accounting for 3.92% of all fractures, are particularly significant due to the ankle's critical role as a major weight-bearing joint.[223] Zhang et al.[224] examined a group of patients who had undergone surgical treatment for high-intensity ankle fractures. The test group received treatment with 3D printed models and 2D CT scans, while the control group was treated using conventional CT/MRI scan reports only. The test group's mean surgery time was 74.1±8 minutes, considerably less than the control group (90.2±10.9 minutes). The amount of blood lost in the control group (159.8±6.5 mL) was more than in the test groups (117.1±20.7 mL). Likewise, Wu et al.[225] used personalized 3D calcaneus models to treat 19 patients with intraarticular calcaneal fractures. The mean surgery time was 45 minutes, and the intraoperative blood loss was 14.5 mL compared to 120 minutes and 21.75 mL in the conventional process. Similarly, Yao et al.[226] introduced physical models of the calcaneus to pre-shape the minimally invasive steel plate for surgical simulation. The results revealed that the planned screw trajectory on the 3D model of the calcaneus showed 88% accuracy for sustentacular screw placement. Furthermore, a substantial 96% reduction was observed in the posterior articular surface of the calcaneus, leading to enhanced foot movement capabilities. However, post-extremity surgery recovery is influenced by age, gender, diabetes, high body mass index, smoking, etc.[223] Therefore, transparent orthopedic 3D printing requires inclusion/exclusion criteria, treatment procedures, patient demographics, clinical factors, and treatment details.[217] Personalized 3D-printed surgical models, implants, and tools can significantly reduce blood losses, surgery duration, and mortality rate among patients, transforming reconstructive orthopedic surgeries.

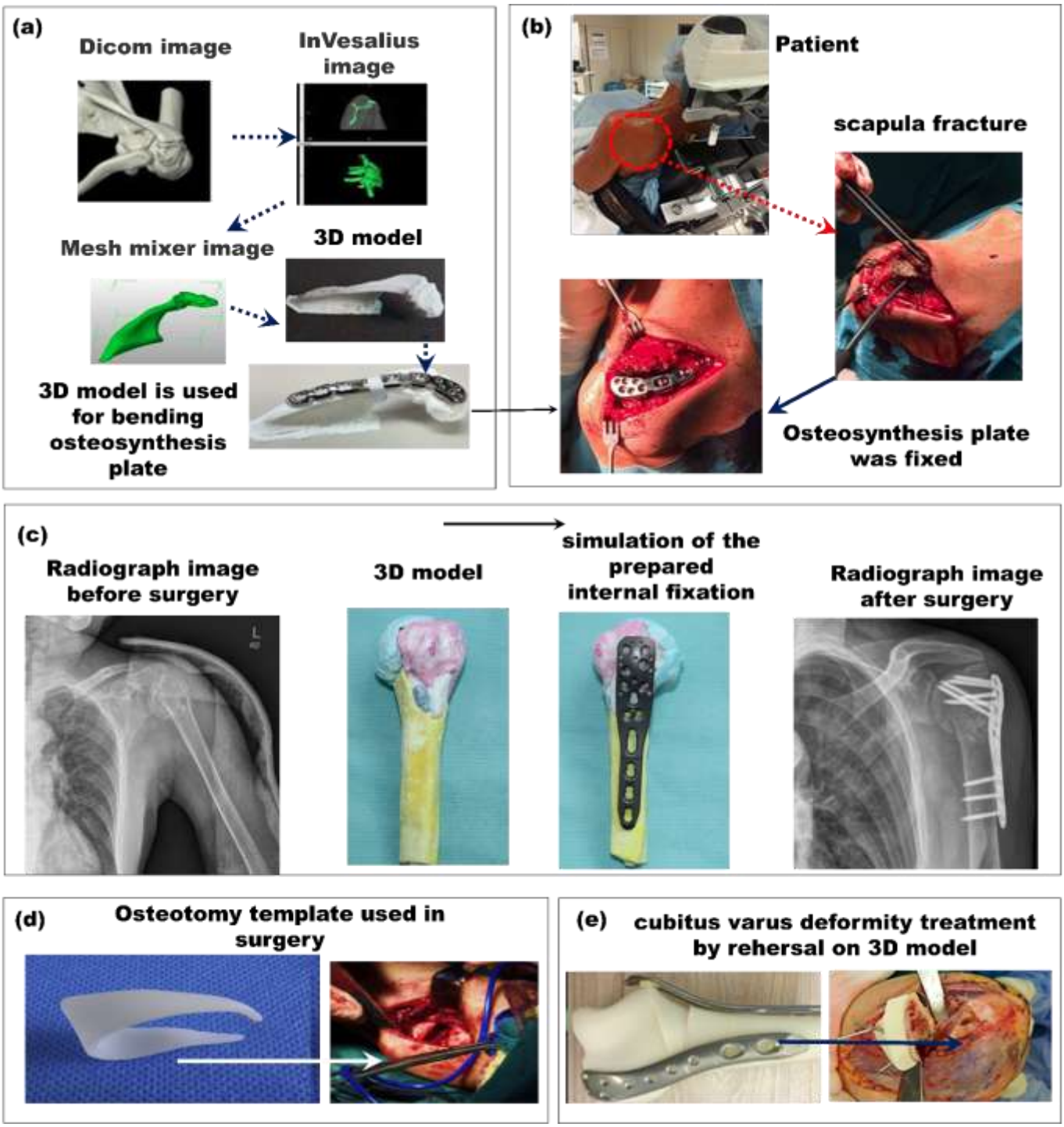

Figure 9. 3D-printed models in upper extremity fracture repair (a) Process of conversion of DICOM files to 3D printed model and bending of osteosynthesis plate with the 3D model; Figure reproduced from Belien et al. [209] with the permission from Springer Nature, copyright (2017) (b) insertion of a pre-contoured plate for clavicle fracture treatment; Figure reproduced from Jeong et al. [211] with the permission from Springer Nature, copyright (2014) (c) 3D printed fracture models of complex proximal humeral fractures and scanned images of the shoulder before and after surgery; Figure reproduced from You et al. [213] (d) Osteotomy templates and their clinical applications; Figure reproduced from Zhang et al. [215] with the permission from Elsevier, copyright (2011) (e) Images of the osteotomy and the subsequent intercalary graft for cubitus varus deformity treatment; Figure reproduced from Gemalamz et al. [216] with the permission from Elsevier, copyright (2017)

3.2.3 Dentistry

The increasing adoption of 3D printing in dentistry is poised to replace traditional methods for crafting dental structures.[227] Dentists utilize this technology to fabricate precise models of teeth and jaws, facilitating the planning of various dental procedures. Additionally, it enables the in-house production of 3D components such as crowns, bridges, and surgical guides. This enhances efficiency by eliminating the need for external laboratory orders.[228] For

example, Williams et al.[229] investigated fibula maxillofacial reconstruction for 12 patients using a point-of-care 3D printing approach to reduce surgery interval. The study revealed that the time needed to produce in-house 3D-printed prostheses from the volume-rendered images was 24 hours, significantly less than two weeks for a laboratory-fabricated prosthesis. Additionally, offsite dental laboratory prostheses are considerably more expensive than in-house 3D-printed prostheses, highlighting the cost-effectiveness of point-of-care 3D printing. Therefore, 3D printing offers point-of-care benefits for dental applications, allowing for immediate dental restoration.[230] Common materials for 3D printing dental prosthetics include photopolymers, titanium, cobalt-chrome alloys, and stainless steel.[231] For example, Lee et al.[232] examined the internal fit of dental crowns produced via 3D printing and CAD/CAM milling methods using stainless steel and vinyl-polysiloxane. The results indicated that the mean discrepancy values measured were 141.1 µm and 91.1 µm for crowns fabricated by two brands of 3D printing systems and 171.6 µm for those produced by the milling system. Moreover, the internal and marginal fit of the crowns manufactured through 3D printing showed significant improvement compared to those produced by the CAD/CAM milling system. Beyond its advantages, 3D printing for dental prosthesis production faces challenges in achieving optimal surface finish for mouth comfort.[233] Additionally, due to the high cost of the necessary tools and supplies, 3D-printed dental prostheses are costly, making the prostheses unaffordable for some patients.[234] In brief, 3D printing offers a high point-of-care approach, precision, and personalization in dentistry. However, the cost and surface finish can hinder some of these practices.

3.2.4 Cardiology

The repair of congenital and structural heart defects is complex due to diverse patient ages, urgency levels, and complexities [235]. Congenital cardiac surgery traditionally relies on a 2D echocardiogram followed by cardiac catheterization to identify complex anatomy. Yet, reconstructing information from a unisensory 2D visual input can be challenging.[236] 3D-printed models offer an interactive solution for understanding complex chest wall tumors, emphasizing the importance of managing cardiovascular complications in cancer therapy. Kim et al. [237] used 3D-printed models with tumors for surgical resectioning of chest wall tumors. The postoperative pathology revealed a reduction in the tumor size from 5.7 cm to 4.5 cm. This reduction was attributed to the detailed tumor insights and its relationship with the neighbouring tissue provided by the personalized 3D models. These insights facilitated patient counselling on cardiac tumor resection. Similarly, left ventricular outflow tract (LVOT) obstruction is a severe side effect during mitral valve repair and replacement.[238] LVOT obstruction impedes blood flow, increasing pressure to maintain forward flow. This raises the pressure gradient between the left ventricle and the aorta, elevating both systolic pressures. This chronic pressure overload can cause adverse heart muscle remodeling, resulting in a left ventricular hypertrophy, dilation, and eventual heart failure.[239] Because of this issue, transcatheter therapies are gaining attention when performing mitral valve procedures to avoid causing or worsening LVOT obstruction. Transcatheter edge-to-edge repair (TEER) is a surgical procedure to place a device that holds the middle parts of the front and back mitral valve leaflets. It creates a double opening in the valve to reduce backward blood leakage in the heart [240]. The MitraClip™ is the only device approved by the Food and Drug Administration (FDA) and has been implanted in over 100,000 patients worldwide.[241] During this process, the surgeon must clearly understand the positions of the interatrial septum, pulmonary veins, left atrial appendage, mitral valve leaflets, and subvalvular apparatus. Therefore, it is crucial to do preoperative simulations to obtain optimal medical decisions regarding the challenging MitraClip procedure.

Computational modeling and patient-specific 3D digital simulations enable in-depth exploration of LVOT biological processes.[242] However, using computational modeling in surgery often involves making assumptions and simplifications. These simplifications may only partially represent the complexities of real-world surgical procedures.[243,244] For example, Mojumder et al. [245] developed a patient-specific computational model to study left ventricular mechanics and myofiber disarray in Hypertrophic Cardiomyopathy (HCM). However, the model did not account for other factors, such as regional and diffuse myofiber disarray, local or diffuse fibrosis, heterogeneous contraction, and electrophysiology in the HCM patients. This limitation hinders the accuracy of the computational simulations. 3D printed models provide a valuable solution for addressing these challenges and assisting clinicians in surgical planning. For example, Bertolini et al.[246] employed 3D printing to develop a training simulator for practicing TEER procedures and successfully tested it using MitraClip equipment. This model aims to enhance TEER training simulators by including anatomical details that can challenge operators during the procedure. However, simulators for mitral valve procedures would be more realistic if they included movable leaflets to simulate leaflet manipulation. These movable dynamic models are crucial for replicating real-time anatomical behavior and improving training accuracy for surgical procedures. 3D dynamic models replace conventional 3D models to resolve such issues. Wang et al.[247] used dynamic 3D printed models to predict LVOT obstruction during preoperative mitral valve replacement and compared their predictions with surgical outcomes. Hemodynamic tests revealed that the dynamic models were consistent with surgical outcomes. For example, the maximum velocity during the cardiac cycle was 113.36 ± 22.10 cm/s in-vitro (3D dynamic model) vs. 115.27 ± 20.96 cm/s in-vivo, and the pressure was 5.33 ± 2.47 mmHg in-vitro (3D dynamic model) vs. 5.48 ± 2.42 mmHg in-vivo. 3D printed models are valuable for surgical training, specifically for practicing the placement of left atrial appendage (LAA) occluders in patients with atrial fibrillation.[239] The LAA is a complex structure that protrudes from the side of the left atrium in a heart. It is a decompression chamber, mainly when increased pressure is within the atrium.[248] In patients with atrial fibrillation, ineffective contraction of the left atrium and LAA can lead to thrombus formation and an increased risk of cardioembolic events. The skill-intensive process of excluding the LAA from the systemic circulation with a device (e.g., WATCHMAN FLX™ and Amulet™) requires significant expertise and substantial learning.[249] 3D-printed LAA models can help surgeons to practice such complex procedures before actual operations (**Figure 10**).

Overall, AM has revolutionized cardiology through highly accurate 3D-printed models for surgical planning and education. However, biomechanical differences exist between 3D-printed models and actual soft tissue, necessitating the integration of soft robotics and

tissue engineering to accurately replicate intracardiac biological structures and motion.

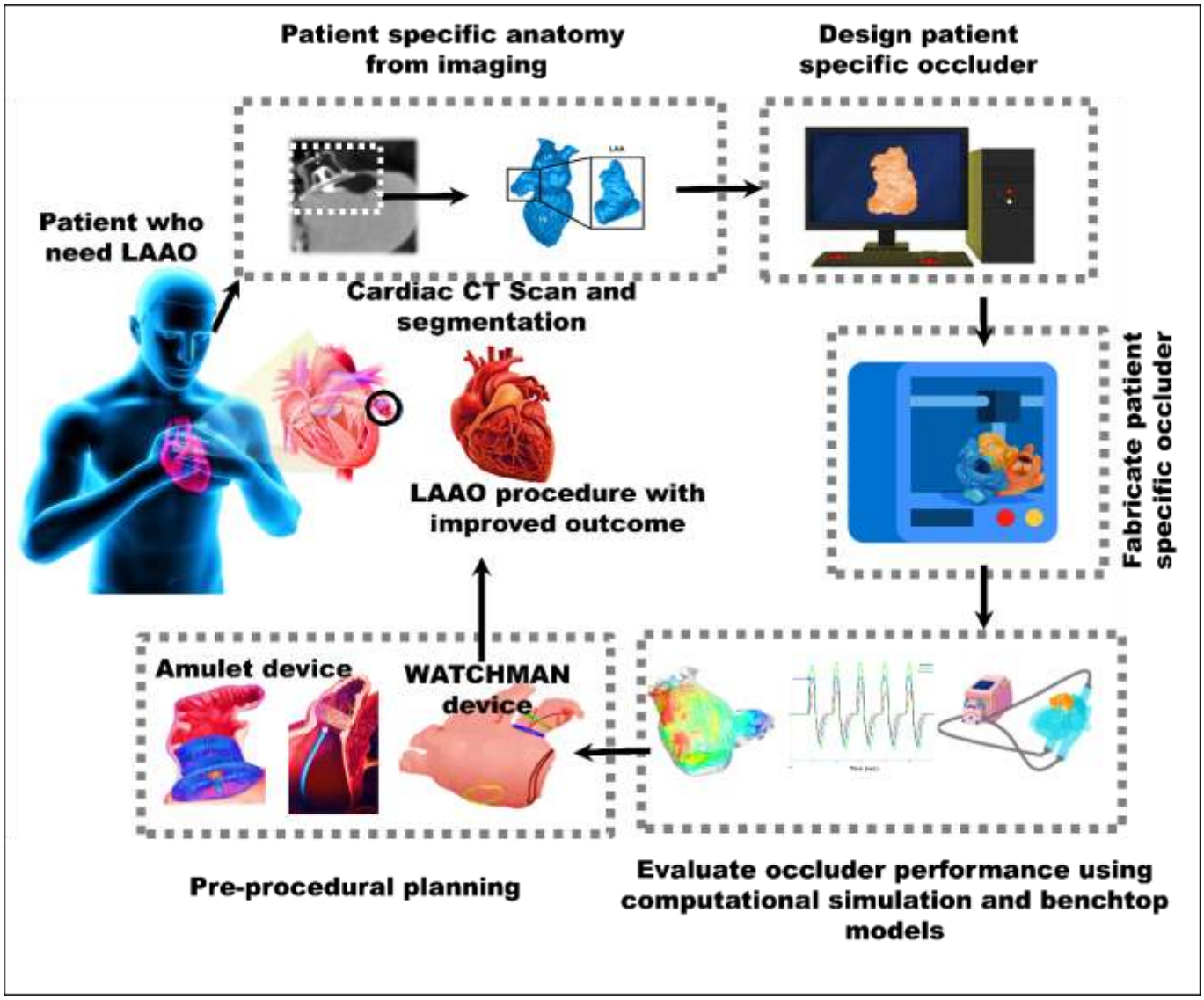

Figure 10. Concept diagram of personalized engineering approach for LAA occlusion; Figure reproduced from Mendez et al. [249] with permission from Elsevier, copyright (2022)

3.2.5 Gynecology

Gynecology is a branch of medicine examining normal and abnormal changes in the female reproductive system.[250] The female reproductive system is commonly affected by various diseases, including endocrine disorders like premature ovarian failure and polycystic ovary syndrome and neoplastic conditions such as cervical cancer, endometrial cancer, ovarian cancer, and uterine fibroids.[251] Among them, uterine fibroids are gynecological tumors affecting about 80% of women globally by an age of fifty.[252] Myomectomy is a medical procedure used to remove these fibroids.[253] However, due to the complexity of the disease, problems such as bleeding can affect the neighboring organs like bladder and colon. This can lead to endometrial perforation and the need for hysterectomy in about 2 to 35% of patients.[254] CT scans display uterine fibroid interactions with surrounding tissues, yet fully grasping the complete information is challenging with 2D images.[255] Cooke et al.[256] used patient-specific 3D-printed models of the pelvis in which uterine fibroids were shown in purple, endometrium in blue, and non-neoplastic anatomy in yellow colour. These different colours enhance the visualization of the underlying disease for pre-operative planning to treat uterine fibroids. 3D models in preoperative planning could reduce the average allotted surgery time by 50 minutes and the estimated blood loss by 120 mL. The postoperative questionnaire was used to understand the benefits of 3D models for fibroid excision. In the survey, 7 out of 11 surgeons agreed that 3D models of uterine fibroids had a good impact on the surgical results of myomectomy. Similarly, endometriosis is another prevalent gynecological illness affecting nearly 15% of females during their reproductive age.[257] Symptoms

such as dysmenorrhea, dysuria, dyschezia, dyspareunia, pelvic pain, and infertility can substantially influence their quality of life.[258] Ajao et al.[259] fabricated a personalized anatomical prototype of a rectovaginal endometriotic nodule with the help of 2D scanned images of patients with a history of endometriosis. The results showed that the location and structural relationship of the endometriotic nodule with that of the uterus and rectum was accurate. 3D models could help surgeons remove the entire endometriotic nodule without harming surrounding tissue. The clinical findings from studies in this section affirm the potential of 3D printing and printed models for safe gynecological surgical simulation. However, its application in studying tumor pathogenesis, metastasis, and treatment is limited.[260] Exploring advanced biomaterials is essential to improve 3D printing outcomes in gynecology. This can boost the confidence of a novice gynecologist, leading to greater surgical accuracy and reducing risks like pelvic pain, heavy bleeding, and infertility in women.

3.2.6 Neurology

Neurosurgery demands high operative standards and skilled neurosurgeons proficient in microsurgical clipping techniques for treating brain aneurysms.[261] While radiologic imaging guides microsurgical clipping, its 2D nature is inadequate for training, highlighting the need for adequate training methods. To mitigate these issues of 2D images, Kimura et al.[262] created elastic hollow models of cerebral aneurysms to replicate the surgical simulation. During surgery, the clips were applied in the same direction and configuration as in the pre-operative simulations. The 3D-printed cerebral aneurysm models made it easy for neurosurgical trainees to understand the vascular configuration and the concept of neck occlusion (narrowing of the carotid arteries, which supplies oxygenated blood to the brain). Likewise, Marciuc et al.[263] fabricated brain vascular lesions to determine the optimal endovascular approach (coil embolization or stent-assisted coil embolization) for 76 cases of cerebral aneurysms. Three interventional neurosurgeons, with experience ranging from ten years to a fourth-year resident, reviewed the cases using computed tomography angiogram with multiplanar reconstructions and volume rendering techniques to decide on coil embolization or stent-assisted coil embolization. The surgeons re-evaluated their treatment plans after using 3D-printed models. The statistical analysis indicated that the endovascular approach was modified in 11.84% of the cases for ten-year experienced neurosurgeons, 13.15% for four-year experienced neurosurgeons, and 21.05% for residents. The 3D-printed models enabled the medical team to reach a consensus on aneurysm treatment plans by providing explicit visual representations **(Figure 11a)**.

3.2.7 Personalised therapy before surgery

Despite the literature highlighting the potential of 3D printing for neurosurgical planning, the static models often fail to replicate the anatomical features and dynamic processes of diseases like Parkinson's and Alzheimer's. This limitation hinders the static models from fully understanding the underlying mechanisms of these conditions. For example, in Alzheimer's disease, mutations in the amyloid-β precursor protein (APP) and presenilin 1 (PS1) genes can cause cellular damage leading to dementia. However, static models cannot fully capture these genetic alterations complex cellular and molecular changes.[264,265] Therefore, Hoon Choi et al. [266] created a 3D cell cultural neural model (organoid) for Alzheimer's disease with elevated mutations in APP and PS1 genes. The organoid replicated Alzheimer's disease, displaying Aβ and hyperphosphorylated tau protein accumulation patterns similar to human brain tissue. However, cell-cultured organoids replicate single-organ structures but not inter-organ interactions, and scaling them up while maintaining structural consistency and integrating vascular networks is challenging.[267,268] 3D bioprinting addresses these challenges by creating organoids that mimic natural tissue complexity, including the main organ, blood vessels, and the immune system **(Figures 11b and 11c)**.[269] Yi et al. [270] employed multimaterial 3D printing to create glioblastoma organoids using patient-derived tumor cells, vascular endothelial cells, and decellularized extracellular matrix from brain tissue. This cancer model replicates glioblastoma's complex ecology and primary pathological features. It included the heterogeneous composition of the extracellular matrix, oxygen gradients leading to central hypoxia, and the mass of cancerous tissue surrounded by dysfunctional microvessels. Heinrich et al.[271] developed 3D-bio-printed mini-brains with glioblastoma cells and macrophages to study their interactions and test targeted therapeutics. The brain models replicated patient macrophage behavior, demonstrating that disrupting interactions between macrophages and glioblastoma cells reduced tumor growth and improved the effectiveness of chemotherapy. In addition to glioblastoma, Parkinson's disease can also benefit from 3D bioprinting. Abdelrahman et al.[272] explored peptide-based bio-ink in Parkinson's disease models, demonstrating its compatibility with mouse and human embryonic stem cell-derived dopaminergic neurons. Vascularization of the models with endothelial cells significantly enhanced neurite outgrowth, suggesting a valuable platform for long-term Parkinson's disease studies.

Additionally, the development of peripheral nerve conduits by 3D printing is a rapidly advancing area that is receiving significant attention in neurobiology research.[273–275] Yoo et al.[276] created elastic nerve guidance conduits (NGCs) with longitudinally oriented collagen hydrogel grafts to repair sciatic nerve defects. The study demonstrated that aligned collagen hydrogels offer an ideal environment for nerve regeneration, serving as a guided pathway. These advanced models can also train surgeons in treating nerve transection injuries.[277,278] Overall, 3D-printed models for surgical planning in neurological diseases show promise but need further development to accurately replicate the dynamic processes of complex neurological conditions for improved patient outcomes.[279][280]

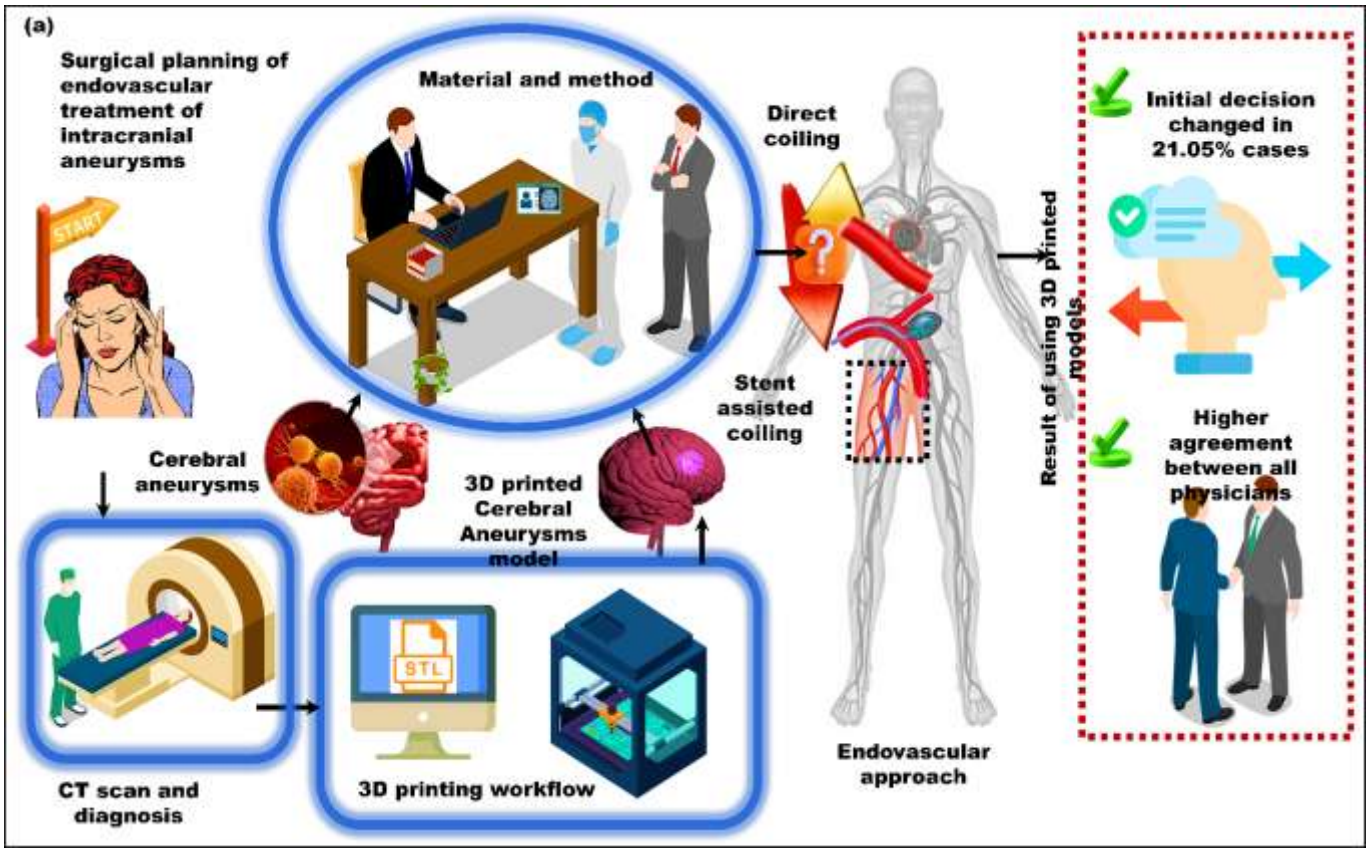
(a)
Surgical planning of endovascular treatment of intracranial aneurysms
START
Material and method
Direct coiling
Stent assisted coiling
Result of using 3D printed models
Initial decision changed in 21.05% cases
Higher agreement between all physicians
Cerebral aneurysms
3D printed Cerebral Aneurysms model
STL
CT scan and diagnosis
3D printing workflow
Endovascular approach

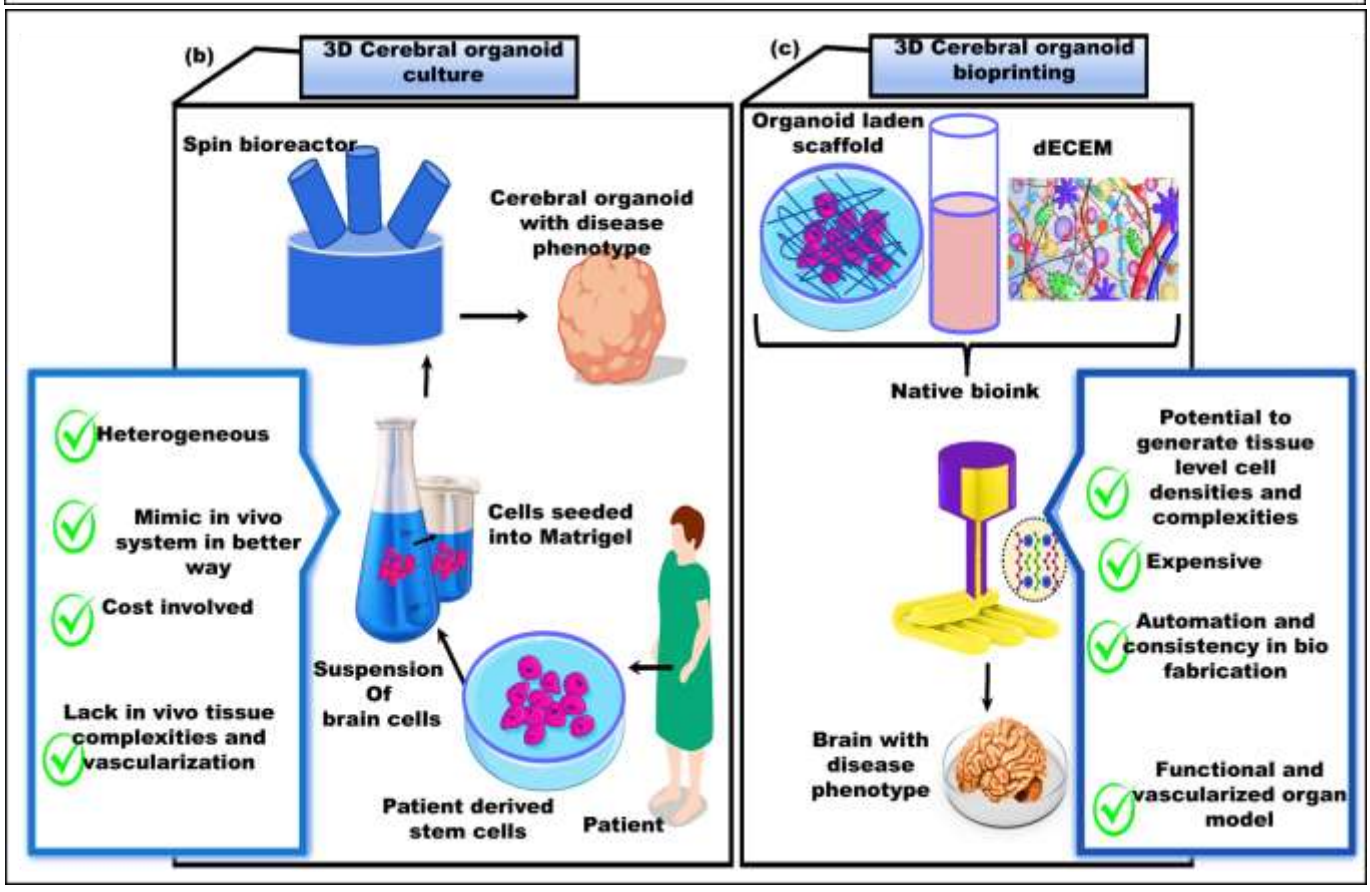
(b)
3D Cerebral organoid culture
Spin bioreactor
Cerebral organoid with disease phenotype
Heterogeneous
Mimic in vivo system in better way
Cost involved
Lack in vivo tissue complexities and vascularization
Cells seeded into Matrigel
Suspension Of brain cells
Patient derived stem cells
Patient
(c)
3D Cerebral organoid bioprinting
Organoid laden scaffold
dECEM
Native bioink
Brain with disease phenotype
Potential to generate tissue level cell densities and complexities
Expensive
Automation and consistency in bio fabrication
Functional and vascularized organ model

Figure. 11 (a) 3D printed models as a valuable tool in endovascular treatment of intracranial aneurysms; Figure reproduced from Marciuc et al.[263] (b) Cerebral organoids are generated by converting patient-derived stem cells into embryoid bodies, forming neuroepithelium in Matrigel. They are then cultured in a spinning bioreactor to enhance nutrient absorption and ensure long-term preservation (c) Cerebral organoid printing; Figure reproduced from Rawal et al. [269] with permission from Springer Nature, copyright (2021)

Considering the above-mentioned surgical cases where 3D printing was involved, it is recommended that surgical prototypes are the best way to allow the surgeons to rehearse before the procedure and prepare them for the actual surgical operation. Personalized 3D-printed implants offer improved outcomes and fewer complications. Their precise fit provides enhanced comfort, quicker recovery, and better integration with surrounding tissues. Overall, 3D printing offers unprecedented precision, patient-specific customization, and enhanced visualization, thereby revolutionizing the field of surgical planning. **Table 4** summarizes the clinical translation of 3D printed models for different surgical planning and procedures included in the surgery-specific section.

Table 4. Summary of the considered 3D-printed models and implants used in various surgical planning and procedures

Diseases	**Use of patient-specific models/implants**	**Materials for models**	**References**
Upper extremity fractures	Clavicle fracture	Plastic	[211]
	Humeral fracture	-	[213]
	Acromial fracture	-	[208]
	Cubitus varus deformity	-	[216]
	Thumb reconstruction	PLA	[219]
Lower extremity fractures	Ankle fracture	-	[224]
	Calcaneal fracture	-	[225]
Dentistry	Dental prosthesis	NextDent Resin	[229]
	Dental crowns	VeroGlaze MED620	[232]
Spine	Congenital scoliosis	-	[198]
	Ankyphosing spondylitis	Ti alloy powder	[202]
	Primary thyroid carcinoma	Ti powder	[199]
	Spinal column tumor	PLA	[197]
Gynecological	Deep infiltrating endometriosis	-	[259]
	Uterine cancer	Photopolymer resin	[256]
Cardiology	Congenital heart disease	-	[12]
	Cardiac tumor	PLA	[237]
	Atrial fibrillation	Flexfill 98A elastic filament	[239]
Neurological	Intracranial aneurysms	Zortax transparent yellow flexible resin	[263]
	Glioblastoma	Brain-derived bioink	[270]
	Parkinson	Peptide bioink	[272]
	Peripheral nerve injury	PLCL and collagen	[276]

4 Prospects in surgical model advancements

Significant progress has been achieved with 3D printing in several subfields of medicine. However, considering surgical planning and procedure, the area is still in its infancy. Additional efforts are required to tackle the difficulties related to printing technologies, printed parts, regulatory considerations, and image segmentation procedures. To overcome these challenges, the adoption of 3D printing with various approaches, such as multi-material techniques,

metamaterials, 4D printing, and machine learning (ML), has been proposed.

4.1 Challenges and concerns in preparation of 3D printed surgical models

4.1.1 Issues and challenges in image segmentation procedures

Medical images are essential in evaluating patients for diagnosis and treatment.[281] Image segmentation results are crucial as they influence all subsequent steps in the image analysis process. Segmentation identifies and separates different ROI within the image. The representation and description of ROI, the measurement of their features, and higher-level tasks like classification all depend on the quality of the initial segmentation.[282] This makes image segmentation crucial for delineating, characterizing, and visualizing ROI in any medical image, which is explained in detail in the data preparation section. The traditional medical image segmentation methods require extensive manual effort and expertise, are prone to errors, and provide only a 2D view of the image at each stage.[283] For example, MRI can provide valuable insights about organ function and perfusion, such as analyzing myocardial perfusion during cardiac tests. However, a significant limitation of MRI is its inability to capture information across multiple biological scales simultaneously, from the molecular and cellular levels to the tissue and organ levels.[284] Such multiscale analysis is crucial for comprehensively understanding physiological and pathological processes. Additionally, the intersection of edges with the background in MRI images can blur the borders of soft tissue, leading to errors in reconstructing edge information. All these multiscale analysis issues combined with blurred borders hamper the overall efficiency of image segmentation and the reliability of the segmentation results. These challenges necessitated the development of advanced technologies to improve image segmentation.[285]

4.1.2 Issues and challenges in the printing process

Inadequate manufacturing speed is a frequent issue observed in 3D printing technologies. In most circumstances, manufacturing biomedical parts utilizing 3D printing takes several hours, if not days.[286] Such printing speed is not suitable for specific biomedical applications, such as life-saving and emergency surgeries. The print resolution is another challenge, as most methods are better suited for medium (meso) and large (macro) dimensions rather than micron-range resolutions needed for specific applications.[287] Additionally, the cost and complexity of 3D-printed models present further challenges, including the need to scale down or divide large parts, which can weaken the final product and introduce dimensional errors.[288–290] Apart from these issues, 3D printing processes can result in the development of thermal gradients.[291] Thermal gradients in 3D printing can lead to directional variations in the microstructures and mechanical properties.[292] For example, FDM-printed fracture fixation plates exhibit more robust mechanical properties along the X and Y axes than the Z-axis (build path), highlighting directional dependence.[293] Beyond mechanical anisotropy, achieving accurate organ mimicry in 3D-printed anatomical models remains challenging, as most models use a single material to represent the variety of tissues present.[294] For example, 3D-printed tumor tissues, made of a single material, lack the varying mechanical textures found in actual tumor tissues.[295] Another example includes the absence of arteries in a 3D-printed dura-mater for neurosurgical rehearsal, which might add complexity during the surgical operation.[296] Although these models accurately reflect the size and shape of real tissues or organs, they fail to capture the full complexity of their structure and function.[30] This limitation persists despite significant advancements in 3D printing technology, as the core workflows have remained unchanged over the past 30 years. The STL file format, still commonly used, links shape and material through surface-based triangle meshes. This limits the ability to use multiple materials and forces all data into surface representations, often increasing computational load, distorting data, and causing loss of critical information, especially in scientific use.[297] A voxel-based approach with multimaterial 3D printing offers improved physical data visualization. By using photopolymer materials such as cyan, magenta, yellow, black, white, and transparent resins, this method produces full-color models with adjustable transparency, enabling accurate representation of complex n manifolds where n is less than or equal to 3, including point clouds, curves, surfaces, and volumes.[298] Commercial multimaterial 3D printers offer high-resolution builds within a 500 × 400 × 200 mm space, achieving up to 929 billion addressable voxels through 600 × 300 dpi droplet resolution and 12 μm layer thickness. This precision enables volumetric color and transparency gradients and fabricating intricate structures with fine details inside clear enclosures. For example, Jacobson et al.[299] used bitmap printing (voxel-based), an AM method that enables precise control over the resin mixing and deposition at ultrahigh resolution. This approach directly translates medical images to replicate human anatomy with 15 μm spatial fidelity, preserving soft tissue variations without data loss or alteration. In addition to progress in printing technologies, there is a growing emphasis on developing advanced materials. Functionally graded materials are gaining attention for their ability to replicate the gradual transitions found in native tissue properties. Zheng et al.[300] designed dental implants with a functionally graded porous structure based on triply periodic minimal surfaces (TPMS). This radial gradient design aimed to reduce stress shielding and support long-term bone integration. Mechanical tests and finite element analysis showed that a 40% gradient (inner porosity 80%, outer porosity 40%) resulted in the highest elastic modulus (14.32 GPa) and yield strength (527.25 MPa). These values fall within the mechanical range of natural bone (2–20 GPa for modulus), supporting their potential suitability for medical applications. Despite progress in 3D printing technologies and materials, there remains a need for systems capable of processing multiple bioinks simultaneously and the spatiotemporal positioning of different bio-inks to accurately replicate the structure, texture, and consistency of native tissues and organs.

4.1.3 Regulatory concerns

Several regulatory challenges exist concerning using the AM process in surgical planning and procedures.[301] The first and most serious concern is the responsibility for deviating from the conventional standard treatment, particularly in the case of anatomical models. It is still doubtful who should be held accountable for any errors in the customization settings of anatomical models.[302] Patient safety is another major concern in the use of 3D printing in surgery. The complexity of using 3D-printed models and devices, which may require mechanical strength, precise positioning, and repeated

loading, necessitates thorough testing and validation.[303] Regulatory bodies such as the U.S. Food and Drug Administration (FDA) are working to establish new testing requirements to ensure the safety of 3D-printed models and devices for clinical use. As AM technologies are relatively new to the medical field, the FDA is focused on developing regulations for 3D-printed components, including organ models, implants, and surgical tools. [304] [305]
A recent review by Brian G. Beitler et al.[306] highlighted the regulatory factors for adopting 3D printing in hospitals, medical centers, or point-of-care to develop patient-specific devices. **Figure 12** summarizes a general guideline recommended by the FDA for establishing point-of-care 3D printing centers. However, the existence of these point-of-care centers blurs the distinction between healthcare providers, medical facilities, and device manufacturers, resulting in regulatory ambiguity.

Globally, governments work to ensure the safety and effectiveness of medical devices, but regulatory systems vary from country to country. Since no single framework meets all countries' needs, each country has developed its regulations and seeks alignment to facilitate international market access. The Global Harmonization Task Force (GHTF), formed by regulators and industry representatives from Australia, Canada, Japan, the European Union, and the US, works to harmonize medical device regulations. A typical regulatory framework includes premarket, on-market, and post-market stages, with devices classified by risk level to determine the level of scrutiny required. For example, the FDA categorizes medical devices into Class I, II, or III, with higher-risk devices subject to more oversight.[307]

Additionally, standardization efforts for AM in medicine are ongoing. ASTM International and ISO have collaborated to develop global standards for AM, with input from over 1,000 experts. Within ASTM's F42 committee, subcommittees focus on industry-specific needs, including medical AM. FDA-recognized standards cover ISO/ASTM 52900(for terminology), ISO/ASTM 52910, 52911 (for design), ISO/ASTM 52915(for data management), ASTM F3001, F3302 (for materials), and ISO/ASTM 52904 for validation. However, these standards do not fully meet all FDA premarket review requirements. For instance, ASTM F3001 outlines material properties for Titanium 6 Aluminium 4 Vanadium ELI. Still, it does not address factors like powder reuse or variations in the build conditions, limiting its application in identifying worst-case material performance.[308] Other organizations, such as IEEE and DICOM, contribute to standardization efforts, particularly in 3D modeling, data management, and medical imaging, although interoperability remains challenging.[309]

Overall, regulatory frameworks must evolve to address the unique characteristics of point-of-care manufacturing, account for the variability in AM processes and materials, and support international collaboration to harmonize standards and reduce market entry barriers.

Evaluation of biocompatibility and functional performance of 3D printed implants

Biocompatibility refers to how biomaterials interact with a living body under various chemical, metabolic, physiological, and physical conditions.[310] It is essential to understand these interactions to ensure the material's safety and effectiveness. Upon implantation, a 3D-printed implant engages in complex interactions with human tissues. Developing safe and biocompatible materials depends on how well these interactions are characterized. As materials may respond differently under various conditions, comprehensive testing is required to ensure their safety.[311] Biocompatibility evaluation involves examining how a material interacts with the biological environment, considering long-term stability, harmful byproduct formation, surface texture, crystallinity, moisture absorption, chemical composition, stiffness, and surface charge. The required testing depends on the material's intended application.[312] For instance, in orthopedic uses, the material must not cause inflammation, interact safely with proteins and blood, and maintain its structural integrity over time. Testing involves both *in vitro* and *in vivo* methods. In vitro testing is essential during the early stages of development to identify potential risks, while in vivo testing provides a comprehensive understanding of biological responses within a living system. [313] Together, these methods are necessary to evaluate the safety and effectiveness of biomaterials for implant applications. However, confirming biocompatibility also requires a thorough assessment of implants' mechanical and chemical properties, as these influence how implants interact with biological tissues over time. Mechanical testing ensures that devices retain structural integrity after implantation and exhibit appropriate degradation behavior. [314] Chemical testing examines extractable and leachable compounds to verify compliance with ISO 10993 standards, reducing potential health risks. [315] In parallel, biological testing is critical in evaluating the overall interaction between implants and the human body. The ISO biocompatibility evaluation matrix further supports this process by classifying medical devices based on the nature and duration of body contact, providing a structured framework for testing.

The ISO 10993 series offers a detailed guideline for evaluating biological safety, specifying the necessary tests and endpoints for different device categories.[316] Key tests in this process include cytotoxicity, which checks for the potential of materials to harm or kill cells; sensitization assays, which identify substances that may cause allergic reactions during repeated exposure; irritation tests, which assess the material's effects on skin and mucous membranes; subchronic toxicity tests, which evaluate prolonged exposure effect; and genotoxicity studies, which look for the substances that could cause genetic damage.[317] Implantation tests observe how materials behave when placed into live tissue, while hemocompatibility tests evaluate interactions with blood tissue. Other tests such as carcinogenicity, reproductive, and developmental toxicity studies are conducted to assess potential risks like cancer or effects on fertility and embryonic development. Biodegradation tests assess how materials degrade in the body, particularly for biodegradable implants. Toxicokinetic studies examine how the body absorbs, distributes, metabolizes, and eliminates potentially toxic substances from medical devices.[310]

International standards play a key role in ensuring such testing is consistent and scientifically robust. Organizations such as the International Organization for Standardization (ISO), ASTM International, and the International Medical Device Regulators Forum (IMDRF) provide structured frameworks that guide the evaluation of biocompatibility, safety, and performance of medical devices globally.

The ISO 10993 series, in particular, outlines detailed procedures for biological and clinical assessments, including tests for implantation effects, systemic toxicity, and carcinogenicity.[318] Regional and national standards play a significant role in shaping medical device regulations worldwide. For instance, European medical devices require a Conformité Européenne (CE) marking, which confirms compliance with European Union (EU) health, safety, and environmental regulations evaluated by accredited Notified Bodies. The FDA regulates device approval in the United States through Premarket Approval and 510(k) pathways, relying on ISO standards combined with FDA-specific guidance.[319] Meanwhile, countries like Japan, India, South Africa, and Israel are developing or harmonizing their regulations with these international frameworks.[320] While progress is being made to align regulations across regions such as Asia-Pacific, Africa, and Latin America, variations remain. In addition to biological testing, many nations impose extra requirements for physicochemical properties and electrical safety.[321]

Organizations, including the American National Standards Institute (ANSI), contribute to consensus standards in the US and collaborate with global bodies like ISO and the International Electrotechnical Commission (IEC).[322] Complementary resources such as the United States Pharmacopeia National Formulary and guidelines like Good Laboratory Practices (GLP) and the International Council for Harmonisation (ICH) support consistent and reliable medical device testing.[323] This evolving regulatory landscape also demands special considerations for specific device categories and emerging technologies.[324] Pediatric devices often rely on clinical data for safety, reducing the need for extensive juvenile toxicity tests. New technologies such as nanomaterials, three-dimensional bioprinting, and regenerative medicine present additional challenges that regulatory agencies, including ISO and FDA, are actively addressing by developing appropriate standards and frameworks.[325] As these regulations continue to change, engaging experts familiar with both regional and international requirements is essential to ensure regulatory compliance and patient safety.[326]

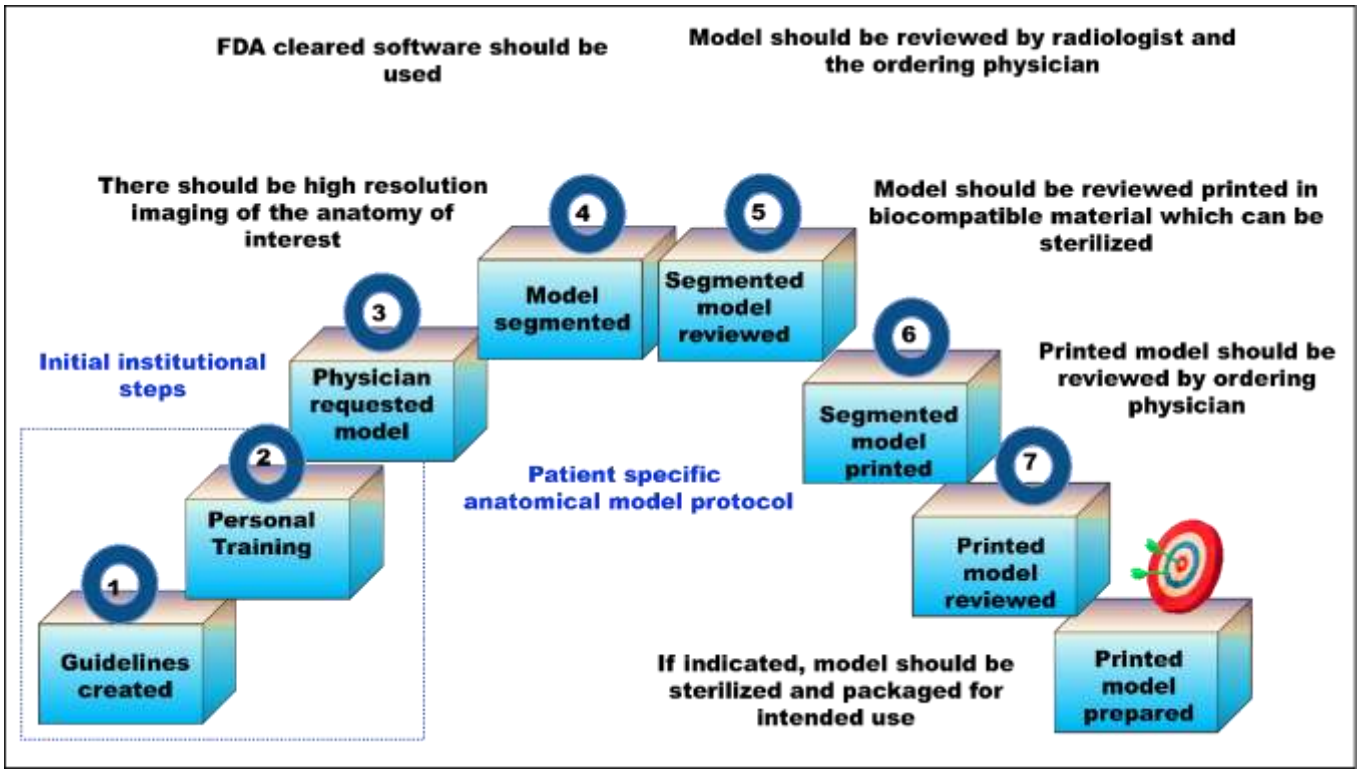

Figure 12. General guidelines recommended by FDA for patient-specific anatomical models; Figure reproduced from Hameed et al. [302]

Overall, existing 3D printing faces several critical issues that require immediate attention. These include limitations in segmenting CT scans and MRIs, printer speed and resolution constraints, and the lack of realistic replication of soft tissue in static, single-material 3D printed models. Addressing these challenges is essential for advancing the technology toward refining the use of AM in surgical planning and procedures.

4.2 Elevating surgical planning with multidisciplinary solutions

4.2.1 Multimaterial 3D printing for personalized anatomical models

Dimensional accuracy in 3D-printed models is vital, and the printed models must respond realistically during rehearsal surgeries to fulfill preoperative planning needs.[327] Although 3D printing can replicate hard tissues like bone, it is challenging to mimic soft tissues like the heart, liver, brain, and kidney. This challenge arises because the materials currently in use, such as photocurable polymers, have limitations in replicating soft tissue's complex structures and functions.[328] Differences in shore hardness and viscoelasticity between existing materials and soft tissues hinder the accurate replication of an organ or tissue. Hence, accurately replicating the mechanical characteristics of native soft tissues in printed models requires close attention to properties such as elastic modulus, hardness, and viscoelasticity.[329] Hydrogels are increasingly used for this purpose due to their tunable mechanical behavior, making them suitable for simulating soft tissue.[330] For example, formulations such as 4% wt. GelMA and 2% wt. Agarose has demonstrated a close mechanical resemblance to the kidney. Reproducing native tissue behavior requires alignment with key parameters like Shore hardness and viscoelastic moduli. The kidney exhibits a Shore hardness of 36 ± 10 Shore 00, which is closely matched by 2% wt agarose (37 ± 5 Shore 00) and 4% wt GelMA (32 ± 4 Shore 00). In terms of viscoelastic behavior, storage and loss moduli of the kidney are 2.38 ± 0.43 kPa and 0.40 ± 0.08 kPa, respectively. Materials like 6% wt. PVA with 1% wt. Phytagel (PHY) provide the closest match for the elastic response (storage modulus), while 1% wt agarose and 4% wt GelMA align well with the viscous component (loss modulus) of the kidney. Brain tissue, being much softer, has a Shore hardness of 4.5 ± 1.5 Shore 00, which is closely mimicked by 2% wt PHY (8 ± 2 Shore 00). Its storage and loss moduli are 2.6 ± 0.84 kPa and 0.47 ± 0.19 kPa, respectively. Again, 6% wt PVA with 1% wt PHY best replicates the elastic response, while 1% wt agarose, 4% wt GelMA, and 2% wt PHY effectively reproduce the viscous properties.[75] Therefore, integrating multi-material 3D printing is critical for minimizing the biomechanical mismatch between printed constructs and actual soft tissues. For example, fabricating a 3D model of the human vascular system requires multiple materials to accurately represent its complex structures.[331,332] Lim et al.[333] used a multimaterial approach with elastomers and hydrogels to produce 3D vascular models through an indirect 3D printing technique. The study revealed that the proposed replicas could facilitate accurate simulation of endovascular surgery. Similarly, Levin et al.[334] used flexible material to print aortic leaflets

and aortic arc geometry in the scope of the intricate structures requirement for transcatheter aortic valve replacement. The hard material was used to print the calcified structure, which was then integrated into the aortic leaflet. One of the challenges is the accurate replication of interfaces at soft and hard tissues. These models precisely mimic the anatomical and functional properties of the actual aortic leaflet of a human. Despite significant advancements, multi-material models struggle to accurately replicate soft tissue's complex biological structures and motions.[75,335]

Soft robotics and tissue engineering can overcome this limitation by achieving intricate biological motions of soft tissue.[336] The functions of these tissue-engineered soft tissues can be augmented through 4D printing, microbots, and cyber-physical systems.[337,338] Park et al.[339] developed a biorobotic hybrid heart that mimics the biomechanics of the heart and preserves its natural internal structure by replicating the cardiac myofiber arrangement found in the left ventricle. The endocardial tissue of the pig heart preserved detailed information on the intracardiac structure. At the same time, soft robotics enabled biomimetic motion. **Figure 13** illustrates the complete process of developing an analogously beating heart model, from pig heart dissection to recreating the dynamic motion of the heart. The high-fidelity beating heart model is a simulator for developing and testing mitral valve repair or replacement interventions. Its simulation capabilities can potentially develop tools for assessing and treating left and right ventricle issues.[340] Singh et al. [341] developed a soft robotic model of the right heart that accurately mimics right ventricle biomechanics and hemodynamics. This soft robotic model enhances the understanding of right ventricle (dys)function, reduces the need for animal testing, provides a foundation for developing tools to correct diseases, and bridges the gap between benchtop and preclinical testing. Noor et al.[342] fabricated the cellularized human heart with integrated blood vessels. The dimensions of the beating heart were 20 mm in height and 14 mm in diameter, with two different bio-inks (multi-material). The blood vessels and cardiac tissue were constructed using customized bio-ink supplemented with dyes (color). The blue for blood vessels and red polystyrene spheres for cardiac tissue were used for better visualization. Additionally, customized bio-ink was used to print functional vascularized patches. These perfusable and vascularized patches were produced by the synergetic use of the patient derived cell and hydrogel. **Figure 14** shows the concept of fabricating a lively human whole heart and vascularized patches. Thus, integrating multi-materials, soft robotics, and tissue engineering into AM can significantly improve the resemblance of 3D-printed tissues to actual soft tissues by reducing biomechanical differences.

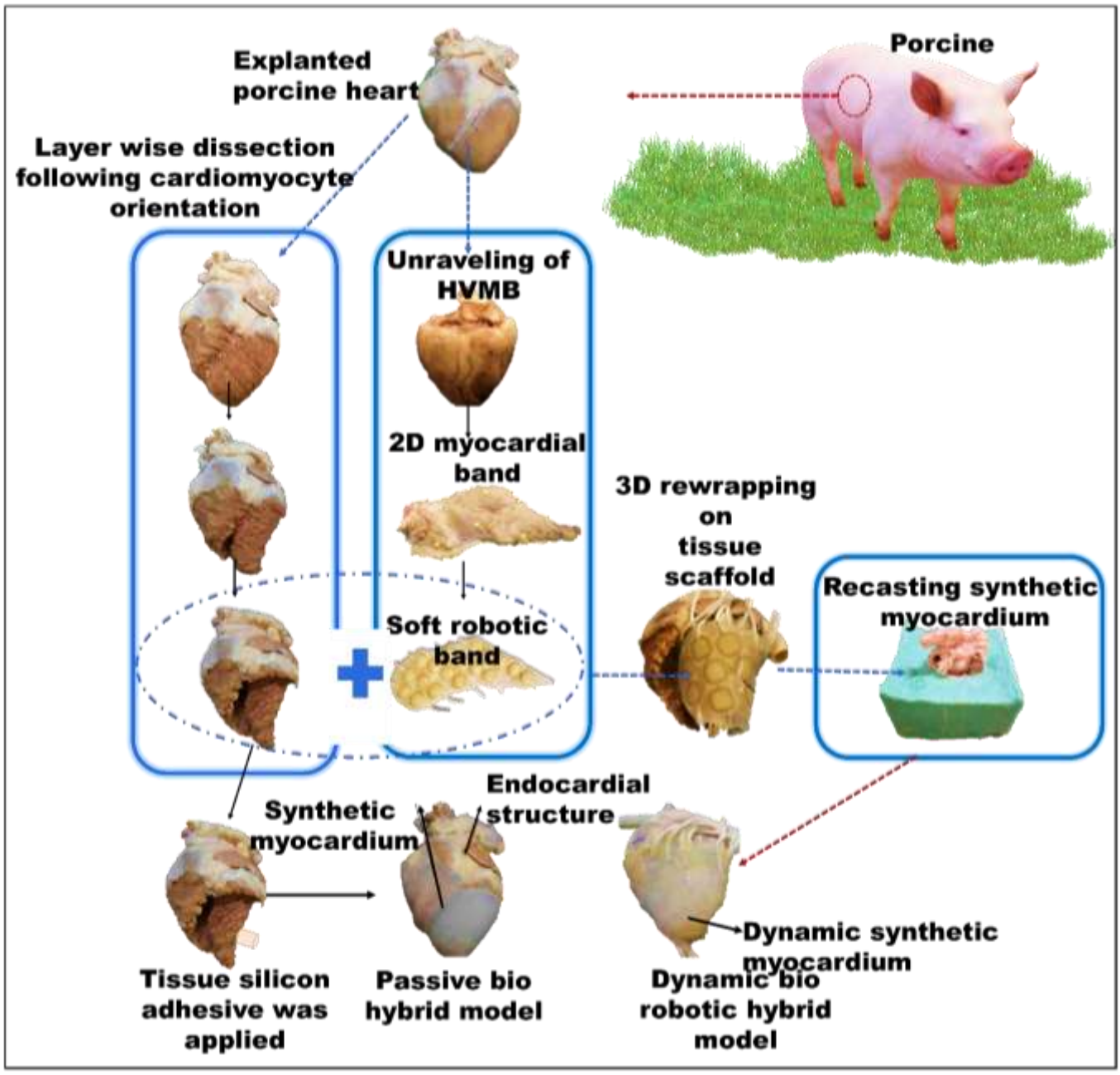

Figure 13. The dynamic bio-robotic hybrid cardiac model fabrication using tissue engineering and soft robotics; Figure reproduced from Park et al. [339] with permission from The American Association for the Advancement of Science, copyright (2020)

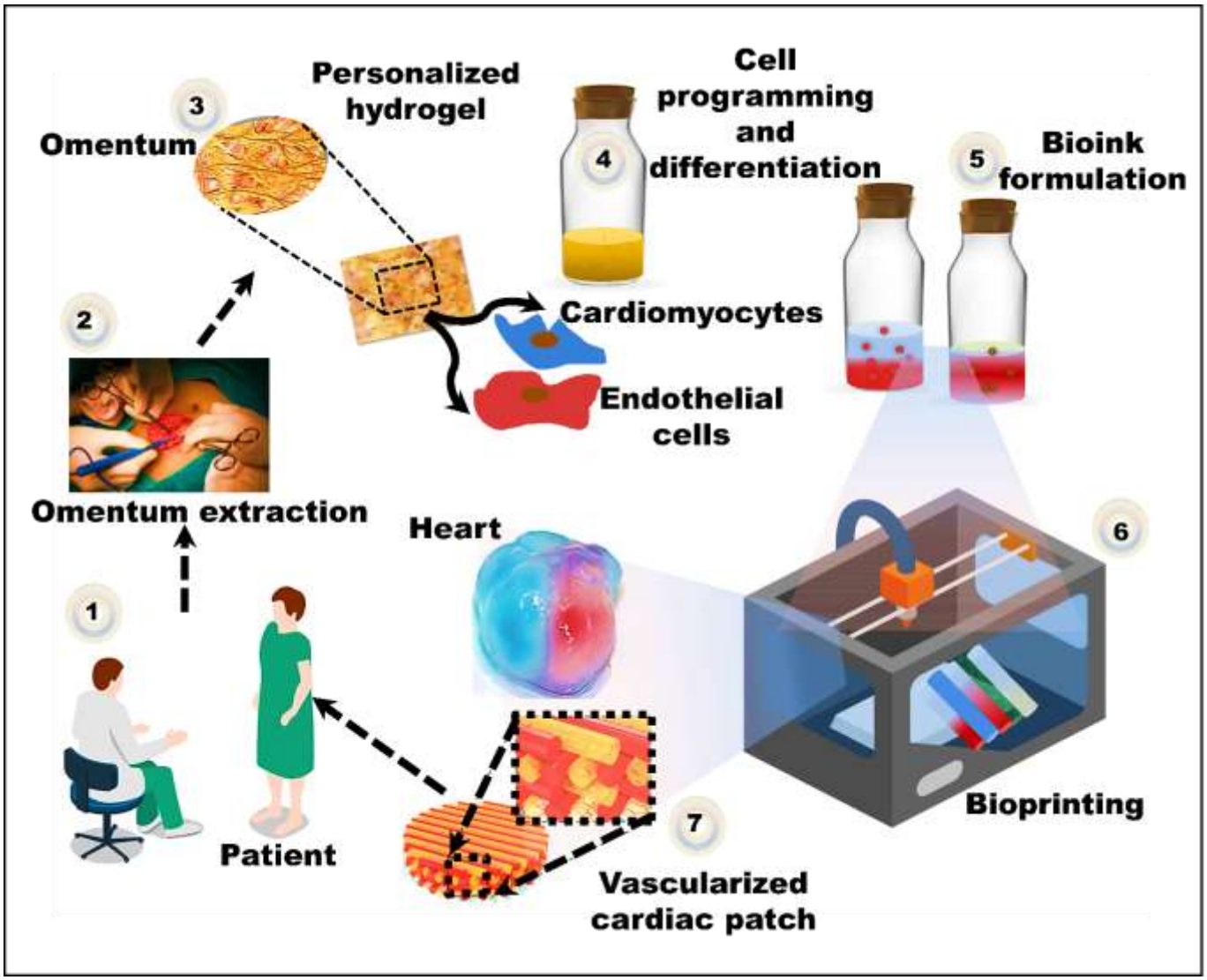

Figure 14. Concept diagram: The omentum tissue is extracted from the human, and cells are separated from the matrix. These cells are reprogrammed and differentiated into cardiomyocytes and endothelial cells. Then cardiomyocytes and endothelial cells are encapsulated within the hydrogel to produce bio-ink for 3D printed hearts and vascularized and perfusable patches. Figure reproduced from Noor et al. [342] with permission from John Wiley and Sons, copyright (2019)

4.2.2 Metamaterial 3D printing: Providing haptic feedback in surgical simulation

The realistic touch sensations are of utmost importance in simulated surgical environments [343]. These systems aim to provide users with an immersive and lifelike experience by incorporating tactile feedback into the training process.[289] To obtain this, a detailed understanding of the mechanical behavior of tissues is essential for the precise selection of materials for 3D printing for surgical simulation.[160] For instance, if the material is excessively stretchable, the needle may penetrate beyond the tissue boundary during surgery. Similarly, an overly soft material lacks tactile feedback for surgeons and may break upon contact. Conventional models used in surgical simulations assume that tissues exhibit either isotropy (equal stretch in all directions) or transverse isotropy (different stretch in different directions). However, actual tissues display nonlinearity, anisotropy, viscoelasticity, and tension-compression asymmetry, affecting the behavior of surgical instruments. Therefore, an accurate 3D surgical model replicating these biomechanical properties is crucial for understanding needle-tissue interactions and ensuring safe and effective surgeries.[344] Recognizing this disparity, researchers are actively improving the accuracy of these models by integrating more advanced features, including rate dependence, hierarchical structure, interstitial flow, and post-yield behaviors.[345,346] Still, there is a mismatch in mechanical properties between materials used in 3D printed models and actual tissue.[346,347] For example, Wang et al.[348] demonstrated that soft tissues and 3D-printed models exhibit distinct behaviors under large deformation. The main difficulty stems from the inherent dissimilarity in stress-strain curves between soft tissues and 3D printable polymers. Soft tissues typically exhibit an initial strain-stiffening behavior, resulting in a convex stress-strain curve during the early stages. On the other hand, polymer materials typically display a strain-softening characteristic, as seen in their stress-strain curve, which is generally concave right from the beginning **(Figure 15a)**.

The latest advancements in 3D-printed metamaterials shed new light on tackling this challenge. The strain-stiffening behavior of soft tissues can be obtained by designing the arrangement and composition of the metamaterials at a microscale or nanoscale level. Metamaterials are specially designed structures with unique mechanical properties that result from the design of their microstructural geometry rather than the materials themselves. The mechanical properties of metamaterials depend on the design and geometry of their unit cells, including cell shape, size, strut and node connectivity, and porosity. Tailoring these elements allows for specific properties, making metamaterials versatile for surgical applications.[349] Hence, manipulating the structure-property relationship in metamaterials makes it possible to create surgical models that accurately replicate the mechanical behavior of anatomical tissues. For instance, a heterogeneous design can be achieved by reinforcing a body-centered cubic (BCC) structure with face-centered cubic (FCC) unit cells arranged in a chessboard-like pattern within each layer, enhancing compressive strength (**Figure 15b).** [350] The feasibility of designing the mechanical properties of metamaterials has increased with the advent of multi-material 3D printing technologies.[351] For instance, Maier et al.[352] replicated human soft tissue using dual-material 3D printing with a support-filled metamaterial to provide bimanual haptic feedback for a hand surgery training system. This method not only improves the overall elasticity of the hand model but also ensures that the support material remains locally constrained. This dual effect allows the model to maintain its shape and adequately align the internal bones, even after repeated deformation. Johnson et al.[353] devised a framework utilizing lattice microstructures to adjust the elastic profile of linear base material, transforming it into nonlinear elastic materials to mimic the biomechanical properties of soft tissues like plantar fat. A stress-strain curve closest to plantar fat was observed in a simple cubic lattice microstructure composed of cylindrical elements with 0.5 mm diameter columns and 1.2 mm spacing. The elastic modulus at 10%, 30%, and 50% strain was 7.55 kPa, 9.50 kPa, and 252 kPa, respectively. At the same strain values, actual plantar fat has modulus values of 1.08 kPa, 7.13 kPa, and 188 kPa. Therefore, fine-tuning the lattice microstructures can reduce Young's modulus of soft 3D-printed materials, allowing them to mimic human soft tissue behavior. Hence, integrating metamaterial 3D printing into surgical simulation significantly enhances the immersive experience.[354] It enables surgeons to develop and refine their skills in a highly realistic and controlled environment **(Figure 15c)**.

Zhang et al.[355] developed microlattice metamaterials for vascular stents, using designs inspired byNiTi alloys' austenite and martensite crystal structures. These structures were fabricated using laser powder bed fusion with strut diameters ranging from 0.4 mm to 0.8 mm to achieve a wide range of tunable mechanical and superelastic properties. The loading direction influenced the mechanical performance. The martensite-inspired design loaded along the x-axis (M_x) exhibited the highest Young's modulus from 1001.5 MPa to 3720.4 MPa and the widest tunable range of 87.32 %. The austenite-inspired design (A) showed complete tunability in yield strength. All designs demonstrated excellent super elasticity with recoverability between 98.10 % and 99.36 %. The M_x model showed the highest recoverability despite a narrower tunable range. Tuning the lattice structure enhances the mechanical properties of NiTi-based microlattice metamaterials by controlling how stress is distributed and absorbed within the material. Modifying the lattice geometry, including strut orientation, size, and shape, directly influences the key mechanical properties such as stiffness (Young's modulus), strength, and superelastic behavior. The strut diameter and orientation play a critical role in load-bearing capacity and energy absorption, with thicker or optimally oriented struts improving stiffness and strength. The lattice symmetry and topology, derived from the austenite (BCC) or martensite (monoclinic) crystal structures, lead to distinct stress distributions and deformation mechanisms. For instance, the M-x structure exhibits higher stiffness due to its alignment with the loading direction. Additionally, the volume fraction, or the amount of solid material present, increases with strut thickness, further enhancing mechanical performance.

The design of the microlattice architecture, including strut orientation, diameter, and geometry, enables precise control over the mechanical behavior, such as load-bearing capacity and shape recovery after compression. This adjustment significantly enhances metamaterials' mechanical strength and shape memory properties, making them suitable for various surgical applications.[356] Overall, manipulating the structure-property relationship in metamaterials enables the creation of surgical models that can accurately replicate the mechanical behavior of an anatomical tissue.

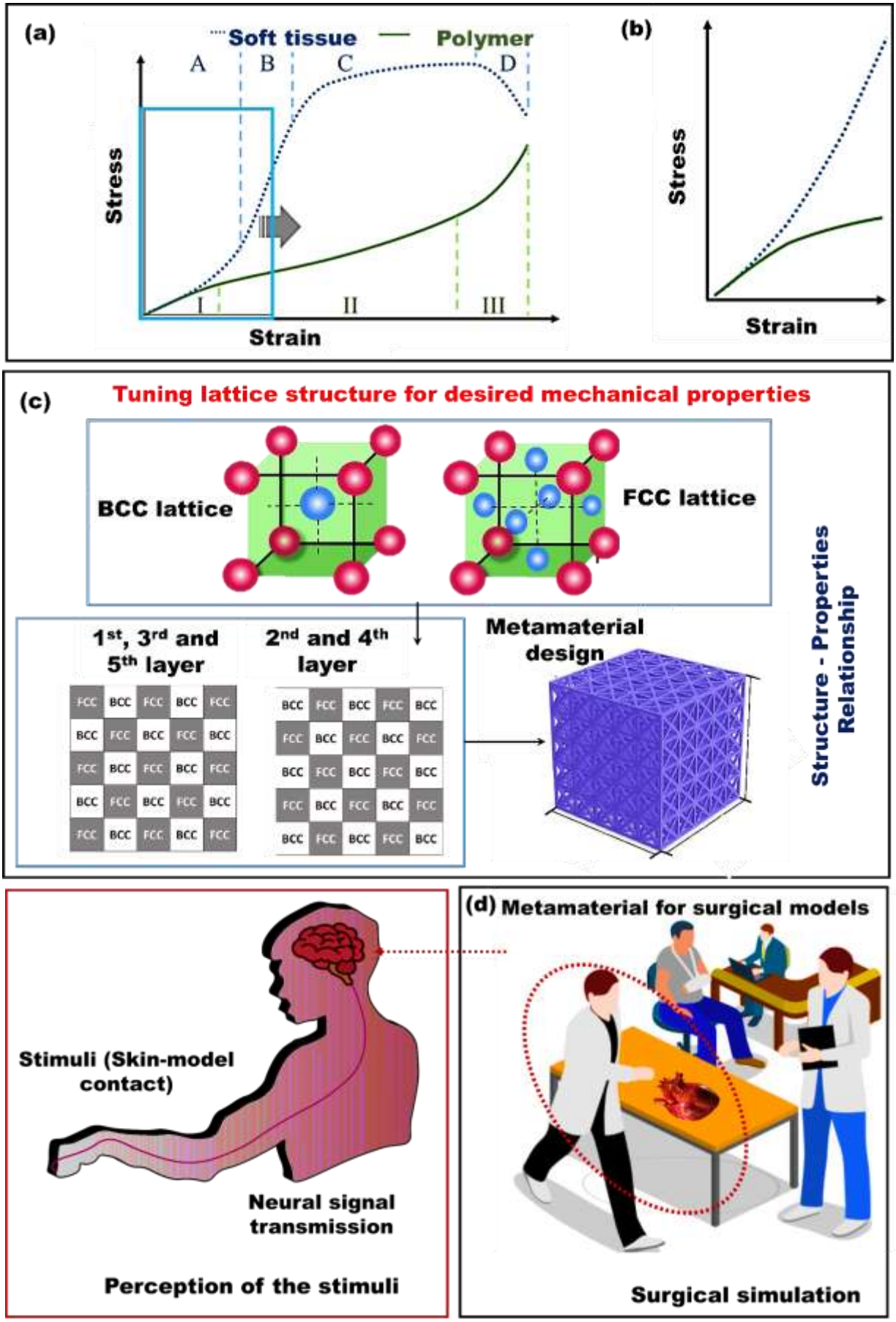

Figure 15. (a) Stress-strain behavior of soft tissue (dashed line) and polymer (solid line): The soft tissue curve includes region A (toe), B (elastic), C (plastic), and D (failure); the Polymer curve shows phase I (primary creep), II (secondary creep), and III (tertiary creep). (b) Enlarged view focusing on the strain range relevant to most tissue-mimicking phantom applications; Figure reproduced from Wang et al. [348] with permission from Elsevier, copyright (2022) (c) Unveiling the Structure-Property Connection: Tailoring the spatial arrangement of lattice cells for desired metamaterial properties ; Figure reproduced from Rahimi et al. [350] with permission from Springer Nature, copyright (2022) (d) Metamaterials in surgical models to attain tactile feedback during surgical simulations; Figure reproduced from Ren et al. [354] with the permission from John Wiley and Sons, copyright (2022)

4.2.3 4D printing towards the development of smart models and implants

3D printing is extensively employed in surgical planning because it can produce complex shapes tailored for use in surgical prototypes, surgical guides, and implants. However, most 3D-printed materials are static and cannot autonomously alter or adjust their characteristics in response to the surrounding dynamic environment.[357] Several studies have demonstrated accurate partial nephrectomies using 3D-printed renal cancer models from MRI data to design surgical plans ahead of laparoscopic surgery. However, these studies cannot accurately translate the surgical plan onto the patient during the procedure, reducing their feasibility for immediate laparoscopic surgery. 4D printing technology enhances 3D-printed models by incorporating active and responsive functionalities, with the distinction between 3D and 4D printing outlined in **Table 5**. 4D printing creates dynamic 3D constructs that evolve. There are two main approaches. The first involves shape-changing constructs, where materials and cells respond to stimuli, causing the printed object to change shape or function.[358] A key example is using materials with an irreversible shape-memory effect for minimally invasive surgery, allowing insertion in a temporary form before expanding into a stable structure. The second approach focuses on dynamic tissue engineering, where scaffolds and grafts mimic human tissue's natural, reversible movements by responding to stimuli. This approach can contribute to surgical planning by providing more realistic preclinical models that simulate tissue behavior under physiological conditions. These models help surgeons anticipate how tissues will respond to interventions, improving the precision of surgical procedures. Essentially, the first approach creates structures that change shape once, while the second enables repeated shape transformations.[359] Like Ock et al.[360] developed a portable, self-expanding surgical guide using 4D printing with shape-memory polymer materials based on medical imaging for laparoscopic partial nephrectomies. The 4D printed surgical guide enhances surgical accuracy and shortens procedure time by marking the resection line on the kidney before clamping blood vessels. It can pass through a laparoscopic port and regain its original shape with heated water, making it suitable for laparoscopic or robotic surgery. Its ability to fit through the trocar and restore its shape is crucial for clinical use. Technical tests confirmed its shape and tumor-targeting accuracy before and after compression. The 4D printed surgical guide demonstrated shape accuracy before compression and after restoration, with limits of agreement between −2.20 to 2.10 mm and −0.94 to 1.04 mm, showing no significant differences between guides. The marking accuracy errors before and after compression ranged from −2.60 to 1.70 mm and −2.20 to 1.80 mm, with no significant differences among operators ($p = 0.899$ and 0.992). These results confirm that novice surgeons can achieve accurate and consistent surgical outcomes using the 4D printed surgical guides.

4D printing technology offers promising advancements in designing adaptive surgical tools that respond to environmental changes, improving precision and control during intricate procedures. Adapting shape and stiffness is vital for surgical tools to effectively conform to diverse anatomical structures and surgical needs, helping to minimize potential harm to nearby tissues. For instance, GE et al.[361] developed a 4D-printed surgical gripper capable of adjusting its shape and stiffness in response to the environmental stimuli within the body, allowing it to navigate confined spaces, handle delicate tissues, and minimize the risk of damage during surgical procedures. Zarek et al. [362] used a 4D printing approach to fabricate personalized endoluminal cylindrical stents to treat central airway obstruction. Methacrylated polycaprolactone (PCL-MA) is a stimuli-responsive biomaterial used for fabricating stents via the SLA method. The PCL-MA stent changes from a closed state at room temperature to an open state at the human body temperature (37°C). By accurately aligning with the arcade structure of the patient and cartilaginous ring positioning, this approach reduces the risk of migration, a common complication during stent placement. The personalized design ensures a precise fit at the damaged site, enabling minimally invasive insertion and optimal stent placement, leading to better patient outcomes. Kim et al.[363] fabricated 4D-printed polyurethane-based bifurcated stents via the FDM process. The use of polyurethane activates the shape memory effects at 55 °C. The stent deforms from an open “Y”-shaped configuration to a temporary metastable closed configuration in the shape of an “I”. During this transition, the multiple branches of the stent converge into a single tube with a smaller diameter. Thus, the 4D-printed stent can pass through the central vessel in its temporary metastable configuration. Once it reaches the target vessel's bifurcation, it can be returned to its original "Y"-shaped configuration by applying a second specific stimulus, raising the temperature to 60 °C. Through 4D printing, stents can be implanted with minimal invasion at the specific bifurcation site, improving the success rate of stent insertion operations in medicine. Apart from stent placement, treating missing or damaged teeth can also benefit from 4D printing. The changing nature of gums and bones around dental prostheses needs careful attention during the design and placement of bridges. Khorsandi et al.[162] demonstrated that 4D printing technology, using shape memory polymers, improves denture flexibility by automatically adjusting to changes in the mouth, thereby reducing potential issues during maxillofacial surgeries. Unlike traditional dentures that require frequent adjustments due to changes in bone structure and pressure, these 4D-printed dentures adapt more effectively to mouth conditions, enhancing patient's comfort and durability of dentures.

Challenges of 4D printing

The emergence of 4DP technology has significantly changed the application of intelligent, tunable materials in fields like regenerative medicine and surgical planning.[364] While 4D printing holds great potential, it is essential to acknowledge the limitations and challenges that prevent its widespread adoption. The development of multi-material and multi-functional 4DP printing technology to create intelligent, tunable materials is still in the early stages and faces several obstacles. The main challenge in 4D printing technology, especially in the biological field, is material limitations. The range of printable materials is limited, and their compatibility for mixing to create multi-component structures is restricted. Biocompatible stimuli-responsive materials that react to physiological signals are crucial for surgical planning, enabling dynamic patient-specific models that enhance preoperative assessment and personalized treatment strategies. Most materials are unsuitable for medical use because they are not biocompatible, do not respond to stimuli, or only respond to specific signals.[359] Besides biocompatibility, biodegradability is crucial in 4D bioprinting and 4D printing with materials like shape-memory polymers. The irreversible shape-memory effect allows for a snug fit, enabling minimally invasive insertion and precise stent placement. However, it complicates removal after healing. Since, permanent stents may lead to hyperplasia, rapidly degradable materials ensure safe removal. There is a need to develop innovative biocompatible and biodegradable materials that can be printed, combined, and respond to various stimuli to overcome these barriers.[365]

The second challenge lies in design-related constraints. The limitations of software capabilities and the inability to control the timing and response rates of materials to stimuli in body conditions are significant obstacles to 4D printing.[366] The third challenge involves technology-related limitations, such as integrating multiple materials, scalability, and achieving high accuracy and resolution. Furthermore, the need for efficient supply chains for raw materials, tools, and infrastructure for large-scale manufacturing and distribution of 4D-printed products increases production costs. These challenges can delay the transition of 4D printing into mass production, and these need to be considered. Overall, 4D printing for surgery has the potential to transform healthcare. Despite challenges, ongoing innovation and collaboration are accelerating progress, paving the way for significant advancements in medicine and biotechnology.

Table 5 Comparisons of 3D and 4D printings

Characteristics	3D printing	4D printing
Principle	Layer-by-layer fabrication of static structures [367]	Shape-changing properties are integrated in layer-by-layer fabrication [368]
Materials used	Plastics, metals, ceramics, composites[369]	Shape-memory polymers, hydrogels, stimuli-responsive composites, metals, and ceramics [370]
Advantages	Personalization, intricate geometry, and minimized waste [370]	Enhanced functionality, flexibility, and responsive behaviour[371]
Complexity	Confined to static structures [372]	Dynamic structures with time-dependent shape transformation [371]
Applications	Prosthetics, implants, tissue scaffolds, medical devices[373]	Soft robotics, self-deploying implants, etc.[374]

4.2.4 AM and AI: An outlook towards synergetic integration

Artificial Intelligence (AI) is essential in elevating the quality of surgical simulations, which are gaining popularity as a valuable tool for enriching the training experiences of surgeons [375]. AI can be applied throughout all stages of 3D surgical models, from pre-printing (such as image processing, computer-aided design, material selection, and setting printing parameters) to the printing process (including method selection, defect control, and failure identification) and finally to post-printing (for quality inspection and real-time monitoring).[297]

Data preparation for 3D printing of surgical models

3D printing anatomical models are highly beneficial in surgical planning, starting with high-quality DICOM files from CT/MRI scans for 3D visualization, segmentation, and mesh creation. Slice thickness under 2 mm ensures accurate rendering, as thicker slices lose fine details. Software like Amira®, Vitrea®, and MIMICS™ extracts the region of interest (ROI) by marking slices within a defined Hounsfield Unit (HU) range (-1024 to 3071). While artifacts in 2D sectioning can complicate interpretation, multiscale volume rendering, such as hierarchical micro imaging (1 µm resolution), aids in analyzing complex structures like soft tissues, blood vessels, and tumors. Nevertheless, manual contouring remains a tedious and time-intensive process, primarily because of the poor soft tissue contrast in CT images, which often results in inaccuracies and inconsistencies in distinguishing target regions from surrounding tissue.[376] For example, Becker et al.[377] noted that an expert could spend approximately 20 to 30 minutes manually segmenting the orbit on a single CT scan. Cooper et al.[378] noted that it typically required around 60 minutes to segment the orbit in a CT scan manually. However, ML, a branch of AI, mimics the human brain for complex

tasks, exploring image features using a data-driven approach to simplify functions like image segmentation.[379] ML-based multiorgan segmentation speeds up contouring and improves accuracy, facilitating online adaptive radiotherapy and enhancing clinical outcomes. Advanced ML algorithms, including convolution neural networks (CNNs), can now automate feature detection for image segmentation.[380] A CNN is a specialized ANN designed for grid-like data, such as images or audio. It processes the input through layers of convolution and pooling to extract key features, progressively reduce data size, and produce prediction outputs. For example, Zreik et al.[381] Patch-based CNN was used to segment the left ventricle (LV) in the cardiac CT angiography scans. The proposed method demonstrated high sensitivity and specificity, significant overlap, and minimal distance between the automatic segmentation and manual annotations, highlighting its accuracy and clinical relevance in medical imaging. This reduced the blur border issues in MRI and enhanced the reliance on medical imaging for producing 3D models for soft tissue surgery.

Generative AI for Imaging modality

Despite the success of supervised learning approaches such as CNNs, these methods often require a large volume of annotated data and rely on pixel-wise classification through the encoder-decoder framework.[382] This dependency limits their flexibility and scalability across diverse clinical applications. Generative AI (GenAI) is gaining attention in medical image data preparation to overcome these issues. [383] Generative adversarial networks (GANs), a subset of Generative AI (GenAI), are recognized as promising medical image analysis tools capable of producing high-quality images that maintain structural accuracy and support potential clinical use.[384] In segmentation tasks, the generator of a GAN is trained to take an input image and create a mask that designates a class label for each pixel in the image. One advantage of employing GANs for segmentation is their capacity to generate high-resolution results with sharp details, making them visually appealing.[385] Introduced by Goodfellow et al.[386], GANs consist of two competing neural networks—a generator that creates synthetic data and a discriminator that distinguishes real from fake. In medical imaging, GANs are highly effective in image reconstruction and enhancement. For instance, the conditional filtered generative adversarial network (CFGAN) achieves high-fidelity, multi-scale reconstruction with high peak signal-to-noise ratio (PSNR), high structural similarity index measure (SSIM), and low frechet inception distance (FID) scores.[387] Compared to other GAN-based methods, its higher SSIM and lower FID values indicate improved image quality and greater diversity. Wavelet-based GANs enhance structural similarity and textural details, while generator–discriminator frameworks help to mitigate hardware limitations and motion artifacts.[388] However, GANs still face limitations like over-smoothing, mode collapse, high computational cost, limited clinical validation, and inconsistent performance across datasets.

To overcome some of these limitations, diffusion models have emerged as a powerful alternative. As proposed by Sohl-Dickstein et al.[389], diffusion models learn data distributions through a forward process that incrementally adds noise and a reverse process that reconstructs the original input. These models offer promising medical image reconstruction and enhancement capabilities, with notable robustness in detail preservation. Discrete residual diffusion mitigates over-smoothing and mode collapse seen in GANs, while wavelet diffusion improves structural detail, aiding Alzheimer's diagnosis.[390] Mao et al.[391] enhanced multi-contrast MRI using a disentangled U-Net with squeeze-and-excitation modules and curriculum learning. Wang et al.[392] propose the Hierarchical Feature Extraction (HiFE) model for generating high-fidelity in-between slices, improving segmentation accuracy. Additionally, Mirza et al.[393] and Cao et al.[394] demonstrate task adaptability by combining forward and reverse diffusion for image upscaling and k-space acceleration. The integration of diffusion models is driving a shift in medical imaging toward more reliable, high-quality, and task-specific solutions in healthcare. However, their practical use still faces challenges, such as high computational demand, slow sampling rates, limited generalization due to single-level wavelet transforms, phase wrapping issues, and dependence on precise noise estimation.[395] Overall, Generative models, including GANs and diffusion models, have advanced MRI by improving image resolution, reducing noise, shortening scan times, and fixing gaps between slices. Combined with other AI techniques, these improvements enhance diagnostic accuracy, increase patient throughput, and help address MRI capacity issues in healthcare.

Part quality/process optimization

Process optimization occurs when new materials or processes are developed to improve 3D-printed surgical models.[395] By adjusting the process parameters, specific qualities can be achieved. A process-structure-properties (PSP) relationship database for a particular AM process and material helps in selecting the correct parameters (temperature, layer thickness, etc.) based on the available information.[396] The high dimensionality of process parameters makes the PSP relationship complex, hindering the development of a governing mathematical formula. ML facilitates the efficient determination of ideal values for parameters like layer thickness, print speed, and temperature, minimizing the reliance on manual adjustments and decreasing material waste. Manually adjusting parameters for the AM process may lack efficiency.[397–399] When trained on data sets, ML models can predict optimal values for parameters such as layer thickness, print speed, and temperature.[400] Moradi et al.[401] enhanced the performance of 3D printing of PLA by analyzing thickness, toughness, and fabrication time in dog bone samples. The parameters considered include printing temperature, infill density, and layer thickness. They used ANN and Artificial Neural Network—Genetic Algorithm (ANN-GA) to predict the studied properties. ANN-GA achieved higher accuracy than ANN, improving part thickness by 11.5%, toughness by 7.5%, and production cost by 4.5%. The study highlighted that reducing production costs is possible without compromising the desired properties, with the interaction between layer thickness and infill density being the most significant factor affecting part thickness. Zhang et al.[402] presented a novel data-driven predictive modelling method to explore the structure-property relationship of carbon fiber-reinforced polymers (CCFRPs) produced by FDM. The ensemble learning-based model predicted the flexural modulus of CCFRP specimens based on design factors like layer number, contours, and infill pattern. It combined eight base learners: linear regression, least absolute shrinkage, and selection operator, multivariate adaptive regression splines, generalized additive model, k-nearest neighbours,

Support Vector Machine, extra trees, and Xtreme Gradient Boosting. The model accurately predicted flexural strength, achieving a minimum root mean square error of 9.87%, minimum relative error of 7.75%, and maximum R^2 of 96.99%.

In-situ monitoring for quality control

Using sensors for closed-loop feedback control in in-situ monitoring can improve the consistency and reliability of 3D-printed parts.[403] Identifying flaws during printing enables corrective actions, making it easier to qualify components during the process. AM quality monitoring research has primarily focused on two areas. The first uses pyrometers and high-speed cameras to capture melt pool temperature data, while the second analyses the workpiece using optical cameras, near-infrared thermal CMOS cameras, photodiodes, and x-ray phase-contrast imaging (XPCI) or x-ray CT. This allows the identification of the defects at each stage. The presence of any flaws in the construction process is subsequently deduced using these metrics. ML algorithms have been applied using visual or sensor-generated data. Gobert et al.[404] indicated that Image quality, illumination, and the quantity of sensors or cameras are crucial factors in enhancing the effectiveness of in-situ monitoring. Since most in-situ monitoring relies on cameras to collect data on the printing process, computer vision (CV) capabilities are crucial for fault detection. In this regard, CNN is gaining significant attention compared to the other ML techniques. For example, using the CNN model, interlayer irregularities resulting from incorrect nozzle height and calibration can be analyzed. A mounted camera was used to monitor nozzle positions, categorized as Good, High, High+, and Low. Their CNN model achieved 97.8% accuracy on test data and 91% on validation data.

AI in Post printing

High material uniformity is essential in biomedical implants to ensure structural integrity and compatibility with biological systems.[405] Implant performance can be compromised by issues like porosity, microcracks, or irregular distribution of the alloying elements, potentially leading to harmful biological effects.[406] AI approaches such as ML and deep learning have effectively detected material inconsistencies. CNN has been applied to analyze X-ray and CT scan data, allowing accurate detection of microstructural defects in titanium and cobalt-chromium implants.[407] In addition, GANs have been used to create ideal, flaw-free material structures that enhance model training and improve defect identification accuracy. Beyond defect detection, AI also assesses dimensional accuracy and fit. Tuker et al. [408] performed tolerance verification to ensure that stereolithography (SLA) dental guides accurately fit the mandible through dimensional analysis using AI. Dimensional apertures of SLA-produced dental guides were analyzed for the implant procedures, and ANNs were used to classify results based on the design flexibility offered by SLA. Using the Mimics program, a 3D anatomical model was created from the patient-specific CBCT data, and three dental guide designs were developed with 3-Matic. These guides and a mandible model were produced using an SLA 3D printer, and dimensional data were captured with a 3D scanner. 3D registration between the mandible and dental guides determined the dimensional aperture values. The dataset was analyzed using Jamovi 2.0.0 and ANNs. The results showed that the aperture values were consistent, indicating a good fit with the mandible. Among the three guide designs, Guide 3 provided the best fit. Integrating AI into post-printing helps accurately measure dimensions, improve the fit of designs, and maintain consistency between printed parts. It also adds automation to the process, making adopting personalized 3D-printed solutions in clinical settings easier and faster.[397]

AI driven design optimization for surgical implants

Modern implant design aims to restore natural function while minimizing complications from mechanical mismatch. In bone repair, this mismatch often leads to stress shielding, where the high stiffness of traditional implants reduces load transfer to surrounding bone, impairing remodeling and causing tissue degeneration. The rising incidence of complex fractures, often linked to osteoporosis and aging populations, further exposes the limitations of standard bone plates and highlights the need for patient-specific solutions. Additive Manufacturing (AM), with its layer-by-layer fabrication process, enables such customization through advanced methods like Topology Optimization (TO) and Generative Design (GD). Xua et al. [409] created patient-specific bone plates using topology optimization and generative design methods, which were fabricated using Directed Energy Deposition. The designs reduced the weight of the bone plates significantly by 43.7 % and 44.2 % for the two generative design versions, GD1 and GD2, and by 36 per cent for the topology optimization version, TO1. These improvements were achieved while also enhancing the strain performance of the implants.

However, physics-based approaches like TO and GD rely on predefined objectives and assumptions, which may limit their ability to address complex anatomical variability or fully personalized needs. Variational autoencoders (VAEs) are generative models that can bridge this gap by learning from large anatomical and mechanical datasets to generate tailored implant geometries. [410] For example, the Swap Disentangled Variational Autoencoder (SD-VAE) can isolate specific anatomical sub-units and assess their influence on the overall shape, supporting precise diagnosis and surgical planning. Foti et al. [411] demonstrated how SD-VAE can analyze and generate 3D craniofacial shapes in syndromic patients, simulate surgical outcomes, and enhance clinical decision-making. Yet, relying on AI-generated norms in planning raises ethical concerns, as the model's perception of "normal" or "ideal" reflects biases within its training data. Although the interpolations step helps reduce this effect, it cannot eliminate such bias. Despite this, integrating AI with conventional methods represents a step toward more personalized, adaptive, and data-driven orthopedic treatments.

Digital Twin and Generative AI for enhancing surgical planning

3D/4D-printed models have improved surgical precision by offering patient-specific anatomical replicas. These models help reduce surgical time and enhance outcomes by allowing surgeons to practice complex procedures and better understand intricate structures with technological advancements.[412] However, sometimes, these models do not provide haptic feedback, such as kinesthetic (force) and cutaneous (tactile) sensations, which are vital for surgeons during procedures.[413] Additionally, they offer limited real-time predictive insights, making them less effective for immediate decision-making during surgery. Unlike using only 3D/4D models, digital twins (DT) can replicate dynamic processes and incorporate real-time data, enabling continuous patient monitoring and predictive analysis.[414] DT

technology connects the physical and digital worlds, addressing the limitations of AR/VR and 3D/4D-printed models. It enhances surgical advancements by complementing physical models with virtual replicas of patients or surgical environments.[415]

"Digital Twin-Guided Surgery (DTGS)" utilizes DT technology to optimize perioperative processes, enhancing surgical training, planning, precision, safety, and patient care.[416] The novelty of DTGS lies in its real-time virtual model, which dynamically represents the relationship between the organs (e.g., kidney, brain, eye) of the patient, their physiological parameters (e.g., blood pressure, heart rate, oxygen levels), and surgical actions (e.g., cutting, suturing, ablation), providing a comprehensive view of the procedure. DTGS begins with data collection from the physical twin, such as tissues, organs, or surgical tools. This can occur before creating the virtual DT, offline, or in real time during surgery.[417] Data is collected from medical images (CT, MRI, X-ray, ultrasound), sensors, medical devices, patient records, biomarkers, and lab tests. This data can be stored in electronic databases, including cloud systems, ensuring access for the 3D modelling team, clinicians, and hospital staff. AI analyzes the data to construct the virtual model. Once the virtual model is created, extended reality technologies improve visualization and interaction and provide haptic feedback for the surgical team. Real-time data acquisition and analysis provide the surgical team with live updates, supporting informed intraoperative decision-making (**Figure 16**)[418]. For example, the DT offers real-time insights on optimal tissue-cutting paths to minimize accidental damage while predicting blood flow changes and potential blood loss, such as when a vessel is clamped or an organ is partially severed. Although research has explored DT applications, frameworks, and tools, a gap remains in automating their development and updates, as the process is complex, time-consuming, and heavily dependent on existing data.[419] Therefore, the next stage of this advancement involves integrating GenAI.

GenAI, powered by deep learning, can enhance DT development by generating data and refining models.[420] This approach improves efficiency, accuracy, and reliability while streamlining the process. By creating synthetic data that mirrors real-world patterns, GenAI addresses data scarcity in surgical planning, enabling more comprehensive testing of treatment outcomes.[421] In clinical applications, GenAI models learn from patient data, including vitals, lab results, and diagnoses, to simulate future patient trajectories. This predictive capability helps surgeons anticipate treatment outcomes and optimize interventions during the surgery. Additionally, automating tasks like data preprocessing and model initialization accelerates development, making DT more efficient and cost-effective.[422] Overall, Integrating GenAI into DT technology enhances surgical precision, safety, and patient care while enabling telesurgery and advancing training for both novice and experienced surgeons. Therefore, implementing digital technologies in future surgery is inevitable.[423]

Challenges of AI in AM

Integrating AI into 3D and 4D printing holds great promise for enhancing precision, efficiency, and customization. ML-based computational models offer greater efficiency than traditional physics-based simulations. Studies have shown that ML models can predict the stress of a 3D printed component in about 0.47 seconds, while finite element models (FEM) take 5–10 hours.[424] Similarly, CNN models operate in milliseconds, compared to minutes for FEM. However, several challenges limit its full potential.[425] Despite the speed advantages, the need for high-speed imaging and large datasets increases computational demands and costs. Optimizing ML models also raises these costs, making it challenging to balance efficiency with cost-effectiveness in AM.[426] Another major hurdle in using AI to predict material properties in 3D printing is the lack of reliable data on new biomaterials. Many of these materials are still under research, meaning there is insufficient data to train machine learning models effectively. Applying advanced generative techniques to produce synthetic posture data may effectively addresses limitations caused by insufficient datasets in traditional AI techniques. The generated synthetic data resemble real data in many aspects. However, accurately assessing their quality remains challenging without a clear benchmark dataset.[427]

Additionally, it is vital to note that GenAI has various limitations like attribution issue.[428] The attribution problem in generative AI refers to the difficulty in understanding and explaining how these models reach their decisions, particularly in healthcare. These deep learning models produce complex outputs, such as patient data and treatment plans, but function as black boxes, making their decision processes unclear. This lack of transparency can hide biases, potentially worsening health disparities. It also raises ethical and legal concerns, as it becomes hard to assign responsibility for mistakes or harm. To tackle this, methods like attention mechanisms, saliency maps, and post-hoc analysis are being explored to make AI decisions more interpretable. Improving attribution enables healthcare providers to better assess AI reliability and biases, ensuring safer and more equitable use. Integrating AI into healthcare requires smooth compatibility with electronic health records, decision-support tools, and existing IT systems.[424] For real-time applications, AI must quickly process data using optimized algorithms and reliable computing resources. At the same time, applying AI and machine learning in additive manufacturing raises concerns about data security, intellectual property, bias, transparency, and effects on jobs. Addressing these challenges by protecting privacy, preventing misuse, managing automation impacts, and improving cybersecurity is essential for successful and widespread adoption.[429]

Several reviews in the literature highlight the contributions of AL and ML to advancing various aspects of 3D and 4D printing, such as monitoring, defect detection, and parameter control, reflecting a significant rise in publications on AI applications in AM in recent years, as shown in **Figure 17a**.[430] The literature highlights the need to integrate AI and ML in AM effectively. While AI and ML enhance certain quality control aspects in AM and surgical planning, the Robotic Automation Process creates a seamless system by combining these technologies to improve the entire quality assurance process from beginning to end.[431] AI-driven AM improves surgical planning by combining real-time diagnostics with patient history analysis while optimizing the development and use of 3D and 4D printed models.[432] By providing personalized surgical recommendations, these systems ensure that printed models are designed to meet needs of the patients. For example, suppose a patient with cardiovascular conditions requires complex reconstruction using 3D-printed implants. In that case, these advance technologies can

analyze their medical history and imaging data to enhance implant design and refine the surgical approach, reducing anesthesia-related risks. This holistic approach ensures that surgical plans and printed models are tailored to the patient's overall health, resulting in more precise and effective procedures (**Figure 17b**).[431] These developments emphasize the importance of incorporating AI in AM. This integration is expected to lead to "5D printing," where AI acts as the fifth dimension, enhancing the capabilities of 3D and 4D printing in surgeries looking ahead (**Figure 17c**).[433] In the future, 5D printing could play a key role in surgical planning by using AI to track real-time health changes, predict complications, and enhance precision in patient-specific implants. This approach may also support robotic-assisted surgeries and enable the development of advanced prostheses for improved patient care.[434,435]

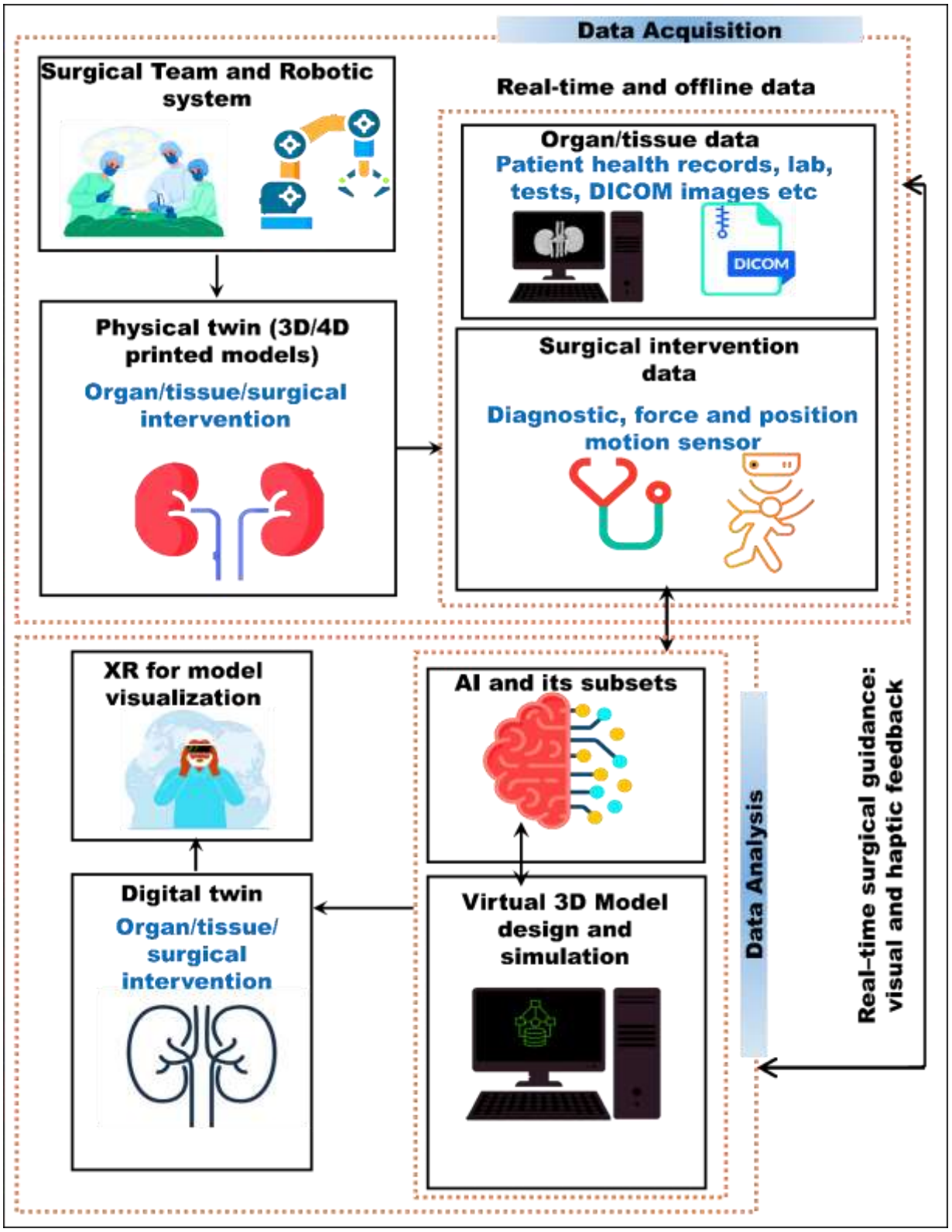

Figure 16 Concept of digital twin-assisted surgery, Figure reproduced from Asciak et al. [418] with permission from Springer Nature, copyright (2025)

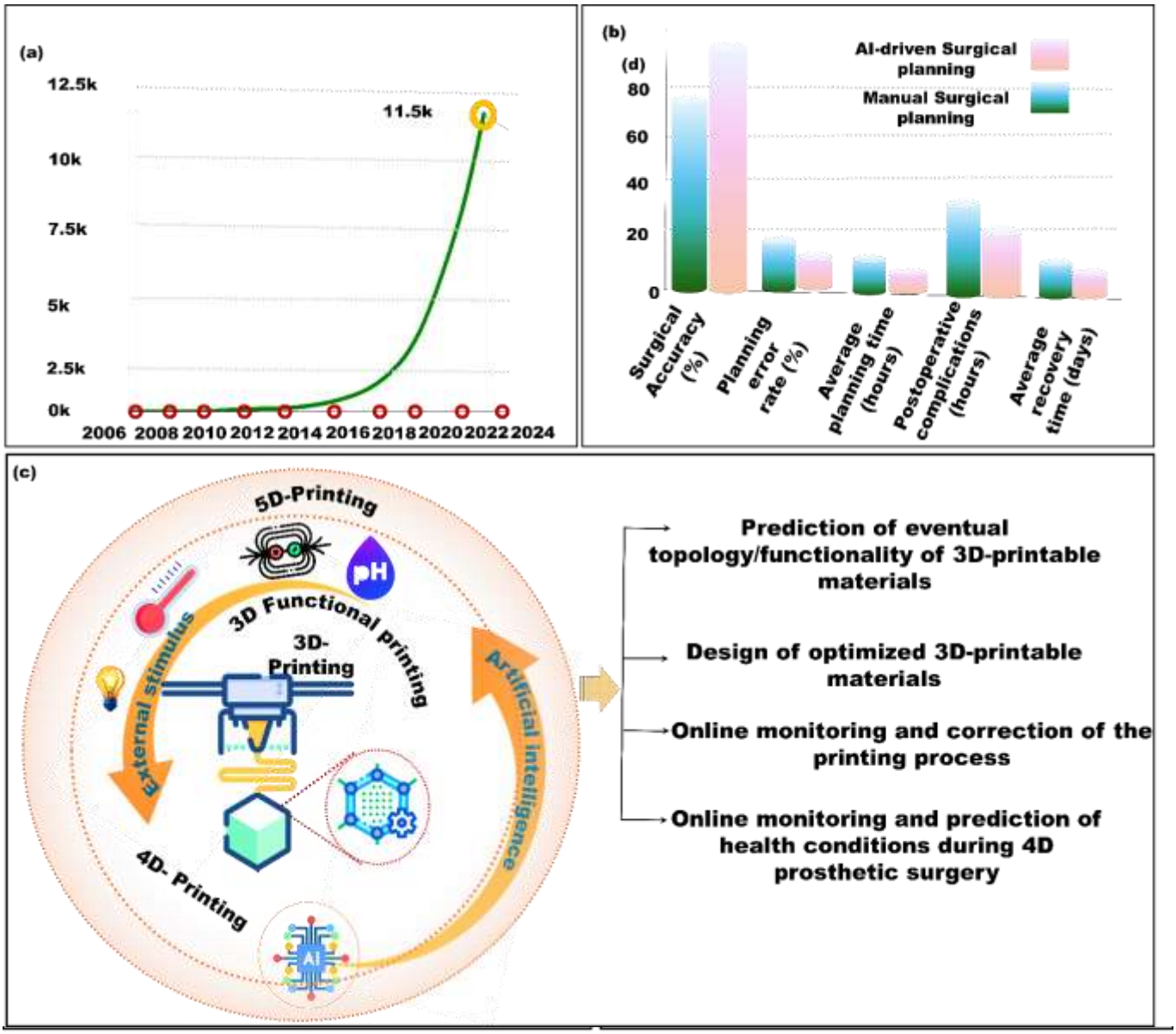

Figure. 17 (a) The count of publications on AI approaches in 3D printing from 2006 to 2024, sourced from the Scopus database, Figure reproduced from Grira et al.[430] with permission from Elsevier, copyright (2025) (b) Advantage of AI-driven RPA in surgical planning (c) From 3D Functional printing to 5D printing via 4D: The advancement of AM in developing innovative constructs with targeted responsiveness, diverse functionalities, and potential applications of AI Integration in AM, Figure reproduced from Milazzo et al. [433] with permission from Wiley-VCH GmbH, copyright (2022)

Overall, surgeons can create models that closely resemble anatomical structures and biological functions of organs by integrating 3D bioprinting, soft robotics, tissue engineering, and AI with 3D and 4D printing **(Figure 18)**.[160] This comprehensive approach goes beyond traditional anatomical resemblance, providing a more profound understanding of the intricate dynamics and complexities of surgical procedures. Though this review integrates some related studies, as shown in **Table 6,** it offers ample scope for further discussion. Continued research and development in this field could revolutionize surgical planning and training, leading to better patient outcomes.

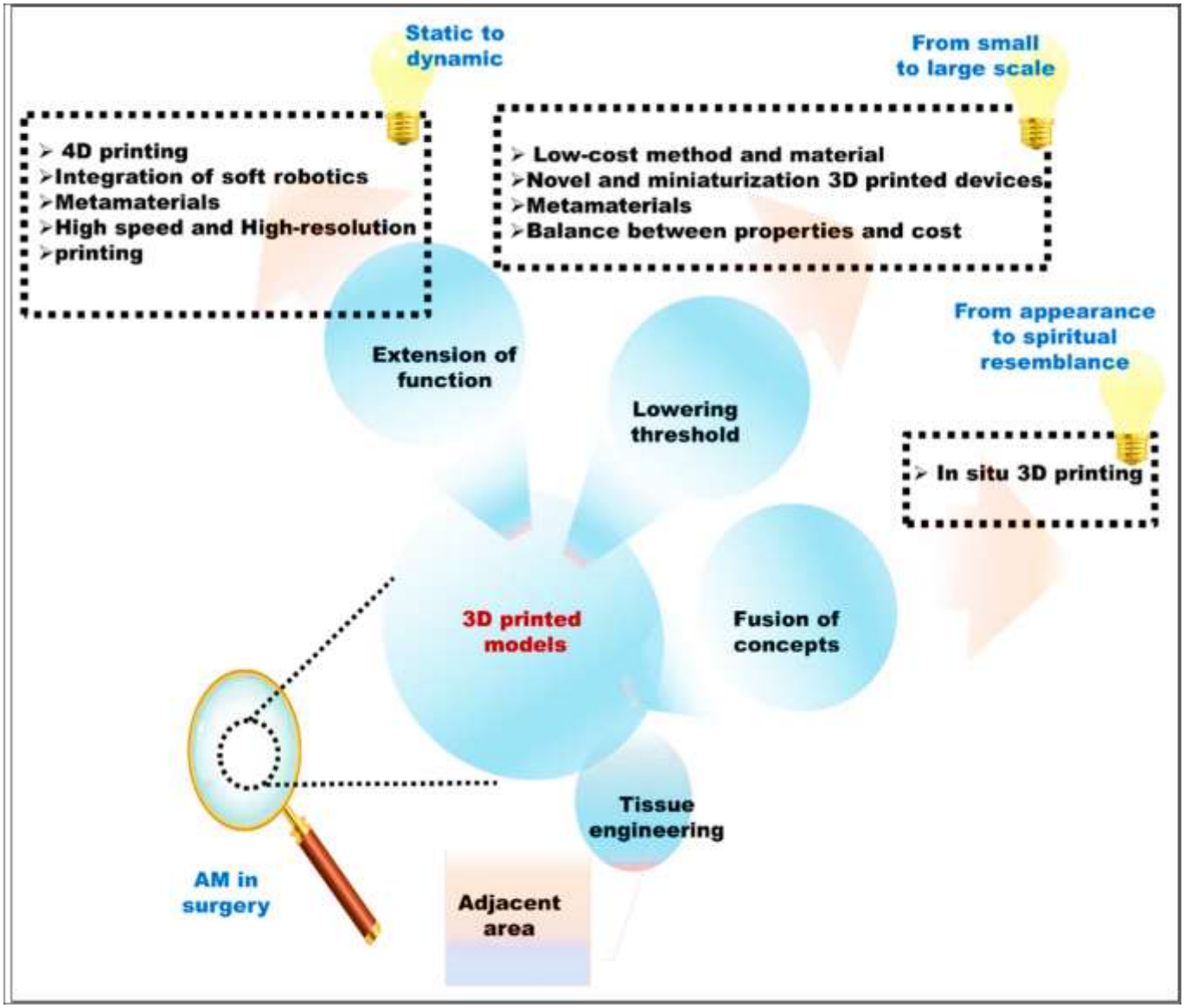

Figure 18. Expansion of the capabilities of 3D models for future advancement in surgical planning: Figure reproduced from He et al. [160] with permission from John Wiley and Sons, copyright (2021)

Table 6. Dynamic AM models for surgical applications

Advanced dynamic 3D model	Material	Advantages	References
Hand model	TangoPlus and support-filled metamaterial	Mimic human soft tissue has haptic properties and elasticity, enabling realistic hand phantom fabrication.	[352]
Cadaveric plantar fat	TangoPlus (FLX930) and support-filled metamaterial	Create nonlinear material from linear base material to mimic human soft tissue	[353]
4D printed surgical guide for laparoscopic surgery	Shape memory polymer resin	Self-expanding 4DP-KSG showed accurate and consistent targeting of kidney tumors.	[360]

4D-printed surgical gripper	Photo-curable methacrylate	Multimaterial grippers that have the potential to function as microgrippers that can grab objects	[361]
Endoluminal cylindrical stents	Methacrylated polycaprolactone	The personalized stent matched the arcade structure and cartilaginous rings, reducing migration, a common cause of tracheal stent failure.	[362]
Bifurcated stents	Polyurethane	The 4D-printed stent stays in a temporary shape to pass through the central vessel and returns to its "Y" shape at the target vessel.	[363]

5 Conclusion and Outlook

Additive manufacturing holds an enormous premise for patient-tailored surgical planning and the evolution of clinical tools. Pre-operative and intra-operative disease evaluation can be done with the help of 3D-printed, tangible anatomical models. Mock surgeries often allow the less experienced surgeons to eliminate the risk associated with their lack of first-hand experience during the surgery. The use of patient-specific 3D models in complex surgeries in cardiac, orthopedic, dentistry, cerebral, and gynecologic tissues has been demonstrated. The utilization of metamaterials in surgical models shows significant potential in enhancing haptic feedback. These 3D patient-specific models allow better pre-operative planning, intra-operative performance, surgeon expertise, and patient outcomes such as shorter surgery time and less intra-operative blood loss. However, it is necessary to transform conventional static 3D models into dynamic or beating models that closely resemble the biological functions of real organs, aiming for a high degree of similarity. 4D printing allows for the creation of structures that can change shape, behaviour, or function over time, opening new possibilities for dynamic and adaptive design in various fields. In accordance with the discussions in this review, the intersection of Artificial intelligence and 3D and 4D printing for surgical planning models is on the cusp of a game-changing transition. The convergence of these advanced technologies offers significant opportunities to enhance sustainable and environmentally friendly manufacturing processes for surgical models. Concerning future perspectives in this field, autonomous in-hospital biofabrication hubs represent a transformative direction for surgical planning. These advanced self-contained units within healthcare settings enable the on-demand fabrication of patient-specific biological constructs or implants. They integrate additive manufacturing technologies such as bioprinting and multi-material 3D printing with robotics, artificial intelligence (AI), and real-time imaging systems, allowing precise and personalized devices to be produced directly at the point of care. The process begins with AI-based segmentation of imaging data such as CT or MRI scans to generate three-dimensional models tailored to the patient's anatomy. Once the design is finalized, automated 3D printers fabricate the surgical models using biocompatible materials, including polymers, hydrogels, or living cells, with minimal human intervention. [436] Advancing these capabilities further, emerging innovations point towards developing nano cyborgs (miniaturized intelligent implants) that extend beyond static structural roles.[437] Fabricated using advanced 3D and 4D printing with multi-material and metamaterial strategies, these implants would autonomously navigate within the body, interact with the biological environment, and integrate seamlessly at the cellular level. They could deliver targeted therapies, support tissue repair in real-time, or provide continuous intraoperative diagnostics, significantly enhancing precision in complex surgical procedures. Apart from these smart patient-specific implants, these hubs can rapidly produce surgical guides, tissue scaffolds, and potentially bioprinted organs, each optimized for clinical use. AI-driven real-time monitoring ensures accuracy, material consistency, and sterility.[438] At the same time, automated quality control checks validate the integrity of each construct before surgical application. Seamless integration within the hospital workflow enables sterilization and direct delivery to the surgical team, significantly reducing waiting times and enhancing procedural accuracy. However, addressing manufacturing challenges, defining regulatory pathways, and further research and development are key to realizing the potential of additive manufacturing in surgery.

Author contributions

All the authors listed have made a substantial, direct, and intellectual contribution to the work and are approved for publication. More details on specific contributions from each author are available in supporting information on CRediT contributor roles.

Data availability

The authors declare that no primary research results, software or code have been included, and no new data were generated or analyzed as part of this review.

Funding and Acknowledgement

This work was supported by a start-up-research grant (SRG/2019/001504) and (SRG/2021/000859) from the Science and Engineering Research Board, Department of Science and Technology (DST), and the Ministry of Education (MOE), Government of India. The authors would like to thank Prince Sultan University for their support. The authors acknowledge the feedback and support from Prof. Seeram Ramakrishna, NUS Singapore, throughout the preparation of the manuscript.

Conflict of Interest

The authors declare there is no conflict of interest in publication of this review article. Kumar P. is one of the co-founders of Iota Design and Innovations Lab Private Limited, a company that provides 3D printing and prototyping services. Madhusmita Dash is an employee in Iota Design and Innovations Lab Private Limited work on sustainable materials for energy applications.

References

[1] Dublin, *The "Additive Manufacturing Market Size, Share, Trends, By Technology, By Material Type, By Application, and By Region Forecast to 2030,"* **2022**.

[2] I. Gibson, D. Rosen, B. Stucker, M. Khorasani, *Additive Manufacturing Technologies*, Springer International Publishing, Cham, **2021**.

[3] C. Li, D. Pisignano, Y. Zhao, J. Xue, *Engineering* **2020**, *6*, 1222.

[4] H. L. Stewart, J. H. Siewerdsen, B. B. Nelson, C. E. Kawcak, *Equine Vet. J.* **2021**, *53*, 872.

[5] T. Martín-Noguerol, F. Paulano-Godino, R. F. Riascos, J. Calabia-del-Campo, J. Márquez-Rivas, A. Luna, *Ann. Transl. Med.* **2019**, *7*, 684.

[6] A. Kantaros, F. Petrescu, H. Abdoli, O. Diegel, S. Chan, M. Iliescu, T. Ganetsos, I. Munteanu, L. Ungureanu, *Appl. Sci.* **2024**, *14*, 2550.

[7] S. L. D. Kanumilli, B. P. Kosuru, F. Shaukat, U. K. Repalle, *J. Med. Phys.* **2024**, *49*, 319.

[8] M. Soori, B. Arezoo, R. Dastres, *Cogn. Robot.* **2023**, *3*, 54.

[9] C. Shuai, X. Yuan, W. Yang, S. Peng, G. Qian, Z. Zhao, *Carbohydr. Polym.* **2021**, *262*, 117937.

[10] K. H. C. Li, C. Kui, E. K. M. Lee, C. S. Ho, S. H. Wong, W. Wu, W. T. Wong, J. Voll, G. Li, T. Liu, B. Yan, J. Chan, G. Tse, I. D. Keenan, *MedEdPublish* **2017**, *6*, 92.

[11] E. Ghizoni, J. P. S. A. S. de Souza, C. E. Raposo-Amaral, R. Denadai, H. B. de Aquino, C. A. Raposo-Amaral, A. F. Joaquim, H. Tedeschi, L. F. Bernardes, A. L. Jardini, *World Neurosurg.* **2018**, *109*, 356.

[12] L. Kiraly, M. Tofeig, N. K. Jha, H. Talo, *Interact. Cardiovasc. Thorac. Surg.* **2016**, *22*, 238.

[13] L. Kiraly, N. C. Shah, O. Abdullah, O. Al-Ketan, R. Rowshan, *Biomolecules* **2021**, *11*, 1703.

[14] F. Proietti, R. S. Flammia, L. C. Licari, E. Bologna, U. Anceschi, M. C. Ferriero, G. Tuderti, R. Mastroianni, A. Brassetti, G. Simone, C. Leonardo, *J. Clin. Med.* **2024**, *13*, 1590.

[15] N. Wake, A. B. Rosenkrantz, R. Huang, K. U. Park, J. S. Wysock, S. S. Taneja, W. C. Huang, D. K. Sodickson, H. Chandarana, *3D Print. Med.* **2019**, *5*, 4.

[16] A. Schweizer, F. Mauler, L. Vlachopoulos, L. Nagy, P. Fürnstahl, *J. Hand Surg. Am.* **2016**, *41*, 59.

[17] E. M. Lindquist, J. M. Gosnell, S. K. Khan, J. L. Byl, W. Zhou, J. Jiang, J. J. Vettukattil, *Ann. 3D Print. Med.* **2021**, *4*, 100034.

[18] R. Toms, R. Singh, in *Princ. Neonatol.*, Elsevier, **2024**, pp. 299–316.

[19] A. Baroutidou, N. Otountzidis, A. S. Papazoglou, D. V. Moysidis, A. Kartas, L. Mantziari, V. Kamperidis, A. Ziakas, G. Giannakoulas, *J. Am. Heart Assoc.* **2024**, *13*, DOI 10.1161/JAHA.123.032102.

[20] Q.-L. Xu, H. Li, Y.-J. Zhu, G. Xu, *J. Cardiothorac. Surg.* **2020**, *15*, 163.

[21] M. Ghidinelli, D. Höntzsch, B. Atici, S. Crespan, *3D Print. Med.* **2025**, *11*, 2.

[22] A. Tejo-Otero, I. Buj-Corral, F. Fenollosa-Arté S, **n.d.**, DOI 10.1007/s10439-019-02411-0.

[23] A. Pietrabissa, S. Marconi, E. Negrello, V. Mauri, A. Peri, L. Pugliese, E. M. Marone, F. Auricchio, *Surg. Endosc.* **2020**, *34*, 1.

[24] R. Told, Z. Ujfalusi, A. Pentek, M. Kerenyi, K. Banfai, A. Vizi, P. Szabo, S. Melegh, J. Bovari-Biri, J. E. Pongracz, P. Maroti, *Mater. Des.* **2022**, *223*, 111119.

[25] M. Gholipourmalekabadi, S. Sapru, A. Samadikuchaksaraei, R. L. Reis, D. L. Kaplan, S. C. Kundu, *Adv. Drug Deliv. Rev.* **2020**, *153*, 28.

[26] S. Petersmann, M. Spoerk, W. Van De Steene, M. Üçal, J. Wiener, G. Pinter, F. Arbeiter, *J. Mech. Behav. Biomed. Mater.* **2020**, *104*, 103611.

[27] M. Wilkat, J. Lommen, M. Rana, N. Kübler, T. Wienemann, S. M. Braß, R. T. Ziegler, A. Mazrekaj, A. Knapsis, H. Schelzig, M. U. Wagenhäuser, A. Arnautovic, *J. Clin. Med.* **2024**, *13*, 1309.

[28] N. Mamidi, F. F. De Silva, A. B. Vacas, J. A. Gutiérrez Gómez, N. Y. Montes Goo, D. R. Mendoza, R. L. Reis, S. C. Kundu, *Adv. Healthc. Mater.* **2024**, *13*, DOI 10.1002/adhm.202401195.

[29] S. Yuan, F. Shen, C. K. Chua, K. Zhou, *Prog. Polym. Sci.* **2019**, *91*, 141.

[30] M. A. A. Ansari, A. A. Golebiowska, M. Dash, P. Kumar, P. K. Jain, S. P. Nukavarapu, S. Ramakrishna, H. S. Nanda, *Biomater. Sci.* **2022**, *10*, 2789.

[31] D. Vaes, P. Van Puyvelde, *Prog. Polym. Sci.* **2021**, *118*, 101411.

[32] W. L. Ng, G. L. Goh, G. D. Goh, J. S. J. Ten, W. Y. Yeong, *Adv. Mater.* **2024**, DOI 10.1002/adma.202310006.

[33] A. Raja, S. T. Chukka, R. Jayaganthan, *Metals (Basel).* **2020**, *10*, 1349.

[34] W. Lee, C. Xu, H. Fu, M. Ploch, S. D'Souza, S. Lustig, X. Long, Y. Hong, G. Dai, *Adv. Funct. Mater.* **2024**, DOI 10.1002/adfm.202313942.

[35] M. Zu, G. Liu, H. Xu, Z. Zhu, J. Zhen, B. Li, X. Shi, M. Shahbazi, R. L. Reis, S. C. Kundu, G. Nie, B. Xiao, *Adv. Mater.* **2024**, *36*, DOI 10.1002/adma.202409138.

[36] R. Sun, H. Chen, J. Zheng, T. Yoshitomi, N. Kawazoe, Y. Yang, G. Chen, *Adv. Healthc. Mater.* **2023**, *12*, DOI 10.1002/adhm.202202604.

[37] J. Hu, *STUDY ON STL-BASED SLICING PROCESS FOR 3D PRINTING*, **n.d.**

[38] T. Stirrat, R. Martin, G. Baek, S. Thiru, D. Lakhani, M. Umair, A. Sayah, *J. Clin. Imaging Sci.* **2024**, *14*, 49.

[39] F. A. Adnan, F. R. M. Romlay, M. Shafiq, *IOP Conf. Ser. Mater. Sci. Eng.* **2018**, *342*, 012016.

[40] B. Shaqour, M. Abuabiah, S. Abdel-Fattah, A. Juaidi, R.

Abdallah, W. Abuzaina, M. Qarout, B. Verleije, P. Cos, *Int. J. Adv. Manuf. Technol.* **2021**, *114*, 1279.
[41] A. Mostafaei, A. M. Elliott, J. E. Barnes, F. Li, W. Tan, C. L. Cramer, P. Nandwana, M. Chmielus, *Prog. Mater. Sci.* **2021**, *119*, 100707.
[42] J. Schweiger, F. Beuer, M. Stimmelmayr, D. Edelhoff, P. Magne, J. F. Güth, *Br. Dent. J.* **2016**, *221*, 555.
[43] H. Shi, Y. Li, Y. Wang, W. Guo, K. Zhang, Y. Du, H. Shi, T. Qian, *Clin. Neurol. Neurosurg.* **2022**, *217*, 107241.
[44] U. K. Roopavath, R. Soni, U. Mahanta, A. S. Deshpande, S. N. Rath, *RSC Adv.* **2019**, *9*, 23832.
[45] Y. Li, H. Zhou, R. Bi, X. Li, M. Zha, Y. Yang, J.-S. Ni, W. H. Liew, M. Olivo, K. Yao, J. Liu, H. Chen, K. Li, *J. Mater. Chem. B* **2021**, *9*, 9951.
[46] J. Jiang, X. Liu, H. Chen, C. Dai, X. Niu, L. Dai, X. Chen, S. Zhang, *Biomater. Sci.* **2020**, *8*, 6362.
[47] O. Gülcan, K. Günaydın, A. Tamer, *Polymers (Basel).* **2021**, *13*, 2829.
[48] R. Udroiu, I. C. Braga, *MATEC Web Conf.* **2017**, *112*, 03011.
[49] A. D. Castiaux, C. W. Pinger, E. A. Hayter, M. E. Bunn, R. S. Martin, D. M. Spence, *Anal. Chem.* **2019**, *91*, 6910.
[50] P. Mishra, *Int. J. Res. Appl. Sci. Eng. Technol.* **2020**, *8*, 956.
[51] E. Benca, B. Eckhart, A. Stoegner, E. Unger, M. Bittner-Frank, A. Strassl, C. Gahleitner, L. Hirtler, R. Windhager, G. M. Hobusch, F. Moscato, *3D Print. Med.* **2024**, *10*, 5.
[52] M. Żukowska, F. Górski, R. Wichniarek, W. Kuczko, *Adv. Sci. Technol. Res. J.* **2019**, *13*, 120.
[53] N. N. Zein, I. A. Hanouneh, P. D. Bishop, M. Samaan, B. Eghtesad, C. Quintini, C. Miller, L. Yerian, R. Klatte, **n.d.**, DOI 10.1002/lt.23729.
[54] I. Sander, T. Liepert, E. Doney, W. Leevy, D. Liepert, *J. Funct. Biomater.* **2017**, *8*, 13.
[55] M. Vaezi, S. Yang, in *Rapid Prototyp. Biomater.*, Elsevier, **2014**, pp. 41–92.
[56] P. H. Salame, A. N., H. H. S., S. R. Pillai, B. Kulsange, in *Med. Addit. Manuf.*, Elsevier, **2024**, pp. 563–597.
[57] M. Afify, D. M. Belk, B. Linkan, Y. Moubachir, J. Hassar, Z. Guennoun, *Int. J. Interact. Des. Manuf.* **2024**, *18*, 11.
[58] V. Yakubov, H. Ostergaard, S. Bhagavath, C. L. A. Leung, J. Hughes, E. Yasa, M. Khezri, S. K. Löschke, Q. Li, A. M. Paradowska, *Heliyon* **2024**, *10*, e27243.
[59] G. Brunello, S. Sivolella, R. Meneghello, L. Ferroni, C. Gardin, A. Piattelli, B. Zavan, E. Bressan, *Biotechnol. Adv.* **2016**, *34*, 740.
[60] S.-H. Um, S.-W. Hwang, C. P. Grigoropoulos, H. Jeon, S. H. Ko, *Appl. Phys. Rev.* **2022**, *9*, 041302.
[61] F. Salmon, H. B. Ghadim, A. Godin, D. Haillot, A. Veillere, D. Lacanette, M. Duquesne, *Appl. Energy* **2024**, *362*, 122983.
[62] G. Skrabalak, A. Stwora, Y. Rumiantseva, A. Bętkowska, K. Chat-Wilk, **2024**, p. 020038.
[63] N. S. Lubimyi, M. Chepchurov, A. A. Polshin, M. D. Gerasimov, B. S. Chetverikov, A. Chetverikova, A. A. Tikhonov, A. Maltsev, *J. Manuf. Mater. Process.* **2024**, *8*, 44.
[64] Y. Song, Y. Ghafari, A. Asefnejad, D. Toghraie, *Opt. Laser Technol.* **2024**, *171*, 110459.
[65] K. V. Wong, A. Hernandez, *ISRN Mech. Eng.* **2012**, *2012*, 1.
[66] J. M. Williams, A. Adewunmi, R. M. Schek, C. L. Flanagan, P. H. Krebsbach, S. E. Feinberg, S. J. Hollister, S. Das, *Biomaterials* **2005**, *26*, 4817.
[67] K. Lussenburg, R. van Starkenburg, A. Sakes, P. Breedveld, *Mater. Des.* **2024**, *240*, 112845.
[68] W. Yang, C. Zhou, C. He, Y. Yang, W. Aiyiti, L. Xu, C. Shuai, *J. Colloid Interface Sci.* **2025**, *678*, 260.
[69] R. Păcurar, P. Berce, A. Petrilak, O. Nemeş, C. Borzan, M. Harničárová, A. Păcurar, *Materials (Basel).* **2021**, *14*, 4240.
[70] S. Kim, S. Yalla, S. Shetty, N. J. Rosenblatt, *PLoS One* **2022**, *17*, e0275161.
[71] A. Tejo-Otero, P. Lustig-Gainza, F. Fenollosa-Artés, A. Valls, L. Krauel, I. Buj-Corral, *J. Mech. Behav. Biomed. Mater.* **2020**, *109*, 103844.
[72] A. K. Kushwaha, M. H. Rahman, E. Slater, R. Patel, C. Evangelista, E. Austin, E. Tompkins, A. McCarroll, D. K. Rajak, P. L. Menezes, in *Tribol. Addit. Manuf. Mater.*, Elsevier, **2022**, pp. 1–37.
[73] J. N. DiNoro, N. C. Paxton, J. Skewes, Z. Yue, P. M. Lewis, R. G. Thompson, S. Beirne, M. A. Woodruff, G. G. Wallace, *Polymers (Basel).* **2022**, *14*, 2336.
[74] J. H. Park, S. J. Tucker, J. Yoon, Y. Kim, S. J. Hollister, *J. Biomed. Mater. Res. Part A* **2024**, *112*, 1015.
[75] A. Tejo-Otero, F. Fenollosa-Artés, I. Achaerandio, S. Rey-Vinolas, I. Buj-Corral, M. Á. Mateos-Timoneda, E. Engel, *Gels* **2022**, *8*, 40.
[76] Á. Aguilar-de-Leyva, M. Casas, C. Ferrero, V. Linares, I. Caraballo, *Pharmaceutics* **2024**, *16*, 437.
[77] G. O. Lara-Topete, J. D. Castanier-Rivas, M. S. Gradilla-Hernández, M. E. González-López, *Sustain. Chem. Pharm.* **2024**, *37*, 101435.
[78] A. Bashirgonbadi, Y. Ureel, L. Delva, R. Fiorio, K. M. Van Geem, K. Ragaert, *Polym. Test.* **2024**, *131*, 108353.
[79] E. Balla, V. Daniilidis, G. Karlioti, T. Kalamas, M. Stefanidou, N. D. Bikiaris, A. Vlachopoulos, I. Koumentakou, D. N. Bikiaris, *Polymers (Basel).* **2021**, *13*, 1822.
[80] P. Imrie, J. Jin, *Macromol. Mater. Eng.* **2024**, *309*, DOI 10.1002/mame.202300272.
[81] M. N. Andanje, J. W. Mwangi, B. R. Mose, S. Carrara, *Polymers (Basel).* **2023**, *15*, 2355.
[82] S. Muta, M. Ikeda, T. Nikaido, M. Sayed, A. Sadr, T. Suzuki, J. Tagami, *J. Prosthodont. Res.* **2020**, *64*, 401.
[83] N. Sarkar, Y. Zhou, W. Grayson, in *3D Bioprinting Nanotechnol. Tissue Eng. Regen. Med.*, Elsevier, **2022**, pp. 311–335.
[84] C. Petropolis, D. Kozan, L. Sigurdson, *Plast. Surg.* **2015**, *23*, 91.
[85] Naghieh Saman, Reihany Alireza, *J. "Regeneration, Reconstr. Restoration"* **2016**.
[86] K. F. Leong, C. M. Cheah, C. K. Chua, *Biomaterials* **2003**, *24*, 2363.
[87] A. C. H. Tsang, J. Zhang, K. N. Hui, K. S. Hui, H. Huang, *Adv. Mater. Technol.* **2022**, *7*, DOI 10.1002/admt.202101358.
[88] L. Wei, Z. Gao, *RSC Adv.* **2023**, *13*, 8427.
[89] S. Kalaba, E. Gerhard, J. S. Winder, E. M. Pauli, R. S. Haluck, J. Yang, *Bioact. Mater.* **2016**, *1*, 2.
[90] R. Ajdary, G. Reyes, J. Kuula, E. Raussi-Lehto, T. S. Mikkola,

E. Kankuri, O. J. Rojas, *ACS Polym. Au* **2022**, *2*, 97.
[91] C. Xu, H. Zhang, S. Yu, W. Wu, L. Zhang, Q. Liu, L. Ren, *J. Mater. Res. Technol.* **2023**, *25*, 4901.
[92] T. Jiang, J. G. Munguia-Lopez, S. Flores-Torres, J. Kort-Mascort, J. M. Kinsella, *Appl. Phys. Rev.* **2019**, *6*, 011310.
[93] R. Chakraborty, A. G. Anoop, A. Thakur, G. C. Mohanta, P. Kumar, *ACS Omega* **2023**, *8*, 5139.
[94] M. Revilla-León, J. L. Sánchez-Rubio, A. Besné-Torre, M. Özcan, *Int. J. Esthet. Dent.* **2018**, *13*, 184.
[95] W. P. Cascón, J. R. de Gopegui, M. Revilla-León, *J. Prosthet. Dent.* **2019**, *121*, 741.
[96] I.-A. Timofticiuc, O. Călinescu, A. Iftime, S. Dragosloveanu, A. Caruntu, A.-E. Scheau, I. A. Badarau, A. C. Didilescu, C. Caruntu, C. Scheau, *J. Funct. Biomater.* **2023**, *15*, 7.
[97] I. Roppolo, M. Caprioli, C. F. Pirri, S. Magdassi, *Adv. Mater.* **2024**, *36*, DOI 10.1002/adma.202305537.
[98] H. Goodarzi Hosseinabadi, D. Nieto, A. Yousefinejad, H. Fattel, L. Ionov, A. K. Miri, *Appl. Mater. Today* **2023**, *30*, 101721.
[99] B. W. Caplins, C. I. Higgins, T. J. Kolibaba, U. Arp, C. C. Miller, D. L. Poster, C. J. Zarobila, Y. Zong, J. P. Killgore, *Addit. Manuf.* **2023**, *62*, 103381.
[100] M. Braian, R. Jimbo, A. Wennerberg, *Dent. Mater.* **2016**, *32*, 853.
[101] D. Bahati, M. Bricha, K. El Mabrouk, *Adv. Eng. Mater.* **2023**, *25*, DOI 10.1002/adem.202200859.
[102] X. Xu, A. Goyanes, S. J. Trenfield, L. Diaz-Gomez, C. Alvarez-Lorenzo, S. Gaisford, A. W. Basit, *Mater. Sci. Eng. C* **2021**, *120*, 111773.
[103] H. Abo Sharkh, N. Makhoul, *J. Oral Maxillofac. Surg.* **2020**, *78*, 651.
[104] M. A. Geven, V. Varjas, L. Kamer, X. Wang, J. Peng, D. Eglin, D. W. Grijpma, *Polym. Adv. Technol.* **2015**, *26*, 1433.
[105] J. T. Lichtenstein, A. N. Zeller, J. Lemound, T. E. Lichtenstein, M. Rana, N.-C. Gellrich, M. E. Wagner, *J. Surg. Educ.* **2017**, *74*, 2.
[106] O. Guillaume, M. A. Geven, V. Varjas, P. Varga, D. Gehweiler, V. A. Stadelmann, T. Smidt, S. Zeiter, C. Sprecher, R. R. M. Bos, D. W. Grijpma, M. Alini, H. Yuan, G. R. Richards, T. Tang, L. Qin, L. Yuxiao, P. Jiang, D. Eglin, *Biomaterials* **2020**, *233*, 119721.
[107] M. Hossain, R. Navaratne, D. Perić, *Int. J. Non. Linear. Mech.* **2020**, *126*, 103546.
[108] C. Aravena, T. R. Gildea, *Ann. Transl. Med.* **2022**, *0*, 0.
[109] F. Dini, S. A. Ghaffari, J. Jafar, R. Hamidreza, S. Marjan, *Met. Powder Rep.* **2020**, *75*, 95.
[110] I. Gibson, D. Rosen, B. Stucker, M. Khorasani, in *Addit. Manuf. Technol.*, Springer International Publishing, Cham, **2021**, pp. 237–252.
[111] S. Mirzababaei, S. Pasebani, *J. Manuf. Mater. Process.* **2019**, *3*, 82.
[112] V. Sarila, H. P. Koneru, S. Pyatla, M. Cheepu, V. C. Kantumunchu, D. Ramachandran, in *Int. Conf. Process. Perform. Mater. (ICPPM 2023)*, MDPI, Basel Switzerland, **2024**, p. 44.
[113] Y. Wang, N. Genina, A. Müllertz, J. Rantanen, *Basic Clin. Pharmacol. Toxicol.* **2024**, *134*, 325.
[114] M. Khademitab, P. R. de Vecchis, P. Staszel, M. K. Vaicik, M. Chmielus, A. Mostafaei, *Mater. Today Commun.* **2024**, *38*, 107716.
[115] A. Mostafaei, E. L. Stevens, J. J. Ference, D. E. Schmidt, M. Chmielus, *Addit. Manuf.* **2018**, *21*, 63.
[116] P. K. Gokuldoss, S. Kolla, J. Eckert, *Materials (Basel).* **2017**, *10*, 672.
[117] Y. Mao, J. Yuan, Y. Heng, K. Feng, D. Cai, Q. Wei, *Virtual Phys. Prototyp.* **2023**, *18*, DOI 10.1080/17452759.2023.2174703.
[118] H. Wang, W. Liu, Z. Tang, Y. Wang, X. Mei, K. M. Saleheen, Z. Wang, H. Zhang, *Opt. Eng.* **2020**, *59*, 1.
[119] N. Tepylo, X. Huang, P. C. Patnaik, *Adv. Eng. Mater.* **2019**, *21*, DOI 10.1002/adem.201900617.
[120] T. Takeuchi, G. Chen, K. Haupt, *J. Mater. Chem. B* **2022**, *10*, 6570.
[121] R. Yan, D. Luo, H. Huang, R. Li, N. Yu, C. Liu, M. Hu, Q. Rong, *Sci. Rep.* **2018**, *8*, 750.
[122] H. D. Nguyen, A. Pramanik, A. K. Basak, Y. Dong, C. Prakash, S. Debnath, S. Shankar, I. S. Jawahir, S. Dixit, D. Buddhi, *J. Mater. Res. Technol.* **2022**, *18*, 4641.
[123] D. A. Hollander, M. von Walter, T. Wirtz, R. Sellei, B. Schmidt-Rohlfing, O. Paar, H.-J. Erli, *Biomaterials* **2006**, *27*, 955.
[124] D. Svetlizky, M. Das, B. Zheng, A. L. Vyatskikh, S. Bose, A. Bandyopadhyay, J. M. Schoenung, E. J. Lavernia, N. Eliaz, *Mater. Today* **2021**, *49*, 271.
[125] A. Nazir, O. Gokcekaya, K. Md Masum Billah, O. Ertugrul, J. Jiang, J. Sun, S. Hussain, *Mater. Des.* **2023**, *226*, 111661.
[126] N. K. K. Arthur, C. W. Siyasiya, M. Tlotleng, S. L. Pityana, **2024**, pp. 299–308.
[127] M. Vukicevic, B. Mosadegh, J. K. Min, S. H. Little, *JACC Cardiovasc. Imaging* **2017**, *10*, 171.
[128] J. W. Choi, N. Kim, *Arch. Plast. Surg.* **2015**, *42*, 267.
[129] P. Ferretti, C. Leon-Cardenas, M. Sali, G. M. Santi, L. Frizziero, G. Donnici, A. Liverani, *Application of TPU-Sourced 3D Printed FDM Organs for Improving the Realism in Surgical Planning and Training*, **n.d.**
[130] A. C. Sousa, R. Alvites, B. Lopes, P. Sousa, A. Moreira, A. Coelho, J. D. Santos, L. Atayde, N. Alves, A. C. Maurício, *J. Funct. Biomater.* **2025**, *16*, 28.
[131] J. M. Unagolla, A. C. Jayasuriya, *Appl. Mater. Today* **2020**, *18*, 100479.
[132] A. Biswas, B. Saha, H. Bora, P. V. Vaidya, K. Dixit, S. Dhara, in *3D Bioprinting from Lab to Ind.*, Wiley, **2024**, pp. 1–37.
[133] M. Ho, A. B. Ramirez, N. Akbarnia, E. Croiset, E. Prince, G. G. Fuller, M. Kamkar, *Adv. Funct. Mater.* **2025**, DOI 10.1002/adfm.202415507.
[134] S. Tripathi, A. A. Ansari, M. Dash, P. K. Jain, H. Singh, S. Ramakrishna, H. S. Nanda, in *Nat. Synth. Hydrogels*, Elsevier, **2025**, pp. 465–505.
[135] D. Wu, S. Pang, J. Berg, Y. Mei, A. S. M. Ali, V. Röhrs, B. Tolksdorf, J. Hagenbuchner, M. J. Ausserlechner, H. E. Deubzer, A. Gurlo, J. Kurreck, *Adv. Funct. Mater.* **2024**, *34*, DOI 10.1002/adfm.202314171.
[136] Y.-W. Moon, T. Dobroski, K. Willson, J.-O. Jeong, C. Bishop, A. Atala, J. J. Yoo, S. J. Lee, *Mater. Today Bio* **2025**, *32*,

101786.
[137] S. Tripathi, M. Dash, R. Chakraborty, H. J. Lukman, P. Kumar, S. Hassan, H. Mehboob, H. Singh, H. S. Nanda, *Biomater. Sci.* **2025**, *13*, 93.
[138] Z. Gu, J. Fu, H. Lin, Y. He, *Asian J. Pharm. Sci.* **2020**, *15*, 529.
[139] R. U. Hassan, S. M. Khalil, S. A. Khan, S. Ali, J. Moon, D.-H. Cho, D. Byun, *Polymers (Basel).* **2022**, *14*, 4373.
[140] Ł. Miazio, *Agric. Eng.* **2019**, *23*, 33.
[141] H. Xun, S. Clarke, N. Baker, C. Shallal, E. Lee, D. Fadavi, A. Wong, G. Brandacher, S. H. Kang, J. M. Sacks, *J. Am. Coll. Surg.* **2021**, *232*, 726.
[142] STEPHANIE HENDRIXSON, **n.d.**
[143] **N.d.**
[144] A. Ganapathy, D. Chen, A. Elumalai, B. Albers, K. Tappa, U. Jammalamadaka, M. J. Hoegger, D. H. Ballard, *Methods* **2022**, *206*, 41.
[145] Y. J. Suh, T. H. Lim, H. S. Choi, M. S. Kim, S. J. Lee, S. H. Kim, C. H. Park, *Materials (Basel).* **2020**, *13*, 4819.
[146] J. M. Justino Netto, I. G. Ragoni, L. E. Frezzatto Santos, Z. C. Silveira, *SN Appl. Sci.* **2019**, *1*, 335.
[147] M. Higgins, S. Leung, N. Radacsi, *Ann. 3D Print. Med.* **2022**, *6*, 100057.
[148] H. Quan, T. Zhang, H. Xu, S. Luo, J. Nie, X. Zhu, *Bioact. Mater.* **2020**, *5*, 110.
[149] Y. P. Shaik, J. Schuster, A. Shaik, *OALib* **2021**, *08*, 1.
[150] M. Manoj Prabhakar, A. K. Saravanan, A. Haiter Lenin, I. Jerin leno, K. Mayandi, P. Sethu Ramalingam, *Mater. Today Proc.* **2021**, *45*, 6108.
[151] A. Redmann, P. Oehlmann, T. Scheffler, L. Kagermeier, T. A. Osswald, *Addit. Manuf.* **2020**, *32*, 101018.
[152] N. Muthuram, P. Sriram Madhav, D. Keerthi Vasan, M. E. Mohan, G. Prajeeth, *Mater. Today Proc.* **2022**, *68*, 1906.
[153] F. Fina, A. Goyanes, S. Gaisford, A. W. Basit, *Int. J. Pharm.* **2017**, *529*, 285.
[154] J. M. Mercado-Colmenero, M. A. Rubio-Paramio, M. D. la Rubia-Garcia, D. Lozano-Arjona, C. Martin-Doñate, *Int. J. Adv. Manuf. Technol.* **2019**, *103*, 1893.
[155] L. C. Duarte, F. Figueredo, C. L. S. Chagas, E. Cortón, W. K. T. Coltro, *Anal. Chim. Acta* **2024**, *1299*, 342429.
[156] P. Patpatiya, K. Chaudhary, A. Shastri, S. Sharma, *Proc. Inst. Mech. Eng. Part C J. Mech. Eng. Sci.* **2022**, *236*, 7899.
[157] S. F. Iftekar, A. Aabid, A. Amir, M. Baig, *Polymers (Basel).* **2023**, *15*, 2519.
[158] R. Patel, C. Desai, S. Kushwah, M. H. Mangrola, *Mater. Today Proc.* **2022**, *60*, 2162.
[159] V. Tsioukas, C. Pikridas, I.-A. Karolos, in *3D Print. Appl. Med. Surg.*, Elsevier, **2020**, pp. 151–155.
[160] Z. Jin, Y. Li, K. Yu, L. Liu, J. Fu, X. Yao, A. Zhang, Y. He, *Adv. Sci.* **2021**, *8*, 2101394.
[161] P. Ukhov, A. Ryapukhin, *Int. J. Technol. Enhanc. Learn.* **2022**, *14*, 217.
[162] D. Khorsandi, A. Fahimipour, P. Abasian, S. S. Saber, M. Seyedi, S. Ghanavati, A. Ahmad, A. A. De Stephanis, F. Taghavinezhaddilami, A. Leonova, R. Mohammadinejad, M. Shabani, B. Mazzolai, V. Mattoli, F. R. Tay, P. Makvandi, *Acta Biomater.* **2021**, *122*, 26.
[163] P. Ravi, L. L. Chepelev, G. V. Stichweh, B. S. Jones, F. J. Rybicki, *J. Digit. Imaging* **2022**, *35*, 613.
[164] V. Goodarzi Ardakani, A. M. Gambaruto, G. Silva, R. Pereira, *Int. j. numer. method. biomed. eng.* **2022**, *38*, DOI 10.1002/cnm.3580.
[165] E. Johnstone, J. J. Wyatt, A. M. Henry, S. C. Short, D. Sebag-Montefiore, L. Murray, C. G. Kelly, H. M. McCallum, R. Speight, *Int. J. Radiat. Oncol.* **2018**, *100*, 199.
[166] B. Msallem, N. Sharma, S. Cao, F. S. Halbeisen, H.-F. Zeilhofer, F. M. Thieringer, *J. Clin. Med.* **2020**, *9*, 817.
[167] K. M. Ogden, C. Aslan, N. Ordway, D. Diallo, G. Tillapaugh-Fay, P. Soman, *J. Digit. Imaging* **2015**, *28*, 654.
[168] X.-B. Wu, J.-Q. Wang, C.-P. Zhao, X. Sun, Y. Shi, Z.-A. Zhang, Y.-N. Li, M.-Y. Wang, *Chin. Med. J. (Engl).* **2015**, *128*, 477.
[169] P. Nguyen, I. Stanislaus, C. McGahon, K. Pattabathula, S. Bryant, N. Pinto, J. Jenkins, C. Meinert, *Front. Med. Technol.* **2023**, *5*, DOI 10.3389/fmedt.2023.1097850.
[170] E. Huotilainen, R. Jaanimets, J. Valášek, P. Marcián, M. Salmi, J. Tuomi, A. Mäkitie, J. Wolff, *J. Cranio-Maxillofacial Surg.* **2014**, *42*, e259.
[171] E. M. Zanetti, G. Fragomeni, M. Sanguedolce, G. Pascoletti, L. De Napoli, L. Filice, G. Catapano, *Chemie Ing. Tech.* **2024**, *96*, 486.
[172] J. M. Nicholas, J. Nicholas, H. Steyn, H. Steyn, *Project Management for Business, Engineering and Technology*, Routledge, **2010**.
[173] D. Martinez-Marquez, M. Jokymaityte, A. Mirnajafizadeh, C. P. Carty, D. Lloyd, R. A. Stewart, *Materials (Basel).* **2019**, *12*, 3110.
[174] D. A. J. Brion, S. W. Pattinson, *Nat. Commun.* **2022**, *13*, 4654.
[175] N. Bhadu, J. Singh, *SSRN Electron. J.* **2021**, DOI 10.2139/ssrn.3883928.
[176] R. Moreta-Martinez, A. Pose-Díez-De-La-Lastra, J. A. Calvo-Haro, L. Mediavilla-Santos, R. Pérez-Mañanes, J. Pascau, **2021**, DOI 10.3390/s21041370.
[177] A. Reinschluessel, R. Fischer, C. Schumann, V. Uslar, T. Muender, U. Katzky, H. Kißner, V. Kraft, M. Lampe, T. Lück, K. Bock-Müller, H. Nopper, S. Pelzl, D. Wenig, A. Schenk, D. Weyhe, G. Zachmann, R. Malaka, *Introducing Virtual & 3D-Printed Models for Improved Collaboration in Surgery*, **n.d.**
[178] B. Langridge, S. Momin, B. Coumbe, E. Woin, M. Griffin, P. Butler, *J. Surg. Educ.* **2018**, *75*, 209.
[179] D. B. Jones, R. Sung, C. Weinberg, T. Korelitz, R. Andrews, *Surg. Innov.* **2016**, *23*, 189.
[180] D. Amparore, A. Pecoraro, F. Piramide, P. Verri, E. Checcucci, S. De Cillis, A. Piana, M. Manfredi, C. Fiori, F. Porpiglia, *Urol. Video J.* **2022**, *13*, 100135.
[181] M. Yan, J. Huang, M. Ding, J. Wang, J. Ni, H. Wu, D. Song, *J. Surg. Educ.* **2023**, *80*, 331.
[182] M. Hanisch, E. Kroeger, M. Dekiff, M. Timme, J. Kleinheinz, D. Dirksen, **n.d.**, DOI 10.3390/ijerph17082901.
[183] V. Waran, V. Narayanan, R. Karuppiah, D. Pancharatnam, H. Chandran, R. Raman, Z. A. A. Rahman, S. L. F. Owen, T. Z. Aziz, *J. Surg. Educ.* **2014**, *71*, 193.
[184] F. Alshomer, F. AlFaqeeh, M. Alariefy, I. Altweijri, T. Alhumsi, *J. Craniofac. Surg.* **2019**, *30*, 1652.
[185] H. A. Atalay, V. Ülker, İ. Alkan, H. L. Canat, Ü. Özkuvancı, F.

Altunrende, *J. Endourol.* **2016**, *30*, 1132.
[186] P. Bhatla, J. T. Tretter, A. Ludomirsky, M. Argilla, L. A. Latson, S. Chakravarti, P. C. Barker, S.-J. Yoo, D. B. McElhinney, N. Wake, R. S. Mosca, *Pediatr. Cardiol.* **2017**, *38*, 103.
[187] S. Anwar, G. K. Singh, J. Miller, M. Sharma, P. Manning, J. J. Billadello, P. Eghtesady, P. K. Woodard, *JACC Basic to Transl. Sci.* **2018**, *3*, 294.
[188] C. Park, M.-M. Jones, S. Kaplan, F. L. Koller, J. M. Wilder, L. E. Boulware, L. M. McElroy, *Int. J. Equity Health* **2022**, *21*, 22.
[189] A. Tejo-Otero, I. Buj-Corral, F. Fenollosa-Artés, *Ann. Biomed. Eng.* **2020**, *48*, 536.
[190] L. Zhou, H. Liu, B. Zhang, C. Wei, S. Zhou, X. Huang, X. Zhong, L. Zhang, W. Bi, J. Liu, Y. Liang, L. Jin, R. Guo, *Adv. Funct. Mater.* **2024**, *34*, DOI 10.1002/adfm.202314330.
[191] K. Yammine, J. Karbala, A. Maalouf, J. Daher, C. Assi, *Eur. J. Trauma Emerg. Surg.* **2022**, *48*, 3479.
[192] H. H. Malik, A. R. J. Darwood, S. Shaunak, P. Kulatilake, A. A. El-Hilly, O. Mulki, A. Baskaradas, *J. Surg. Res.* **2015**, *199*, 512.
[193] D. G. Alemayehu, Z. Zhang, E. Tahir, D. Gateau, D.-F. Zhang, X. Ma, *Biomed Res. Int.* **2021**, *2021*, 1.
[194] R. J. Mobbs, M. Coughlan, R. Thompson, C. E. Sutterlin Iii, K. Phan, *J Neurosurg Spine* **2017**, *26*, 513.
[195] H. Zhou, S. Liu, Z. Li, X. Liu, L. Dang, Y. Li, Z. Li, P. Hu, B. Wang, F. Wei, Z. Liu, *J. Neurosurg. Spine* **2022**, *37*, 274.
[196] T. H. Land, Y. A. Chowdhury, Y. T. Woo, M. F. Chowdhury, M. Grainger, M. Czyz, *Cureus* **2022**, DOI 10.7759/cureus.27758.
[197] J. Xiao, W. Huang, X. Yang, W. Yan, D. Song, H. Wei, T. Liu, Z. Wu, C. Yang, *Orthop. Surg.* **2016**, *8*, 171.
[198] Z. Wu, L. Huang, H. Sang, Z. Ma, S. Wan, G. Cui, W. Lei, *J. Spinal Disord. Tech.* **2011**, *24*, 444.
[199] X. Li, Y. Wang, Y. Zhao, J. Liu, S. Xiao, K. Mao, *Spine (Phila. Pa. 1976).* **2017**, *42*, E1326.
[200] O. P. Leary, J. Crozier, D. D. Liu, T. Niu, N. J. Pertsch, J. Q. Camara-Quintana, K. A. Svokos, S. Syed, A. E. Telfeian, A. A. Oyelese, A. S. Woo, Z. L. Gokaslan, J. S. Fridley, *World Neurosurg.* **2021**, *145*, e116.
[201] M. M. Safaee, P. R. Maloney, V. Deviren, C. P. Ames, *Oper. Neurosurg.* **2022**, *22*, e245.
[202] Q. Tu, H. Ding, H. Chen, Q. Miao, X. Yang, K. Li, K. Zhang, Z. Wu, Y. Tang, H. Xia, J. Xu, *World Neurosurg.* **2019**, *130*, e961.
[203] A. Habib, N. Jovanovich, N. Muthiah, A. Alattar, N. Alan, N. Agarwal, A. Ozpinar, D. K. Hamilton, *Eur. Spine J.* **2022**, *31*, 1682.
[204] E. Wade, S. Messner, E. Richer, in *Handb. Interpers. Violence Abus. Across Lifesp.*, Springer International Publishing, Cham, **2022**, pp. 449–508.
[205] *Prosthetics And Orthotics Market Size, Share & Trend Analysis Report By Type (Orthotics (Upper Limb, Lower Limb, Spinal), Prosthetics (Upper Extremity, Lower Extremity), And Segment Forecasts, 2022 - 2030*, **2020**.
[206] F. Kordon, A. Maier, B. Swartman, M. Privalov, J. S. El Barbari, H. Kunze, *J. Imaging* **2022**, *8*, 108.
[207] R. O. Stanborough, J. M. Bestic, J. J. Peterson, *Radiol. Clin. North Am.* **2022**, *60*, 593.
[208] T. B. Weir, J. M. Abzug, in *Congenit. Acquir. Deform. Pediatr. Shoulder Girdle*, Springer International Publishing, Cham, **2022**, pp. 29–44.
[209] H. Beliën, H. Biesmans, A. Steenwerckx, E. Bijnens, C. Dierickx, *J. Exp. Orthop.* **2017**, *4*, 34.
[210] L. A. Rossi, in *Orthop. Trauma*, Springer International Publishing, Cham, **2024**, pp. 113–120.
[211] H.-S. Jeong, K.-J. Park, K.-M. Kil, S. Chong, H.-J. Eun, T.-S. Lee, J.-P. Lee, *Arch. Orthop. Trauma Surg.* **2014**, *134*, 1551.
[212] R. M. Greiwe, in *Shoulder Elb. Trauma Its Complicat.*, Elsevier, **2015**, pp. 83–112.
[213] W. You, L. J. Liu, H. X. Chen, J. Y. Xiong, D. M. Wang, J. H. Huang, J. L. Ding, D. P. Wang, *Orthop. Traumatol. Surg. Res.* **2016**, *102*, 897.
[214] C. Zindel, P. Fürnstahl, A. Hoch, T. Götschi, A. Schweizer, L. Nagy, S. Roner, *J. Orthop. Surg. Res.* **2021**, *16*, 159.
[215] Y. Z. Zhang, S. Lu, B. Chen, J. M. Zhao, R. Liu, G. X. Pei, *J. Shoulder Elb. Surg.* **2011**, *20*, 51.
[216] H. C. Gemalmaz, K. Sarıyılmaz, O. Ozkunt, M. Sungur, İ. Kaya, F. Dikici, *Int. J. Surg. Case Rep.* **2017**, *41*, 438.
[217] F. Fillat-Gomà, F. A. Marcano-Fernández, S. Coderch-Navarro, L. Martínez-Carreres, A. Berenguer, *Injury* **2021**, *52*, S117.
[218] Z. Xuefeng, G. Jian, D. Jiayue, Z. Chuchen, W. Shenglin, Y. Xiao'en, *Med. Hypotheses* **2020**, *134*, 109435.
[219] C. Zang, J. Zhang, Z. Meng, L. Liu, W. Zhang, Y. Chen, R. Cong, *Orthop. Surg.* **2017**, *9*, 215.
[220] M. Javaid, A. Haleem, R. P. Singh, R. Suman, *Glob. Heal. J.* **2022**, DOI 10.1016/j.glohj.2022.11.001.
[221] T. S. Polonsky, M. M. McDermott, *JAMA* **2021**, *325*, 2188.
[222] R. J. Kadakia, C. M. Wixted, N. B. Allen, A. E. Hanselman, S. B. Adams, *3D Print. Med.* **2020**, *6*, 29.
[223] A. Lorente, L. Pelaz, P. Palacios, M. Benlloch, J. E. de la Rubia Ortí, C. Barrios, G. Mariscal, R. Lorente, *J. Clin. Med.* **2024**, *13*, 1188.
[224] Y.-W. Zhang BCDE, X. Xiao CDE, Y. Xiao CDE, X. E. Chen, S.-L. Zhang ABCDEFG, L. Deng Corresponding Author, L. Deng, **2019**, *25*, 4233.
[225] M. Wu, J. Guan, Y. Xiao, Z. Wang, X. Chen, Z. Zhao, K. Zhang, J. Zhu, *Zhongguo Xiu Fu Chong Jian Wai Ke Za Zhi* **2017**, *31*, 1316.
[226] L. Yao, H. Wang, F. Zhang, L. Wang, J. Dong, *Math. Biosci. Eng.* **2019**, *16*, 1597.
[227] C. Valenti, S. Pagano, I. Xhimitiku, M. Kutrolli, F. Masciotti, T. Zara, T. Truffarelli, G. Tribbiani, A. Nanussi, L. Marinucci, *Prosthesis* **2024**, *6*, 263.
[228] Y. Balel, R. Grillo, *J. Stomatol. Oral Maxillofac. Surg.* **2024**, 101945.
[229] F. C. Williams, D. A. Hammer, T. R. Wentland, R. Y. Kim, *J. Oral Maxillofac. Surg.* **2020**, *78*, 1320.
[230] V. J. Gómez, A. Martín-González, V. Zafra-Vallejo, I. Zubillaga-Rodríguez, A. Fernández-García, G. Sánchez-Aniceto, *Int. J. Oral Maxillofac. Surg.* **2024**, DOI 10.1016/j.ijom.2024.01.005.
[231] S. R. Chandra, V. Pillai, in *Oral Maxillofac. Surg. Clin.*,

Springer Nature Singapore, Singapore, **2021**, pp. 1997–2008.
[232] W.-S. Lee, D.-H. Lee, K.-B. Lee, *J. Adv. Prosthodont.* **2017**, *9*, 265.
[233] T. T. Oliveira, A. C. Reis, *J. Prosthet. Dent.* **2019**, *122*, 270.
[234] A. N. Garza-Cisneros, M. M. García-Pérez, W. J. Rodriguez-Guajardo, G. Elizondo-Riojas, A. A. Negreros-Osuna, *Plast. Surg.* **2024**, *32*, 70.
[235] K. K. Stout, C. S. Broberg, W. M. Book, F. Cecchin, J. M. Chen, K. Dimopoulos, M. D. Everitt, M. Gatzoulis, L. Harris, D. T. Hsu, J. T. Kuvin, Y. Law, C. M. Martin, A. M. Murphy, H. J. Ross, G. Singh, T. L. Spray, *Circulation* **2016**, *133*, 770.
[236] O. T. A. Lyons, M. Baguneid, T. D. Barwick, R. E. Bell, N. Foster, S. Homer-Vanniasinkam, S. Hopkins, A. Hussain, K. Katsanos, B. Modarai, J. A. T. Sandoe, S. Thomas, N. M. Price, *Eur. J. Vasc. Endovasc. Surg.* **2016**, *52*, 758.
[237] M. P. Kim, A. H. Ta, W. A. Ellsworth, R. A. Marco, P. Gaur, J. S. Miller, *Int. J. Surg. Case Rep.* **2015**, *16*, 127.
[238] S. Sehovic, D. Behram, M. Karavdic, S. Pandur, M. Kacila, *Anatol. J. Cardiol.* **2021**, *25*, 280.
[239] M. Hozman, D. Herman, D. Zemanek, O. Fiser, D. Vrba, M. Poloczek, I. Varvarovsky, P. Obona, T. Pokorny, P. Osmancik, *Catheter. Cardiovasc. Interv.* **2023**, *102*, 1331.
[240] J. Hausleiter, T. J. Stocker, M. Adamo, N. Karam, M. J. Swaans, F. Praz, *EuroIntervention* **2023**, *18*, 957.
[241] T. Matsumoto, S. Kubo, M. Izumo, S. Mizuno, S. Shirai, *Circ. J.* **2022**, *86*, CJ.
[242] D. D. Wang, Z. Qian, M. Vukicevic, S. Engelhardt, A. Kheradvar, C. Zhang, S. H. Little, J. Verjans, D. Comaniciu, W. W. O'Neill, M. A. Vannan, *JACC Cardiovasc. Imaging* **2021**, *14*, 41.
[243] R. Vashistha, P. Kumar, A. K. Dangi, N. Sharma, D. Chhabra, P. Shukla, *J. Biol. Eng.* **2019**, *13*, 12.
[244] V. Vijayaraghavan, A. Garg, J. S. L. Lam, B. Panda, S. S. Mahapatra, *Int. J. Adv. Manuf. Technol.* **2015**, *78*, 781.
[245] J. Mojumder, L. Fan, T. Nguyen, K. S. Campbell, J. F. Wenk, J. M. Guccione, T. Abraham, L. C. Lee, *Sci. Rep.* **2023**, *13*, 958.
[246] M. Bertolini, M. Mullen, G. Belitsis, A. Babu, G. Colombo, A. Cook, A. Mullen, C. Capelli, *Materials (Basel).* **2022**, *15*, 4284.
[247] H. Wang, H. Song, Y. Yang, Z. Wu, R. Hu, J. Chen, J. Guo, Y. Wang, D. Jia, S. Cao, Q. Zhou, R. Guo, *Int. J. Cardiol.* **2021**, *331*, 296.
[248] G. Musotto, A. Monteleone, D. Vella, S. Di Leonardo, A. Viola, G. Pitarresi, B. Zuccarello, A. Pantano, A. Cook, G. M. Bosi, G. Burriesci, *Front. Cardiovasc. Med.* **2022**, *9*, DOI 10.3389/fcvm.2022.894187.
[249] K. Mendez, D. G. Kennedy, D. D. Wang, B. O'Neill, E. T. Roche, *J. Soc. Cardiovasc. Angiogr. Interv.* **2022**, *1*, 100405.
[250] I. D. Muhammad, U. A. Umar, U. S. Sabo, I. Rabiu, A. M. Ahmad, M. A. Yusuf, *Parasitol. Int.* **2024**, *101*, 102878.
[251] B.-L. Kemah, N. Bhagat, A. Pandya, R. Sullivan, S. S. Sundar, *Int. J. Gynecol. Cancer* **2023**, ijgc.
[252] W. D. Schlaff, R. T. Ackerman, A. Al-Hendy, D. F. Archer, K. T. Barnhart, L. D. Bradley, B. R. Carr, E. C. Feinberg, S. M. Hurtado, J. Kim, R. Liu, R. G. Mabey, C. D. Owens, A. Poindexter, E. E. Puscheck, H. Rodriguez-Ginorio, J. A. Simon, A. M. Soliman, E. A. Stewart, N. B. Watts, O. Muneyyirci-Delale, *N. Engl. J. Med.* **2020**, *382*, 328.
[253] F. Xu, L. Deng, L. Zhang, H. Hu, Q. Shi, *Int. J. Hyperth.* **2021**, *38*, 24.
[254] C. Nezhat, N. Vang, M. Vu, J. Grossman, J. Skinner, K. Robinson, K. Saini, A. Vaid, L. Maule, J. R. Adler, J. W. Jang, I. C. Gibbs, *Curr. Obstet. Gynecol. Rep.* **2020**, *9*, 1.
[255] T. Akiba, **n.d.**, DOI 10.1007/s11748-013-0336-z.
[256] C. Cooke, T. Flaxman, A. Sheikh, O. Miguel, M. McInnes, S. Singh, *J. Obstet. Gynaecol. Canada* **2021**, *43*, 670.
[257] E. G. Richards, T. Falcone, *J. Minim. Invasive Gynecol.* **2017**, *24*, 1053.
[258] V. Nisenblat, L. Prentice, P. M. Bossuyt, C. Farquhar, M. L. Hull, N. Johnson, *Cochrane Database Syst. Rev.* **2016**, DOI 10.1002/14651858.CD012281.
[259] M. O. Ajao, N. V. Clark, T. Kelil, S. L. Cohen, J. I. Einarsson, *J. Minim. Invasive Gynecol.* **2017**, *24*, 1239.
[260] S. A. Z. Bin Sayed Aluwee, X. Zhou, H. Kato, H. Makino, C. Muramatsu, T. Hara, M. Matsuo, H. Fujita, *Radiol. Phys. Technol.* **2017**, *10*, 279.
[261] C. J. Stam, *Nat. Rev. Neurosci.* **2014**, *15*, 683.
[262] T. Kimura, A. Morita, K. Nishimura, H. Aiyama, H. Itoh, S. Fukaya, S. Sora, C. Ochiai, *Neurosurgery* **2009**, *65*, 719.
[263] E. A. Marciuc, B. I. Dobrovat, R. M. Popescu, N. Dobrin, A. Chiriac, D. Marciuc, L. Eva, D. Haba, *Brain Sci.* **2021**, *11*, 598.
[264] S. Thakral, A. Yadav, V. Singh, M. Kumar, P. Kumar, R. Narang, K. Sudhakar, A. Verma, H. Khalilullah, M. Jaremko, A.-H. Emwas, *Ageing Res. Rev.* **2023**, *88*, 101960.
[265] A. Nakamura, N. Kaneko, V. L. Villemagne, T. Kato, J. Doecke, V. Doré, C. Fowler, Q.-X. Li, R. Martins, C. Rowe, T. Tomita, K. Matsuzaki, K. Ishii, K. Ishii, Y. Arahata, S. Iwamoto, K. Ito, K. Tanaka, C. L. Masters, K. Yanagisawa, *Nature* **2018**, *554*, 249.
[266] S. H. Choi, Y. H. Kim, M. Hebisch, C. Sliwinski, S. Lee, C. D'Avanzo, H. Chen, B. Hooli, C. Asselin, J. Muffat, J. B. Klee, C. Zhang, B. J. Wainger, M. Peitz, D. M. Kovacs, C. J. Woolf, S. L. Wagner, R. E. Tanzi, D. Y. Kim, *Nature* **2014**, *515*, 274.
[267] I. Alić, P. A. Goh, A. Murray, E. Portelius, E. Gkanatsiou, G. Gough, K. Y. Mok, D. Koschut, R. Brunmeir, Y. J. Yeap, N. L. O'Brien, J. Groet, X. Shao, S. Havlicek, N. R. Dunn, H. Kvartsberg, G. Brinkmalm, R. Hithersay, C. Startin, S. Hamburg, M. Phillips, K. Pervushin, M. Turmaine, D. Wallon, A. Rovelet-Lecrux, H. Soininen, E. Volpi, J. E. Martin, J. N. Foo, D. L. Becker, A. Rostagno, J. Ghiso, Ž. Krsnik, G. Šimić, I. Kostović, D. Mitrečić, A. Strydom, E. Fisher, F. Wiseman, D. Nizetic, J. Hardy, V. Tybulewicz, A. Karmiloff-Smith, P. T. Francis, K. Blennow, A. Strydom, J. Hardy, H. Zetterberg, D. Nižetić, *Mol. Psychiatry* **2021**, *26*, 5766.
[268] X.-Y. Tang, S. Wu, D. Wang, C. Chu, Y. Hong, M. Tao, H. Hu, M. Xu, X. Guo, Y. Liu, *Signal Transduct. Target. Ther.* **2022**, *7*, 168.
[269] P. Rawal, D. M. Tripathi, S. Ramakrishna, S. Kaur, *Bio-Design Manuf.* **2021**, *4*, 627.
[270] H.-G. Yi, Y. H. Jeong, Y. Kim, Y.-J. Choi, H. E. Moon, S. H.

Park, K. S. Kang, M. Bae, J. Jang, H. Youn, S. H. Paek, D.-W. Cho, *Nat. Biomed. Eng.* **2019**, *3*, 509.
[271] M. A. Heinrich, R. Bansal, T. Lammers, Y. S. Zhang, R. Michel Schiffelers, J. Prakash, *Adv. Mater.* **2019**, *31*, 1806590.
[272] S. Abdelrahman, W. F. Alsanie, Z. N. Khan, H. I. Albalawi, R. I. Felimban, M. Moretti, N. Steiner, A. G. Chaudhary, C. A. E. Hauser, *Biofabrication* **2022**, *14*, 044103.
[273] B. S. Crook, M. M. Cullen, T. S. Pidgeon, *J. Hand Surg. Glob. Online* **2024**, DOI 10.1016/j.jhsg.2024.01.024.
[274] Y. Leng, S. F. Ackley, M. M. Glymour, K. Yaffe, W. D. Brenowitz, *Ann. Neurol.* **2021**, *89*, 177.
[275] E. Redolfi Riva, M. Özkan, E. Contreras, S. Pawar, C. Zinno, E. Escarda-Castro, J. Kim, P. Wieringa, F. Stellacci, S. Micera, X. Navarro, *Biomater. Sci.* **2024**, *12*, 1371.
[276] J. Yoo, J. H. Park, Y. W. Kwon, J. J. Chung, I. C. Choi, J. J. Nam, H. S. Lee, E. Y. Jeon, K. Lee, S. H. Kim, Y. Jung, J. W. Park, *Biomater. Sci.* **2020**, *8*, 6261.
[277] S. Das, J. Thimukonda Jegadeesan, B. Basu, *ACS Biomater. Sci. Eng.* **2024**, *10*, 1620.
[278] E. M. Steele, Z. L. Carr, E. Dosmar, *Biophysica* **2024**, *4*, 58.
[279] Z. Wu, R. Liu, N. Shao, Y. Zhao, *Lab Chip* **2025**, DOI 10.1039/D4LC00769G.
[280] M. Blekhman, A. J. B. James, R. Roberson, F. Adams, Z. Zheng, R. Llull, A. Katz, N. Levi, in *Polym. Mater. Biomed. Implant.*, Elsevier, **2024**, pp. 377–456.
[281] M. Delemeester, K. M. Pawelec, J. M. L. Hix, J. R. Siegenthaler, M. Lissy, P. C. Douek, A. Houmeau, S. A. Si-Mohamed, E. M. Shapiro, *Adv. Funct. Mater.* **2024**, DOI 10.1002/adfm.202404860.
[282] C. Nikolaou, E. Polyzos, Y. Zhu, D. Polyzos, L. Pyl, *Addit. Manuf.* **2024**, *85*, 104181.
[283] J. Zeng, Z. Liu, G. Shen, Y. Zhang, L. Li, Z. Wu, D. Luo, Q. Gu, H. Mao, L. Wang, *Int. J. Infect. Dis.* **2019**, *82*, 138.
[284] J. Reinhard, P. Urban, S. Bell, D. Carpenter, M. S. Sagoo, *Nat. Commun.* **2024**, *15*, 1360.
[285] A. Hosny, C. Parmar, J. Quackenbush, L. H. Schwartz, H. J. W. L. Aerts, *Nat. Rev. Cancer* **2018**, *18*, 500.
[286] C. K. Chua, K. F. Leong, J. An, *Rapid Prototyp. Biomater. Tech. Addit. Manuf.* **2020**, 1.
[287] T. D. Ngo, A. Kashani, G. Imbalzano, K. T. Q. Nguyen, D. Hui, *Compos. Part B Eng.* **2018**, *143*, 172.
[288] J. Yang, B. Zhou, D. Han, N. Cui, B. Li, J. Shen, Z. Zhang, A. Du, *ES Mater. Manuf.* **2021**, DOI 10.30919/esmm5f526.
[289] J. Lai, C. Wang, M. Wang, *Appl. Phys. Rev.* **2021**, *8*, 021322.
[290] P. B.A, L. N, A. Buradi, S. N, P. B L, V. R, *Mater. Today Proc.* **2022**, *52*, 1309.
[291] Z. Liu, Y. Wang, B. Wu, C. Cui, Y. Guo, C. Yan, *Int. J. Adv. Manuf. Technol.* **2019**, *102*, 2877.
[292] W. Oropallo, L. A. Piegl, *Eng. Comput.* **2016**, *32*, 135.
[293] A. El Magri, S. Ouassil, S. Vaudreuil, *Polym. Eng. Sci.* **2022**, *62*, 848.
[294] L. Jaksa, D. Pahr, G. Kronreif, A. Lorenz, *Int. J. Bioprinting* **2021**, *7*, 420.
[295] N. Ashammakhi, S. Ahadian, C. Xu, H. Montazerian, H. Ko, R. Nasiri, N. Barros, A. Khademhosseini, *Mater. Today Bio* **2019**, *1*, 100008.
[296] P. Morer-Camo, J. Paredes-Puente, M. Llorente-Ortega, X. Unamuno-Iñurritegui, **2022**, pp. 182–190.
[297] L. Ma, S. Yu, X. Xu, S. Moses Amadi, J. Zhang, Z. Wang, *Mater. Today Bio* **2023**, *23*, 100792.
[298] C. Bader, D. Kolb, J. C. Weaver, S. Sharma, A. Hosny, J. Costa, N. Oxman, *Sci. Adv.* **2018**, *4*, DOI 10.1126/sciadv.aas8652.
[299] N. M. Jacobson, L. Smith, J. Brusilovsky, E. Carrera, H. McClain, R. MacCurdy, *J. Vis. Exp.* **2022**, DOI 10.3791/63214.
[300] W. Zheng, S. Zeng, J. Wang, G. Bai, J. Ye, *J. Mater. Eng. Perform.* **2024**, DOI 10.1007/s11665-024-10608-1.
[301] A. Bandyopadhyay, I. Mitra, S. B. Goodman, M. Kumar, S. Bose, *Prog. Mater. Sci.* **2023**, *133*, 101053.
[302] O. Abdulhameed, A. Al-Ahmari, W. Ameen, S. H. Mian, **2019**, *11*, 1.
[303] H. B. Mamo, M. Adamiak, A. Kunwar, *J. Mech. Behav. Biomed. Mater.* **2023**, *143*, 105930.
[304] M. Fogarasi, K. L. Snodderly, M. A. Di Prima, *Nat. Rev. Bioeng.* **2023**, *1*, 687.
[305] W. Long Ng, J. An, C. Kai Chua, *Engineering* **2024**, DOI 10.1016/j.eng.2024.01.028.
[306] B. G. Beitler, P. F. Abraham, A. R. Glennon, S. M. Tommasini, L. L. Lattanza, J. M. Morris, D. H. Wiznia, *3D Print. Med.* **2022**, *8*, 7.
[307] Khalid Rafi, Alexander Zhonghong Liu, Matthew Di Prima, Paul Bates, Mohsen Seifi, **n.d.**
[308] *Standard Specification for Additive Manufacturing Titanium-6 Aluminum-4 Vanadium ELI (Extra Low Interstitial) with Powder Bed Fusion*, **n.d.**
[309] U.S Food and Drug Administration, "https:// www. acces sdata. fda. gov/ scrip ts/ cdrh/ cfdocs/ cfsta ndards/ search. cfm.," **n.d.**
[310] W. Al-Zyoud, D. Haddadin, S. A. Hasan, H. Jaradat, O. Kanoun, *Materials (Basel).* **2023**, *16*, 6881.
[311] A. B. Singh, C. Khandelwal, G. S. Dangayach, *Polym. Technol. Mater.* **2024**, *63*, 1608.
[312] M. Rahmati, E. A. Silva, J. E. Reseland, C. A. Heyward, H. J. Haugen, *Chem. Soc. Rev.* **2020**, *49*, 5178.
[313] A. Abdul Samat, Z. A. Abdul Hamid, M. Jaafar, C. C. Ong, B. H. Yahaya, *Bioengineering* **2023**, *10*, 394.
[314] K. Moghadasi, M. S. Mohd Isa, M. A. Ariffin, M. Z. Mohd jamil, S. Raja, B. Wu, M. Yamani, M. R. Bin Muhamad, F. Yusof, M. F. Jamaludin, M. S. bin Ab Karim, B. binti Abdul Razak, N. bin Yusoff, *J. Mater. Res. Technol.* **2022**, *17*, 1054.
[315] "Chemical characterization of medical device materials within a risk management process," **n.d.**
[316] J. C. L. Schuh, K. A. Funk, *Toxicol. Pathol.* **2019**, *47*, 344.
[317] R. Jayabal, *Regen. Eng. Transl. Med.* **2025**, DOI 10.1007/s40883-025-00416-x.
[318] K. M. Jurczak, T. A. B. van der Boon, R. Devia-Rodriguez, R. C. L. Schuurmann, J. Sjollema, L. van Huizen, J. P. M. De Vries, P. van Rijn, *Bioeng. Transl. Med.* **2025**, *10*, DOI 10.1002/btm2.10721.
[319] F. Pappalardo, J. Wilkinson, F. Busquet, A. Bril, M. Palmer, B. Walker, C. Curreli, G. Russo, T. Marchal, E. Toschi, R. Alessandrello, V. Costignola, I. Klingmann, M. Contin, B.

Staumont, M. Woiczinski, C. Kaddick, V. Di Salvatore, A. Aldieri, L. Geris, M. Viceconti, *IEEE J. Biomed. Heal. Informatics* **2022**, *26*, 5282.

[320] M. Kazemzadeh-Narbat, A. Memic, K. B. McGowan, A. Memic, A. Tamayol, *Prog. Biomed. Eng.* **2024**, *6*, 032002.

[321] L. Reeve, P. Baldrick, *Expert Rev. Med. Devices* **2017**, *14*, 161.

[322] F. Atouf, in *Cell Ther.*, Springer International Publishing, Cham, **2022**, pp. 589–608.

[323] V. Hasirci, N. Hasirci, in *Fundam. Biomater.*, Springer International Publishing, Cham, **2024**, pp. 363–388.

[324] M. E. Bhatnagar, G. J. Burckart, D. L. Snyder, R. Bax, L. Yao, D. J. Green, in *Essentials Transl. Pediatr. Drug Dev.*, Elsevier, **2024**, pp. 385–419.

[325] M. P. Sekar, H. Budharaju, A. Zennifer, S. Sethuraman, N. Vermeulen, D. Sundaramurthi, D. M. Kalaskar, *J. Tissue Eng.* **2021**, *12*, 204173142110276.

[326] N. Beheshtizadeh, M. Gharibshahian, Z. Pazhouhnia, M. Rostami, A. R. Zangi, R. Maleki, H. K. Azar, V. Zalouli, H. Rajavand, A. Farzin, N. Lotfibakhshaiesh, F. Sefat, M. Azami, T. J. Webster, N. Rezaei, *Biomed. Pharmacother.* **2022**, *153*, 113431.

[327] S. Bose, D. Ke, H. Sahasrabudhe, A. Bandyopadhyay, *Prog. Mater. Sci.* **2018**, *93*, 45.

[328] J. Cheng, R. Wang, Z. Sun, Q. Liu, X. He, H. Li, H. Ye, X. Yang, X. Wei, Z. Li, B. Jian, W. Deng, Q. Ge, *Nat. Commun.* **2022**, *13*, 7931.

[329] A. S. Verga, S. J. Tucker, Y. Gao, A. M. Plaskett, S. J. Hollister, *Front. Mech. Eng.* **2022**, *8*, DOI 10.3389/fmech.2022.862375.

[330] P. Lu, D. Ruan, M. Huang, M. Tian, K. Zhu, Z. Gan, Z. Xiao, *Signal Transduct. Target. Ther.* **2024**, *9*, 166.

[331] S.-J. Estermann, D. H. Pahr, A. Reisinger, *J. Mech. Behav. Biomed. Mater.* **2020**, *104*, 103630.

[332] I. S. Kinstlinger, S. H. Saxton, G. A. Calderon, K. V. Ruiz, D. R. Yalacki, P. R. Deme, J. E. Rosenkrantz, J. D. Louis-Rosenberg, F. Johansson, K. D. Janson, D. W. Sazer, S. S. Panchavati, K.-D. Bissig, K. R. Stevens, J. S. Miller, *Nat. Biomed. Eng.* **2020**, *4*, 916.

[333] J. Lim, J. Kim, *Adv. Funct. Mater.* **2020**, *30*, 2003395.

[334] D. Levin, G. B. Mackensen, M. Reisman, J. M. McCabe, D. Dvir, B. Ripley, *Curr. Cardiol. Rep.* **2020**, *22*, 23.

[335] N. Annabi, A. Tamayol, J. A. Uquillas, M. Akbari, L. E. Bertassoni, C. Cha, G. Camci-Unal, M. R. Dokmeci, N. A. Peppas, A. Khademhosseini, *Adv. Mater.* **2014**, *26*, 85.

[336] L. Rosalia, C. Ozturk, J. Coll-Font, Y. Fan, Y. Nagata, M. Singh, D. Goswami, A. Mauskapf, S. Chen, R. A. Eder, E. M. Goffer, J. H. Kim, S. Yurista, B. P. Bonner, A. N. Foster, R. A. Levine, E. R. Edelman, M. Panagia, J. L. Guerrero, E. T. Roche, C. T. Nguyen, *Nat. Biomed. Eng.* **2022**, *6*, 1134.

[337] P. Kumar, K. B. Mirza, K. Choudhury, M. Cucchiarini, H. Madry, P. Shukla, *Adv. Funct. Mater.* **2021**, *31*, 2009663.

[338] Y. Wang, H. Cui, T. Esworthy, D. Mei, Y. Wang, L. G. Zhang, *Adv. Mater.* **2022**, *34*, 2109198.

[339] C. Park, Y. Fan, G. Hager, H. Yuk, M. Singh, A. Rojas, A. Hameed, M. Saeed, N. V. Vasilyev, T. W. J. Steele, X. Zhao, C. T. Nguyen, E. T. Roche, *Sci. Robot.* **2020**, *5*, DOI 10.1126/scirobotics.aay9106.

[340] C. Park, M. Singh, M. Y. Saeed, C. T. Nguyen, E. T. Roche, *Device* **2024**, *2*, 100217.

[341] M. Singh, J. Bonnemain, C. Ozturk, B. Ayers, M. Y. Saeed, D. Quevedo-Moreno, M. Rowlett, C. Park, Y. Fan, C. T. Nguyen, E. T. Roche, *Nat. Cardiovasc. Res.* **2023**, *2*, 1310.

[342] N. Noor, A. Shapira, R. Edri, I. Gal, L. Wertheim, T. Dvir, *Adv. Sci.* **2019**, *6*, 1900344.

[343] A. Gutiérrez-Fernández, C. Fernández-Llamas, A. M. Vázquez-Casares, E. Mauriz, V. Riego-del-Castillo, N. W. John, *Vis. Comput.* **2024**, DOI 10.1007/s00371-023-03227-9.

[344] A. I. Journal, C. Li, B. Wang, X. Liu, Z. Pan, C. Liu, H. Ma, X. Liu, L. Liu, C. Jiang, *Nanomedicine, Biotechnol.* **2019**, *47*, 1823.

[345] Q. Sun, Z. Dai, X. Meng, F.-S. Xiao, *Chem. Soc. Rev.* **2015**, *44*, 6018.

[346] Z. Jia, X. Xu, D. Zhu, Y. Zheng, *Prog. Mater. Sci.* **2023**, *134*, 101072.

[347] P. Foti, N. Razavi, A. Fatemi, F. Berto, *Prog. Mater. Sci.* **2023**, *137*, 101126.

[348] K. Wang, C. Wu, Z. Qian, C. Zhang, B. Wang, M. A. Vannan, *Addit. Manuf.* **2016**, *12*, 31.

[349] F. S. L. Bobbert, K. Lietaert, A. A. Eftekhari, B. Pouran, S. M. Ahmadi, H. Weinans, A. A. Zadpoor, *Acta Biomater.* **2017**, *53*, 572.

[350] S. Rahimi, M. Asghari, *Heliyon* **2025**, *11*, e40911.

[351] M. J. Mirzaali, M. Cruz Saldívar, A. Herranz de la Nava, D. Gunashekar, M. Nouri-Goushki, E. L. Doubrovski, A. A. Zadpoor, *Adv. Eng. Mater.* **2020**, *22*, 1901142.

[352] J. Maier, M. Weiherer, M. Huber, C. Palm, *Quant. Imaging Med. Surg.* **2019**, *9*, 30.

[353] L. K. Johnson, C. Richburg, M. Lew, W. R. Ledoux, P. M. Aubin, E. Rombokas, *Bioinspir. Biomim.* **2018**, *14*, 016001.

[354] L. Ren, W. Wu, L. Ren, Z. Song, Q. Liu, B. Li, Q. Wu, X. Zhou, *Adv. Mater. Technol.* **2022**, *7*, 2101546.

[355] Z. Zhang, J. Gao, S. Wei, B. Song, Y. Yao, X. Zheng, Y. Zhang, L. Zhang, Q. Li, J. Wu, Y. Shi, *Virtual Phys. Prototyp.* **2025**, *20*, DOI 10.1080/17452759.2024.2444572.

[356] A. Álvarez-Trejo, E. Cuan-Urquizo, D. Bhate, A. Roman-Flores, *Mater. Des.* **2023**, *233*, 112190.

[357] J. Zhang, M. Xu, N. Zhang, T. Wang, Y. Zhang, Z. Yang, Q. Wang, *Addit. Manuf. Front.* **2024**, *3*, 200115.

[358] P. Imrie, J. Jin, *Macromol. Mater. Eng.* **2025**, DOI 10.1002/mame.202400386.

[359] L. A. Damiati, S. A. Alsudir, R. Y. Mohammed, M. A. Majrashi, S. H. Albrahim, A. algethami, F. O. Alghamdi, H. A. Alamari, M. M. Alzaydi, *Bioprinting* **2025**, *45*, e00386.

[360] J. Ock, E. Gwon, T. Kim, S. On, S. Moon, Y. S. Kyung, N. Kim, *Sci. Rep.* **2024**, *14*, 5722.

[361] Q. Ge, A. H. Sakhaei, H. Lee, C. K. Dunn, N. X. Fang, M. L. Dunn, *Sci. Rep.* **2016**, *6*, 31110.

[362] M. Zarek, N. Mansour, S. Shapira, D. Cohn, *Macromol. Rapid Commun.* **2017**, *38*, DOI 10.1002/marc.201600628.

[363] T. Kim, Y.-G. Lee, *Sci. Rep.* **2018**, *8*, 13911.

[364] A. Sadraei, S. M. Naghib, *Polym. Rev.* **2025**, *65*, 104.

[365] S. Tripathi, M. Dash, R. Chakraborty, H. J. Lukman, P.

Kumar, S. Hassan, H. Mehboob, H. Singh, H. S. Nanda, *Biomater. Sci.* **2024**, DOI 10.1039/D4BM01192A.
[366] G. Vashishtha, S. Chauhan, N. Yadav, D. Chhabra, M. K. Gupta, R. Kumar, Z. Li, *Int. J. Adv. Manuf. Technol.* **2025**, *136*, 4215.
[367] E. G. Milano, C. Capelli, J. Wray, B. Biffi, S. Layton, M. Lee, M. Caputo, A. M. Taylor, S. Schievano, G. Biglino, *Br. J. Radiol.* **2019**, *92*, DOI 10.1259/bjr.20180389.
[368] L. Bonetti, G. Scalet, *Prog. Addit. Manuf.* **2024**, DOI 10.1007/s40964-024-00743-5.
[369] S. Park, W. Shou, L. Makatura, W. Matusik, K. (Kelvin) Fu, *Matter* **2022**, *5*, 43.
[370] P. Kumar, P. Suryavanshi, S. Kumar Dwivedy, S. Banerjee, *J. Mol. Liq.* **2024**, *410*, 125553.
[371] R. Sajjad, S. T. Chauhdary, M. T. Anwar, A. Zahid, A. A. Khosa, M. Imran, M. H. Sajjad, *Adv. Ind. Eng. Polym. Res.* **2024**, *7*, 20.
[372] N. Burns, A. Rajesh, A. Manjula-Basavanna, A. Duraj-Thatte, *Adv. Drug Deliv. Rev.* **2025**, *217*, 115505.
[373] N. Tyagi, V. Bhardwaj, D. Sharma, R. Tomar, V. Chaudhary, M. Khanuja, M. K. Singh, G. Sharma, *Biomed. Mater. Devices* **2024**, *2*, 178.
[374] A. Sharma, P. N. Vishwakarma, S. Gupta, S. Dixit, S. R. Kumar, *Materwiss. Werksttech.* **2024**, *55*, 496.
[375] H. Chen, S. Lou, Q. Wang, P. Huang, H. Duan, Y. Hu, *Appl. Phys. Rev.* **2024**, *11*, DOI 10.1063/5.0191977.
[376] S. Rehman, H. Ajmal, U. Farooq, Q. U. Ain, F. Riaz, A. Hassan, in *Pattern Recognit. Track. XXIX* (Ed.: M. S. Alam), SPIE, **2018**, p. 26.
[377] M. Becker, K.-I. Friese, F.-E. Wolter, N.-C. Gellrich, H. Essig, in *2015 IEEE Int. Symp. Med. Meas. Appl. Proc.*, IEEE, **2015**, pp. 285–290.
[378] T. Cooper, B. Schmutz, E. Hsu, A. Lynham, *Int. J. Oral Maxillofac. Surg.* **2020**, *49*, 483.
[379] X. Zhou, **2020**, pp. 135–147.
[380] M. Chua, D. Kim, J. Choi, N. G. Lee, V. Deshpande, J. Schwab, M. H. Lev, R. G. Gonzalez, M. S. Gee, S. Do, *Nat. Biomed. Eng.* **2022**, DOI 10.1038/s41551-022-00988-x.
[381] M. Zreik, T. Leiner, B. D. de Vos, R. W. van Hamersvelt, M. A. Viergever, I. Isgum, in *2016 IEEE 13th Int. Symp. Biomed. Imaging*, IEEE, **2016**, pp. 40–43.
[382] X. Zhao, L. Wang, Y. Zhang, X. Han, M. Deveci, M. Parmar, *Artif. Intell. Rev.* **2024**, *57*, 99.
[383] C.-L. Fan, *Heliyon* **2024**, *10*, e38104.
[384] J. Hussain, M. Båth, J. Ivarsson, *Comput. Biol. Med.* **2025**, *191*, 110094.
[385] P. Sharma, M. Kumar, H. K. Sharma, S. M. Biju, *Multimed. Tools Appl.* **2024**, *83*, 88811.
[386] Goodfellow, Jean Pouget-Abadie, Mehdi Mirza, Bing Xu, David Warde-Farley, Sherjil Ozair, Aaron Courville, Yoshua Bengio, NeurIPS Proceedings, **n.d.**
[387] J. Kim, Y. Li, B.-S. Shin, *IEEE J. Biomed. Heal. Informatics* **2024**, *28*, 2904.
[388] F. Zhou, Y. Qiao, Q. Li, *J. Technol. Informatics Eng.* **2025**, *4*, 1.
[389] Jascha Sohl-Dickstein, Eric Weiss, Niru Maheswaranathan, Surya Ganguli, in *Proc. 32nd Int. Conf. Mach. Learn.*, **n.d.**
[390] M. G. Alsubaie, S. Luo, K. Shaukat, *Mach. Learn. Knowl. Extr.* **2024**, *6*, 464.
[391] Y. Mao, L. Jiang, X. Chen, C. Li, **2023**, pp. 387–397.
[392] X. Wang, Z. Shen, Z. Song, S. Wang, M. Liu, L. Zhang, K. Xuan, Q. Wang, **2024**, pp. 23–32.
[393] M. U. Mirza, F. Arslan, T. Çukur, in *2024 32nd Signal Process. Commun. Appl. Conf.*, IEEE, **2024**, pp. 1–4.
[394] Y. Cao, L. Wang, J. Zhang, H. Xia, F. Yang, Y. Zhu, in *2022 16th IEEE Int. Conf. Signal Process.*, IEEE, **2022**, pp. 479–484.
[395] G. D. Goh, S. L. Sing, W. Y. Yeong, *Artif. Intell. Rev.* **2021**, *54*, 63.
[396] L. Bognár, T. Fauszt, *Comput. Educ. Artif. Intell.* **2022**, *3*, 100100.
[397] Z. Zhu, D. W. H. Ng, H. S. Park, M. C. McAlpine, *Nat. Rev. Mater.* **2020**, *6*, 27.
[398] F. Meng, J. Huang, B. Ping, P. Yuan, N. Bai, X. Zhang, X. Shi, J. Zhou, P. Li, P. Zhao, *J. Intell. Manuf.* **2024**, *35*, 575.
[399] A. Conev, E. E. Litsa, M. R. Perez, M. Diba, A. G. Mikos, L. E. Kavraki, *Tissue Eng. Part A* **2020**, *26*, 1359.
[400] Z. Hu, W. Yan, *npj Adv. Manuf.* **2024**, *1*, 3.
[401] M. Moradi, M. Rezayat, F. A. R. Rozhbiany, S. Meiabadi, G. Casalino, M. Shamsborhan, A. Bijoy, S. Chakkingal, M. Lawrence, N. Mohammed, M. Karamimoghadam, *Machines* **2023**, *11*, 950.
[402] Z. Zhang, J. Shi, T. Yu, A. Santomauro, A. Gordon, J. Gou, D. Wu, *J. Comput. Inf. Sci. Eng.* **2020**, *20*, DOI 10.1115/1.4047477.
[403] K.-H. Yu, A. L. Beam, I. S. Kohane, *Nat. Biomed. Eng.* **2018**, *2*, 719.
[404] C. Gobert, E. W. Reutzel, J. Petrich, A. R. Nassar, S. Phoha, *Addit. Manuf.* **2018**, *21*, 517.
[405] A. Karadag, O. Ulkir, *Int. J. Precis. Eng. Manuf.* **2025**, *26*, 1187.
[406] C. Song, L. Liu, Z. Deng, H. Lei, F. Yuan, Y. Yang, Y. Li, Jiakuo Yu, *J. Mater. Res. Technol.* **2023**, *23*, 2626.
[407] S. You, Y. Fan, Y. Chen, X. Jiang, W. Liu, X. Zhou, J. Zhang, J. Zheng, H. Yang, X. Hou, *Cell Reports Phys. Sci.* **2024**, *5*, 102116.
[408] H. Türker, B. Aksoy, K. Özsoy, *J. Mech. Behav. Biomed. Mater.* **2022**, *126*, 105071.
[409] Weiting Xua, Fengyuan Liu, Aydin Nassehi, **2024**, 272.
[410] S. Manogaran, P. K. Yadalam, R. Ramadoss, **2024**, DOI 10.2139/ssrn.5030089.
[411] S. Foti, A. J. Rickart, B. Koo, E. O' Sullivan, L. S. van de Lande, A. Papaioannou, R. Khonsari, D. Stoyanov, N. u. O. Jeelani, S. Schievano, D. J. Dunaway, M. J. Clarkson, *Comput. Methods Programs Biomed.* **2024**, *256*, 108395.
[412] Z. Zhu, S. M. Amadi, J. Mao, M. Zhou, M. Xia, N. J. Parikh, J. Hu, Z. Wang, *Sci. Rep.* **2025**, *15*, 636.
[413] C. Hou, K. Wang, F. Wang, H. Li, L. Lou, S. Zhang, Y. Gu, H. Liu, T. Chen, L. Sun, *Adv. Funct. Mater.* **2023**, *33*, DOI 10.1002/adfm.202302812.
[414] J. Chen, E. Kobayashi, I. Sakuma, N. Tomii, *IEEE Robot. Autom. Lett.* **2024**, *9*, 9789.
[415] H. Hassani, B. Irani, S. Reihaninia, in *Blockchain Digit. Twin Smart Hosp.*, Elsevier, **2025**, pp. 399–411.

[416] P. Tyagi, K. Mittal, in *Artif. Intell. Cybersecurity Healthc.*, Wiley, **2025**, pp. 443–460.
[417] A. Oulefki, A. Amira, S. Foufou, *Health Technol. (Berl).* **2025**, DOI 10.1007/s12553-025-00947-x.
[418] L. Asciak, J. Kyeremeh, X. Luo, A. Kazakidi, P. Connolly, F. Picard, K. O'Neill, S. A. Tsaftaris, G. D. Stewart, W. Shu, *npj Digit. Med.* **2025**, *8*, 32.
[419] Z. Wang, S. Li, J. Peng, Y. Tai, Z. Yu, *IEEE Trans. Multimed.* **2024**, 1.
[420] K.-B. Ooi, G. W.-H. Tan, M. Al-Emran, M. A. Al-Sharafi, A. Capatina, A. Chakraborty, Y. K. Dwivedi, T.-L. Huang, A. K. Kar, V.-H. Lee, X.-M. Loh, A. Micu, P. Mikalef, E. Mogaji, N. Pandey, R. Raman, N. P. Rana, P. Sarker, A. Sharma, C.-I. Teng, S. F. Wamba, L.-W. Wong, *J. Comput. Inf. Syst.* **2025**, *65*, 76.
[421] J. Chen, Y. Shi, C. Yi, H. Du, J. Kang, D. Niyato, *IEEE Internet Things J.* **2024**, *11*, 34749.
[422] M. Bordukova, N. Makarov, R. Rodriguez-Esteban, F. Schmich, M. P. Menden, *Expert Opin. Drug Discov.* **2024**, *19*, 33.
[423] X. Huang, H. Yang, C. Zhou, M. He, X. Shen, W. Zhuang, *IEEE Netw.* **2024**, 1.
[424] M. A. Equbal, A. Equbal, Z. A. Khan, I. A. Badruddin, *Int. J. Light. Mater. Manuf.* **2024**, DOI 10.1016/j.ijlmm.2024.10.002.
[425] D. Kumar Banerjee, A. Kumar, K. Sharma, *Artificial Intelligence on Additive Manufacturing*, **n.d.**
[426] S. Mondal, R. Maity, A. Nag, *Sci. Rep.* **2025**, *15*, 4827.
[427] M. Sharifi Renani, A. M. Eustace, C. A. Myers, C. W. Clary, *Sensors* **2021**, *21*, 5876.
[428] X. Huang, Y. Lou, Y. Duan, H. Liu, J. Tian, Y. Shen, X. Wei, *Bioact. Mater.* **2024**, *33*, 129.
[429] S. Sai, A. Gaur, R. Sai, V. Chamola, M. Guizani, J. J. P. C. Rodrigues, *IEEE Access* **2024**, *12*, 31078.
[430] S. Grira, M. S. Mozumder, A.-H. I. Mourad, M. Ramadan, H. A. Khalifeh, M. Alkhedher, *Bioprinting* **2025**, *46*, e00385.
[431] R. Pingili, *www.irjmets.com @International Res. J. Mod. Eng.* **n.d.**, *185*, DOI 10.56726/IRJMETS64845.
[432] S. Apoorva, N.-T. Nguyen, K. R. Sreejith, *Lab Chip* **2024**, *24*, 1833.
[433] M. Milazzo, F. Libonati, *Adv. Intell. Syst.* **2022**, *4*, DOI 10.1002/aisy.202100278.
[434] M. Elbadawi, H. Li, S. Sun, M. E. Alkahtani, A. W. Basit, S. Gaisford, *Appl. Mater. Today* **2024**, *36*, 102061.
[435] H. Khan, K. K. Kushwah, S. Singh, J. S. Thakur, K. K. Sadasivuni, in *Nanotechnology-Based Addit. Manuf.*, Wiley, **2023**, pp. 601–636.
[436] L. Pinto-Coelho, *Bioengineering* **2023**, *10*, 1435.
[437] J. Huang, H. Dong, W. Zhang, J. Cui, Q. Li, J. Wang, Z. Zhao, X. Zang, *Adv. Sens. Res.* **2025**, *4*, DOI 10.1002/adsr.202400138.
[438] O. Okuyelu, O. Adaji, *J. Adv. Math. Comput. Sci.* **2024**, *39*, 81.